

TESIS DOCTORAL**2021****Propagation of statistical uncertainty in
mesh-based R2S calculations****Javier Alguacil Orejudo***Ingeniería Energética****PROGRAMA DE DOCTORADO EN
TECNOLOGÍAS INDUSTRIALES****DIRECTOR: Patrick Sauvan**CODIRECTOR: Juan Pablo Catalan*

Acknowledgments

First of all, I would like to express my gratitude to my two supervisors, who have been fundamental for the development of the thesis. To Patrick, for his support and inestimable help in any technical issue. To Juan, for his advice and patience to understand my opinions even when I do not find the correct words.

I would also like to thank the support of everyone at the TECF3IR research group, and in special to Javier, for giving me the opportunity to start in the investigation, and to Paco for keeping the cluster operational, despite all the time that this supposes.

In addition, I would like to thank to my family and friends, who support me and allow me to disconnect from the work. In special to Alba, Mario and Andrea, who always listen to me, and to Lara and Jordi without them, it probably would have taken me another year to write this thesis.

Finally, it is worth mentioning that this thesis was carried out as part of the project BES-2016-078586 and ENE2015-70733-R supported by Spanish MINECO and by Fondo Social Europeo (FSE).

Index

ACKNOWLEDGMENTS	3
INDEX	4
LIST OF FIGURES	8
LIST OF TABLES	10
ABBREVIATIONS AND ACRONYMS.....	13
RESUMEN	14
ABSTRACT	16
CHAPTER 1. INTRODUCTION	18
1.1 RADIATION FIELDS IN FUSION FACILITIES.....	19
1.2 COMPUTATIONAL NEUTRONIC ANALYSES TO ESTIMATE DECAY GAMMA FIELD.....	20
1.2.1 <i>Transport codes</i>	21
1.2.2 <i>Activation codes</i>	22
1.2.3 <i>Coupling transport and activation simulations to the estimation of decay gamma fields and their associated responses</i>	23
1.3 R2S METHODOLOGY.....	24
1.4 THE STOCHASTIC UNCERTAINTY IN R2S SIMULATIONS.....	25
1.5 MOTIVATION AND SCOPE OF THE THESIS	27
1.6 OUTLINE OF THE THESIS.....	28
CHAPTER 2. REVIEW OF THE METHODOLOGIES TO ASSESS THE STOCHASTIC UNCERTAINTY IN R2S SIMULATIONS 30	
2.1 BRUTE FORCE METHOD	31
2.2 ADJOINT BASED METHODS.....	32
2.2.1 <i>Explicit adjoint-based method</i>	32
2.2.2 <i>Implicit adjoint-based method</i>	33
2.3 ON-FLY METHOD	34
2.4 SUMMARY AND CONCLUSIONS	34
CHAPTER 3. TRANSPORT AND ACTIVATION STEPS IN R2S	36
3.1 SPATIAL DISTRIBUTION OF THE NEUTRON FLUX	38
3.2 ACTIVATION STEP IN R2S-UNED	38
3.2.1 <i>Mathematical description of the activation step</i>	39
3.2.2 <i>Discrete activation equations applied in R2S-UNED</i>	40
3.3 PHOTON TRANSPORT TO ESTIMATE THE SDR	41

3.4	SOLVING THE TEMPORAL EVOLUTION OF THE ISOTOPIC INVENTORY ODES SYSTEM	42
3.4.1	<i>ACAB code and solver algorithm</i>	43
3.4.2	<i>Single Neutron Interaction and Low Burn-Up (SNILB) conditions</i>	43
3.5	DERIVATIVE OF THE ISOTOPIC CONCENTRATION TO THE REACTION RATES	45
3.6	SUMMARY AND CONCLUSIONS	46
CHAPTER 4.	ANALYTICAL EXPRESSIONS TO ASSESS THE STOCHASTIC UNCERTAINTY IN R2S	
SIMULATIONS	47	
4.1	UNCERTAINTY PROPAGATION LAW.....	48
4.2	UNCERTAINTY OF THE DECAY GAMMA SOURCE INTENSITY	48
4.3	UNCERTAINTY OF THE PHOTON RESPONSE	50
4.4	UNCERTAINTY OF THE SDR	51
4.5	SUMMARY AND CONCLUSIONS	53
CHAPTER 5.	IMPLEMENTATION OF THE METHODOLOGY TO ESTIMATE THE SDR UNCERTAINTY	
IN R2S-UNED	54	
5.1	ESTIMATION OF THE STOCHASTIC NEUTRON UNCERTAINTY DUE TO THE MC TRANSPORT CODE.....	57
5.2	ACTIVATION SUMMARY	58
5.2.1	<i>Contents of the activation summary file</i>	59
5.2.2	<i>Consuming time during the activation step</i>	59
5.3	ESTIMATION OF THE DGS CONTRIBUTION DURING THE PHOTON TRANSPORT	60
5.4	FILTERING STEPS APPLIED TO SPEED UP THE ESTIMATION OF THE SDR UNCERTAINTY	61
5.4.1	<i>Spatial contribution of the DGS to the SDR</i>	61
5.4.2	<i>Isotopic contribution to the SDR</i>	61
5.4.3	<i>Pathway contribution to the production of the relevant isotopes</i>	62
5.5	ESTIMATION OF THE SENSITIVITY COEFFICIENTS	68
5.5.1	<i>SNILB method</i>	68
5.5.2	<i>General activation system</i>	69
5.6	SAVING FORMAT OF THE SENSITIVITY COEFFICIENT DATA. "P1C" COEFFICIENTS	69
5.7	ESTIMATION OF THE STOCHASTIC UNCERTAINTY IN R2S-UNED	71
5.8	SUMMARY AND CONCLUSIONS.....	73
CHAPTER 6.	VERIFICATION OF THE DEVELOPMENTS IN R2S-UNED.....	74
6.1	VERIFICATION OF THE ALGORITHM THAT CALCULATES THE NEUTRON FLUX CORRELATION MATRIX IN R2S-UNED.....	76
6.2	VERIFICATION OF THE ALGORITHM THAT CALCULATES THE ISOTOPIC CONTRIBUTION IN R2S-UNED.....	78
6.3	VERIFICATION AND VALIDATION OF THE ALGORITHM THAT CALCULATES THE CONTRIBUTING PRODUCTION PATHWAYS IN R2S-UNED.....	79
6.3.1	<i>Estimation of the pathway contributions in a simple matrix</i>	80

6.3.2	<i>Verification and Validation of the pathway contribution calculation method in ITER ...</i>	82
6.4	VERIFICATION OF THE ALGORITHM THAT CALCULATES THE DERIVATIVES OF THE CONCENTRATION TO THE REACTION RATES PER TARGET ISOTOPE IN R2S-UNED.....	86
6.4.1	<i>Verification of the algorithm when SNILB conditions are met.....</i>	86
6.4.2	<i>Verification of the general-purpose algorithm.....</i>	88
6.5	VERIFICATION OF THE ALGORITHM THAT TRANSPORTS THE STOCHASTIC UNCERTAINTY IN THE NEUTRON FLUX UNTIL THE SDR UNCERTAINTY	90
6.5.1	<i>Verification of the uncertainty estimation when SNILB conditions are met.....</i>	91
6.5.2	<i>Verification of the uncertainty estimation using the general-purpose method.....</i>	98
6.6	SUMMARY AND CONCLUSIONS.....	101
CHAPTER 7.	APPLICATION OF THE UNCERTAINTY MODULE OF R2S-UNED	102
7.1	ITER BENCHMARK EXERCISE.....	104
7.1.1	<i>Computational assumptions.....</i>	104
7.1.2	<i>Guideline to estimate the SDR stochastic uncertainty of the R2S-UNED calculation....</i>	105
7.1.3	<i>Stochastic uncertainty estimated with R2S-UNED.....</i>	109
7.1.4	<i>Comparison between D1S-UNED and R2S-UNED results of the ITER benchmark.....</i>	111
7.1.5	<i>Effect of the GVR on the correlation of the neutron flux in the ITER benchmark</i>	114
7.2	APPLICATION OF THE R2S-UNED UNCERTAINTY MODULE IN 2016 DD CAMPAIGN OF JET	118
7.2.1	<i>General computational assumptions of R2S air kerma estimation in octant 2 of JET ..</i>	120
7.2.2	<i>Estimation of the air-kerma and the bounding limits of its uncertainty using R2S-UNED</i>	122
7.2.3	<i>Estimation of the air-kerma and its actual stochastic uncertainty using R2S-UNED....</i>	126
7.3	SUMMARY AND CONCLUSIONS	134
CHAPTER 8.	SUMMARY AND CONCLUSIONS	137
8.1	IMPLEMENTATION AND VALIDATION OF THE METHODOLOGY.....	138
8.2	APPLICABILITY OF R2S-UNED TO ESTIMATE THE SDR STOCHASTIC UNCERTAINTY.....	139
8.3	TRANSFER OUTCOME.....	141
CHAPTER 9.	FUTURE WORK	142
9.1	CODE AND METHODOLOGY IMPROVEMENTS.....	143
9.1.1	<i>Code improvements.....</i>	143
9.1.2	<i>Methodology improvements</i>	144
9.2	OTHER APPLICATIONS OF THE DEVELOPED METHODOLOGY.....	145
9.3	OTHER UNCERTAINTY SOURCES IN R2S METHOD	145
ANNEX A.	NEUTRON UNCERTAINTY IN JET	146
ANNEX B.	MESHES COVERING JET GEOMETRY	147

ANNEX C.	DECAY GAMMA GROUPS RECOMMENDED BY FISPACT.....	150
ANNEX D.	ISOTOPIC CONTRIBUTION TO THE AIR-KERMA.....	151
ANNEX E.	COMPARISON OF THE BRUTE FORCE METHOD AND THE IMPLEMENTED METHOD IN JET	152
REFERENCES	153

List of Figures

FIGURE 1.1 STAGES TO ESTIMATE DETAILED 3D DECAY GAMMA FIELD IN FUSION FACILITIES.....	20
FIGURE 1.2 SIMULATION STEPS IN D1S AND R2S METHODOLOGIES	23
FIGURE 2.1 SCHEMATIC REPRESENTATION OF THE BRUTE FORCE METHOD FOR 2MC STEP SIMULATION [32]	31
FIGURE 3.1 RELEVANT QUANTITIES CALCULATED DURING R2S SIMULATION	36
FIGURE 5.1 INDEPENDENT LINEAR CHAIN DECOMPOSITION IN SOLVERS BASED ON LINEAR CHAIN SOLVERS [35].....	64
FIGURE 5.2 ALGORITHM SCHEME USED TO FIND THE CONTRIBUTING PATHWAYS TO THE RELEVANT ISOTOPE	66
FIGURE 5.3 VISUAL TREE FOR THE NUCLEI 1. POINTS REPRESENT THE ISOTOPE WHILE THE LINES JOINT THE FATHER WITH THE DAUGHTER ISOTOPE (THE ARROW INDICATES THE DAUGHTER ISOTOPE).....	67
FIGURE 5.4 DETECTED PATHWAYS IN THE EXAMPLE OF FIGURE 5.3	67
FIGURE 6.1 NEUTRON SOURCE SPECTRUM	77
FIGURE 6.2 RELATIVE DIFFERENCE OF THE CORRELATION (COR) CALCULATED USING NUMPY LIBRARY (N) OR THE SOLVER OF THE TRANSPORT CODE (T) OF R2S-UNED	77
FIGURE 6.3 SCHEME OF THE ACTIVATION CASE FOR VERIFYING THE ALGORITHM TO LOOK FOR THE RELEVANT PATHWAYS	80
FIGURE 6.4 ITER PORT CELL (PC) AND PORT INTERSPACE (PI) AREAS [67]......	83
FIGURE 6.5 NEUTRON FLUX USED FOR ACTIVATION CALCULATION [67]	83
FIGURE 6.6 NEUTRON FLUX CORRELATION	93
FIGURE 6.7 CORRELATION OF THE REACTION RATE CALCULATED BY BRUTE FORCE (LEFT) OR BY R2S-UNED UNCERTAINTY MODULE (RIGHT).....	93
FIGURE 6.8 CORRELATION OF THE ISOTOPIC ACTIVITY CALCULATED BY BRUTE FORCE (LEFT) OR BY R2S-UNED UNCERTAINTY MODULE (RIGHT).....	94
FIGURE 6.9 CORRELATION MATRIX OF THE DGS INTENSITY	95
FIGURE 6.10 CORRELATION OF THE 6-VOXEL NEUTRON FLUX	96
FIGURE 7.1 ITER BENCHMARK SCHEME	104
FIGURE 7.2 COMPUTATIONAL SCHEME OF THE GUIDELINE APPLIED IN THE ITER BENCHMARK	106
FIGURE 7.3 COMPLETE MESH SUPERIMPOSED TO THE ITER BENCHMARK GEOMETRY	107
FIGURE 7.4 NEUTRON FLUX AT POWER OF $2 \cdot 10^{19} \text{ N} \cdot \text{S}^{-1}$ AND ITS UNCERTAINTY (REPRESENTED IN 2D USING AXIAL SYMMETRY AROUND THE Z-AXIS).....	107
FIGURE 7.5 DGS CONTRIBUTION TO THE SDR (REPRESENTED IN 2D USING CYLINDRICAL SYMMETRY AROUND THE Z-AXIS)	108
FIGURE 7.6 CAD MODEL OF PRINCIPAL REGIONS OF THE OCTANT 2 OF JET	121
FIGURE 7.7 PZ=100 OF THE NEUTRON FLUX UNCERTAINTY OVER ALL JET GEOMETRY	123
FIGURE 7.8 DGS CONTRIBUTION TO THE AIR-KERMA IN THE DETECTOR (YELLOW SPHERE) DUE TO THE DD NEUTRON ACTIVATION.....	124
FIGURE 7.9 CONTRIBUTING REGIONS TO THE AIR-KERMA [87].	124
FIGURE 7.10 CONTRIBUTION ELEMENT OF THE MESH 3 (LEFT) AND 4 (RIGHT)	127

FIGURE 7.11 ALGORITHM IMPLEMENTED TO DEFINE THE MESHES THAT CONTAIN THE RELEVANT REGIONS	128
FIGURE 7.12 DISTRIBUTION OF THE MESHES TO CONSIDER 95% OF THE CONTRIBUTING REGIONS.....	130
FIGURE 7.13 NEUTRON FLUX UNCERTAINTY IN EACH MESH.....	130
FIGURE 7.14 CONTRIBUTION OF EACH SMALL MESH INSIDE OF MESH 3 TO THE AIR KERMA AND ITS UNCERTAINTY DUE TO THE NEUTRON FLUX.....	131
FIGURE 7.15 CONTRIBUTION OF EACH SMALL MESH INSIDE OF MESH 4 TO THE AIR KERMA AND ITS UNCERTAINTY DUE TO THE NEUTRON FLUX.....	132
FIGURE 7.16 UNCERTAINTY UNDERESTIMATION OF THE UNCORRELATED ASSUMPTION OF THE CORRELATION MATRIX OF THE NEUTRON FLUX IN JET	132

List of tables

TABLE 1.1 NEUTRON BUDGET AND POWER EXPECTED IN JET ITER AND DEMO [2] [3].....	19
TABLE 1.2 PRINCIPAL ADVANTAGES AND WEAKNESSES OF THE CURRENT METHODOLOGIES THAT ESTIMATE THE MC SDR UNCERTAINTY IN R2S SIMULATIONS	26
TABLE 5.1 COMPUTATIONAL STAGES IN AN R2S SIMULATION INCLUDING THE UNCERTAINTY ESTIMATION. THE TABLE HIGHLIGHTS: I) * MANDATORY NEW INPUT DATA TO ESTIMATE THE SDR UNCERTAINTY. II) ** OPTIONAL NEW INPUT DATA TO ESTIMATE THE SDR UNCERTAINTY.....	55
TABLE 5.2 TIME CONSUMPTION OF THE DIFFERENT VERSIONS OF THE ACTIVATION MODULE OF R2S-UNED.....	60
TABLE 5.3 DEFINITION OF THE PHASE 1 COEFFICIENTS (P ₁ C).....	71
TABLE 6.1 DEFINITION OF SS316LN-IG.....	76
TABLE 6.2 CONTRIBUTION TO THE PHOTON FLUX CALCULATED FROM THE ISOTOPIC ACTIVITY USING R2S-UNED ACTIVATION SOLVER OR FROM R2S-UNED UNCERTAINTY MODULE.....	79
TABLE 6.3 PATHWAYS DETECTED BY THE METHOD ACCORDING TO THE SEARCH OPTION.....	82
TABLE 6.4 PATHWAYS FOR RADIONUCLIDES OF INTEREST FROM ACAB+EAF-2007 ACTIVATION SIMULATION FOR CONVENTIONAL CONCRETE.	84
TABLE 6.5 PATHWAYS FOR RADIONUCLIDES OF INTEREST FROM ACAB+EAF-2007 ACTIVATION SIMULATION FOR BARITE CONCRETE.....	84
TABLE 6.6 PATHWAYS FOR RADIONUCLIDES OF INTEREST FROM ACAB+EAF-2007 ACTIVATION SIMULATION FOR L2N CONCRETE.....	85
TABLE 6.7 PATHWAYS FOR RADIONUCLIDES OF INTEREST FROM ACAB+EAF-2007 ACTIVATION SIMULATION FOR CU.	85
TABLE 6.8 PATHWAYS FOR RADIONUCLIDES OF INTEREST FROM ACAB+EAF-2007 ACTIVATION SIMULATION FOR W.....	86
TABLE 6.9 MIXTURE MATERIAL	87
TABLE 6.10 DERIVATIVE OF THE ISOTOPIC CONCENTRATION RESPECT TO THE REACTION RATE PER TARGET ISOTOPE (AT·S)....	87
TABLE 6.11 DERIVATIVES OF THE CONCENTRATION RESPECT TO THE REACTION RATE (AT·S) WHEN THE BURN UP IS EXTREMELY IMPORTANT.....	88
TABLE 6.12 RELEVANT DATA TO DEFINE THE ACTIVATION SYSTEM TO PRODUCE ¹⁸² Ta	89
TABLE 6.13 DERIVATIVES OF THE ISOTOPIC CONCENTRATION OF TANTALUM 182 WITH RESPECT TO THE REACTIONS. THE REACTIONS ARE REPRESENTED IN BOLD FONT.....	90
TABLE 6.14 RELEVANT PARAMETERS OF THE R2S-UNED UNCERTAINTY MODULE IN THE NICKEL SLAB SIMULATION	92
TABLE 6.15 ISOTOPE CONTRIBUTION TO THE PHOTON FLUX AND PATHWAYS THAT PRODUCE THEM.....	92
TABLE 6.16 REACTION RATE AND ITS UNCERTAINTY ESTIMATED USING THE BRUTE FORCE OF A SET OF CASES OR THE R2S- UNED UNCERTAINTY MODULE IN A PARTICULAR CASE.....	93
TABLE 6.17 SENSITIVITY COEFFICIENTS OF THE MOST RELEVANT REACTIONS IN THE ACTIVATION OF THE NICKEL.....	94
TABLE 6.18 ISOTOPIC ACTIVITY AND ITS UNCERTAINTY ESTIMATED USING THE BRUTE FORCE OF A SET OF CASES OR THE R2S- UNED UNCERTAINTY MODULE IN A PARTICULAR CASE.....	94

TABLE 6.19 GAMMAS PER DISINTEGRATION EMITTED IN THE NICKEL SLAB BY THE RELEVANT ISOTOPES TO THE PHOTON FLUX	94
TABLE 6.20 DGS INTENSITY AND ITS UNCERTAINTY ESTIMATED USING THE BRUTE FORCE METHOD OR THE R2S-UNED UNCERTAINTY MODULE	95
TABLE 6.21 CONTRIBUTION OF THE DGS INTENSITY TO THE PHOTON FLUX EMITTED FROM THE NICKEL SLAB AND ITS UNCERTAINTY, WHERE $\gamma_s - 1$ IS PER PHOTON SOURCE	95
TABLE 6.22 TOTAL SOURCE FACTOR AND PHOTON FLUX EMITTED FROM THE NICKEL SLAB AND ITS UNCERTAINTIES ESTIMATED USING THE BRUTE FORCE OF A SET OF CASES OR THE R2S-UNED UNCERTAINTY MODULE IN A PARTICULAR CASE	95
TABLE 6.23 ISOTOPIC ACTIVITY IN THE NICKEL SLAB AND ITS UNCERTAINTY ESTIMATED USING THE BRUTE FORCE OF A SET OF CASES OR THE R2S-UNED UNCERTAINTY MODULE IN A PARTICULAR CASE	97
TABLE 6.24 TOTAL SOURCE FACTOR AND PHOTON FLUX AND ITS UNCERTAINTIES ESTIMATED USING THE BRUTE FORCE OF A SET OF CASES OR THE R2S-UNED UNCERTAINTY MODULE IN A PARTICULAR CASE	97
TABLE 6.25 PATHWAYS PRODUCED IN THE TUNGSTEN SLAB	98
TABLE 6.26 INPUT PARAMETER OF UNCERTAINTY MODULE OF R2S-UNED CONSIDERED RUNNING THE UNCERTAINTY MODULE OF R2S-UNED IN THE TUNGSTEN SLAB SIMULATION	99
TABLE 6.27 ISOTOPIC ACTIVITY AND ITS UNCERTAINTY ESTIMATED USING THE BRUTE FORCE OF A SET OF CASES OR THE R2S- UNED UNCERTAINTY MODULE IN A PARTICULAR CASE.....	99
TABLE 6.28 TOTAL SOURCE FACTOR AND PHOTON FLUX AND ITS UNCERTAINTIES ESTIMATED USING THE BRUTE FORCE OF A SET OF CASES OR THE R2S-UNED UNCERTAINTY MODULE IN A PARTICULAR CASE	100
TABLE 6.29 TOTAL SOURCE FACTOR AND PHOTON FLUX AND ITS UNCERTAINTIES ESTIMATED USING THE BRUTE FORCE OF A SET OF CASES OR THE R2S-UNED UNCERTAINTY MODULE IN A PARTICULAR CASE OF THE R2S SIMULATION WHERE ONLY TANTALUM 182 IS CONSIDERED.....	100
TABLE 7.1 SA-2 IRRADIATION SCENARIO.....	105
TABLE 7.2 SIZE OF THE DEFINED MESHES AND THE COVARIANCE MATRIX OF THE NEUTRON FLUX.....	109
TABLE 7.3 STATISTICAL UNCERTAINTY OF THE ISOTOPIC ACTIVITY CALCULATED WITH R2S-UNED.....	110
TABLE 7.4 ⁹⁵ Nb PRODUCTION PATHWAYS FOUND IN THE RELEVANT REGIONS OF THE REDUCED MESH	110
TABLE 7.5 D1S REACTION DATA INCLUDED IN THE SIMULATION	112
TABLE 7.6 D1S TIME FACTOR NORMALIZED TO $1.0714 \cdot 10^{17}$ N/s	113
TABLE 7.7 RADIOISOTOPE CONTRIBUTIONS TO THE SDR CALCULATED BY R2S AND D1S METHODOLOGIES.....	113
TABLE 7.8 SDR AND ITS STATISTICAL UNCERTAINTY (ONE STANDARD DEVIATION) OF R2S AND D1S SIMULATIONS OF ITER BENCHMARK EXERCISE	114
TABLE 7.9 UNCERTAINTY OF THE ITER BENCHMARK EXERCISE CALCULATED IN DIFFERENT R2S-UNED SIMULATIONS.....	115
TABLE 7.10 SDR AND ITS UNCERTAINTY CALCULATED WITH DIFFERENT CORRELATION MATRIXES OF THE NEUTRON FLUX, DIVIDED IN DIFFERENT CONTRIBUTIONS	118
TABLE 7.11 2011-2016 YEARLY DD AND DT NEUTRON BUDGET[85]	121
TABLE 7.12 CONTRIBUTION TO THE AIR KERMA TALLY.....	123
TABLE 7.13 UNCERTAINTY ESTIMATION OF THE AIR-KERMA CONTRIBUTION OF MESH 3 AND 4. CORRELATED NEUTRON FLUX APPROACH.	125

TABLE 7.14 UNCERTAINTY ESTIMATION OF THE AIR-KERMA CONTRIBUTION OF MESH 3 AND 4. UNCORRELATED NEUTRON FLUX APPROACH.	125
TABLE 7.15 NUMBER OF MESHES DEFINED.....	129
TABLE 7.16 R2S ESTIMATION OF THE AIR KERMA AND ITS STOCHASTIC UNCERTAINTY IN THE OCTANT 2 OF JET	133

Abbreviations and acronyms

CAD	Computer Aided Design
CADIS	Consistent Adjoint Driven Importance Sampling
CDGS	Common Decay Gamma Source
CDR	Contact Dose Rate
D1S	Direct One Step
DGS	Decay Gamma Source
DEMO	DEMOstration
EAF	European Activation File
ENDF	US Evaluated Nuclear Data Library
FENDL	Fusion Evaluated Nuclear Data Library
GVR	Global Variance Reduction
GT-CADIS	Group-wise Transmutation Consistent Adjoint-Driven Importance Sampling
ILA	ITER Like Antenna
ITER	International Thermonuclear Experimental Reactor
MC	Monte Carlo
MCNP	Monte Carlo N-particle
MS-CADIS	Multi-Step Consistent Adjoint Driven Importance Sampling
JET	Joint European Torus
R2S	Rigorous 2 Steps
SDR	Shutdown Dose Rate
SNILB	Single Neutron Interaction and Low Burn-up
S_N	Discrete ordinate
TEC3FIR	Tecnologías de Fusión Fisión y Fuentes de Irradiación
UNED	Universidad Nacional de Educación a Distancia
VR	Variance Reduction

Resumen

Durante el funcionamiento de las instalaciones experimentales de fusión, se generan intensos campos de neutrones que interactúan con los distintos componentes de la instalación. Esto provoca que dichos componentes se vuelvan radiactivos, y por tanto, que emitan un campo de fotones de decaimiento, incluso cuando la instalación experimental está apagada. La estimación de estos campos de fotones, así como las funciones respuesta asociadas a estos campos, como puede ser la dosis recibida en los componentes y/o trabajadores, es esencial en las fases de diseño, ingeniería y licenciamiento de estas instalaciones de fusión.

Hoy en día, una de las metodologías más potentes para estimar los campos de fotones residuales en parada es Rigorous 2 Steps (R2S). Esta metodología acopla las salidas y entradas de códigos de transporte y activación para simular, paso a paso, todos los procesos físicos relevantes en el cálculo de los campos de fotones residuales. Para ello, primero se realiza una simulación del transporte de neutrones, cuyo objetivo es calcular el flujo de neutrones en cada región de la instalación. Después se simula detalladamente la activación de cada componente debida a la interacción de dichos neutrones con la materia, con lo que se consigue estimar la distribución de fotones que emite el material activado de la instalación al tiempo de interés. Finalmente, el último paso consiste en transportar dicha fuente de fotones por la instalación, calculando el campo de fotones residual y las funciones respuestas deseadas asociadas a este.

Los sistemas R2S más avanzados empleados en el ámbito de la fusión están basados en códigos de transporte Monte Carlo (MC), debido a que este método de cálculo es considerado hoy en día el más preciso para simular el transporte de radiación. Este método permite estimar la incertidumbre estadística del cálculo durante el transporte de neutrones y de fotones de decaimiento. Sin embargo, el método de acople empleado en la metodología R2S no permite transportar las incertidumbres a través del esquema de cálculo. Por lo tanto, la metodología R2S basadas en códigos de transporte MC no es capaz de considerar el error estadístico, introducido durante el transporte de neutrones, en las funciones respuesta asociadas a los fotones de decaimiento.

Este problema ha sido una línea de investigación activa durante los últimos años. Esto ha dado como resultado la propuesta e implementación de varios esquemas computacionales que permiten considerar esta fuente de incertidumbre en los cálculos de R2S. Sin embargo, estos esquemas asumen simplificaciones durante el paso de activación, las cuales limitan su aplicabilidad.

Por ello, el objetivo de esta tesis es proponer e implementar un esquema computacional en el código R2S-UNED, el cual permita considerar esta fuente de incertidumbre sin introducir nuevas

asunciones que aquellas heredadas directamente de la metodología R2S. Este esquema debe ser aplicable a cualquier caso donde se pueda requerir el uso de R2S-UNED.

Esta tesis describe dicho esquema, así como todas las nuevas capacidades de R2S-UNED implementadas para poder aplicarlo. Estas capacidades son enumeradas a continuación:

- i. Cálculo de la matriz de covarianza del flujo neutrónico (incertidumbre estadística del flujo neutrónico)
- ii. Contribución de cada radioisótopo a la dosis o función respuesta deseada
- iii. Contribución de cada camino que genera los radioisótopos de interés durante la activación del material
- iv. Estimación de la derivada de la concentración de isótopos respecto del ratio de reacción
- v. Estimación de la incertidumbre estadística, debida al flujo neutrónico, en las diferentes cantidades calculadas durante un cálculo de R2S (ratios de reacción, concentración isotópica, fuente de decaimiento y dosis o función respuesta deseada).

Cada una de estas capacidades fue implementada dentro del esquema de R2S-UNED y verificada durante esta tesis. Entre todas estas capacidades, la capacidad de estimar la incertidumbre estadística del flujo neutrónico destaca por su importancia en el esquema de cálculo, dado que limita la aplicabilidad del esquema al no poder estimar la matriz de covarianza del flujo neutrónico en muchos casos prácticos, debido al tamaño de dicha matriz. Esta limitación es, hoy en día, una de las mayores limitaciones para poder aplicar la metodología propuesta en esta tesis, así como otras desarrolladas durante estos años.

Por ello, durante esta tesis se ha desarrollado una guía de aplicación que trata de dedicar los recursos computacionales disponibles al cálculo de la incertidumbre de las regiones más importantes que contribuyen a la dosis. Lo cual aumenta considerablemente el rango de aplicabilidad de la nueva herramienta desarrollada para el cálculo de incertidumbre estadística en cálculos de R2S, sin ser aun de aplicación general.

Esta guía ha sido clave para poder aplicar esta nueva herramienta a los dos casos prácticos considerados en esta tesis: El benchmarking computacional de ITER de cálculo de dosis residual y el cálculo de air-kerma en el octante dos de JET. Ambas aplicaciones muestran la necesidad de incluir la información precisa de la matriz de correlación del flujo neutrónico para estimar la incertidumbre en la dosis, en vez de considerar está completamente correlada o anticorrelada, asunciones que estiman límites superiores e inferiores al valor de la incertidumbre estadística en la dosis sin necesidad de obtener la matriz de correlación del flujo neutrónico completa.

Abstract

During the operation of experimental fusion facilities, intense neutron fields are generated, which interact with the different components of the facility. Due to this, such components become radioactive, and therefore, emit a decay gamma field even when the facility is not operating. The estimation of these decay gamma fields, and the corresponding responses in the components and/or workers is essential during the design, engineering, and licencing phases of the fusion facilities.

Nowadays, one of the most powerful methodologies to estimate the decay gamma field and its associated responses is the Rigorous 2 Steps (R2S). This methodology couples the input and outputs of the transport and activation codes in order to simulate, step by step, the most relevant physical processes to calculate the decay gamma field. In order to do that, three simulations are sequentially carried out. The first one consists of a neutron transport where the neutron flux is estimated in all regions of the facility. The second one is an activation simulation, which considers the neutron reactions within the materials in order to estimate the radioactive isotopes at a particular time; consequently, it computes the decay gamma source at that time. Finally, the last simulation consists of a photon transport of this decay gamma source in order to compute the decay gamma field and its associated responses, such as shutdown dose rate (SDR).

The most advanced R2S systems, applied in the fusion field, use Monte Carlo (MC) transport codes, since currently they are considered the most accurate to perform the radiation transport step. The MC method enables the assessment of the stochastic uncertainty caused by the calculation method during the transport simulations. However, R2S coupling scheme does not transport the neutron flux uncertainty to the SDR uncertainty. This means that MC R2S simulations cannot provide the estimation of the stochastic uncertainty due to the calculation method in the calculated response.

This issue has been an active research line during the last years. Consequently, several schemes, which estimate the SDR uncertainty due to MC method in R2S calculations, have been proposed. However, these schemes assume simple activation conditions that simplify the activation calculation, while also limiting the application of these methodologies.

The aim of this thesis is to propose and to implement a computational scheme that calculates the stochastic uncertainty of the SDR responses in R2S calculations. This scheme must not introduce new assumptions that those inherit from R2S methodology. In addition, the scheme must be applicable to any analysis where R2S is used.

This thesis describes this scheme, as well as all new R2S-UNED capabilities that were implemented in order to apply this scheme. They are:

- i. Estimation of the covariance matrix of the neutron flux (stochastic uncertainty of the neutron flux).
- ii. Contribution of each radioisotope to the SDR response.
- iii. Contribution of each pathway that produce the relevant radioisotopes during the activation of the material.
- iv. Estimation of the derivative of the isotopic concentration respect to the reaction rates
- v. Estimation of the stochastic uncertainty, due to the neutron flux uncertainty, of the different quantities estimated during the R2S simulation; those are the reaction rates, the isotopic concentration, the decay gamma source, and the SDR response.

During this thesis, all these capabilities were implemented in R2S-UNED and verified. Among all of them, the capability to estimate the stochastic uncertainty of the neutron flux stands out due to its importance to the applicability of the developed tool. The methodology implemented to estimate the neutron flux uncertainty cannot be applied in most of the practical cases where R2S is applied, because the size of the correlation matrix of the neutron flux is usually too large. Nowadays, this is the most relevant limitation to apply the methodology proposed in this thesis. It is worth highlighting that this limitation also affects the other methodologies developed during the last years.

For this reason, we also propose a guideline to improve the applicability of this tool. This is based on the optimization of the computational resources, calculating only the stochastic uncertainty due to the activated regions which contribute significantly to the SDR. It is worth noting that although this guideline improves the applicability of the tool, its application is still not universal.

This guideline was essential in order to apply the new tool to the two practical cases that have been carried out during this thesis: The SDR computational benchmark of ITER and the estimation of the air-kerma in the octant 2 of JET. Both applications show the importance of estimating the correlation matrix of the neutron flux, instead of considering this matrix completely correlated or uncorrelated (superior or inferior boundaries to the value of the SDR uncertainty).

Chapter 1.

Introduction

In fusion devices, high-energy neutrons are emitted from the plasma source, penetrating deep into the facility. One of the effects of the neutron radiation field is the activation of the different components of the facility producing radioactive nuclides, which persist after the shutdown of the facility. Consequently, decay gamma fields, which result from gamma emitted by these radionuclides, are expected along the fusion facility even after its shutdown. Important efforts are directed to the analysis of the effects of the decay gamma field, such as the shutdown dose rate, due to their relevance to the licensing of the fusion facilities.

Nowadays, one of the most relevant methodologies to carry out these analyses is the Rigorous-two-Step (R2S) method. This method estimates the decay gamma radiation field and associate responses by coupling particle transport and activation calculations. However, one of the weaknesses of this methodology is that the coupling scheme does not enable the transport of the uncertainty of the different simulations to the response. The stochastic uncertainty due to the MC calculation method used by the radiation transport codes is of special relevance.

The research topic of this thesis is the development and implementation of a methodology that overcomes this open issue of the R2S methodology. This chapter aims to introducing the R2S method to nuclear analysis in fusion facilities as well as to motivate the study of the uncertainty transport of the MC uncertainty in R2S systems. In addition, this chapter also summarizes the principal contributions of this thesis to the field of research and describes the organization of this document.

1.1 Radiation fields in fusion facilities

Several fusion facilities are being built as part of the roadmap to using nuclear fusion as a commercial energy source [1]. In them, intense neutron fields are produced as a result of the fusion reactions. Furthermore, each new proposed fusion facility increases the intensity of these neutron fields and the neutron budget expected in the corresponding device. Table 1.1 presents the quantitative example of the neutron sources of three relevant fusion experiments in order to contextualize the expected neutron fields in fusion facilities.

Table 1.1 Neutron budget and power expected in JET ITER and DEMO [2] [3]

<i>Facility</i>	<i>Maximum Power</i>	<i>Neutron budget during the facility lifetime</i>
<i>The Joint European Torus¹ [4] (JET)</i>	16.1 MW ($\sim 10^{19}$ n/s)	$\sim 10^{22}$
<i>("The way" in latin) ITER² [5]</i>	500 MW ($\sim 10^{20}$ n/s)	$\sim 10^{27}$
<i>The DEMOnstration reactor³ [6] (DEMO)</i>	2000-5000MW ($\sim 10^{21}$ n/s)	$\sim 10^{28} - 10^{29}$

The neutrons, produced in the fusion process, interact with the structure of the corresponding facility producing the material activation ⁴. As a consequence of the material activation along the fusion facility, different radiation fields are produced. In practice, the most problematic one, from the point of view of the nuclear analysis, is the decay gamma field. The principal reason being that it is propagated along the whole facility. Consequently, it causes damage to electronic systems and health problems in the workers, and therefore, drastically affects the licensing of the whole fusion facility. Hence, the quantification of the radiation effects on both components and workers is essential to the design of the facilities, and subsequently, it is also indispensable to achieve the fusion as a viable energy source.

The computational neutronic field, which covers the general frame of this thesis, studies the problems associated with the radiation fields produced by the neutron fields. The following sections briefly describe the usual computational schemes applied in neutronic analysis of fusion facilities, focusing on the decay gamma fields estimation.

¹ JET is the largest tokamak in operation nowadays, and furthermore, one of the most relevant experimental fusion facilities dedicated to test technologies for ITER

² ITER will be the world's largest experimental tokamak nuclear fusion reactor, whose main goal is to demonstrate the scientific and technological of fusion energy for future electricity generation. It is currently being built in France.

³ DEMO will be the ITER's successor. DEMO is intended to demonstrate the large-scale production of electrical power

⁴ Radioactive isotopes produced by the transmutations or excitations of the nuclei due to the neutron interaction

1.2 Computational neutronic analyses to estimate decay gamma field

As previously commented, this section presents the typical scheme and computational tools applied in common neutronic analyses, paying special attention to those aspects related to the estimation of the decay gamma field in fusion facilities. A detailed state of art of the methods and tools used for neutronic analyses of relevant fusion facilities can be found in references [7] and [8].

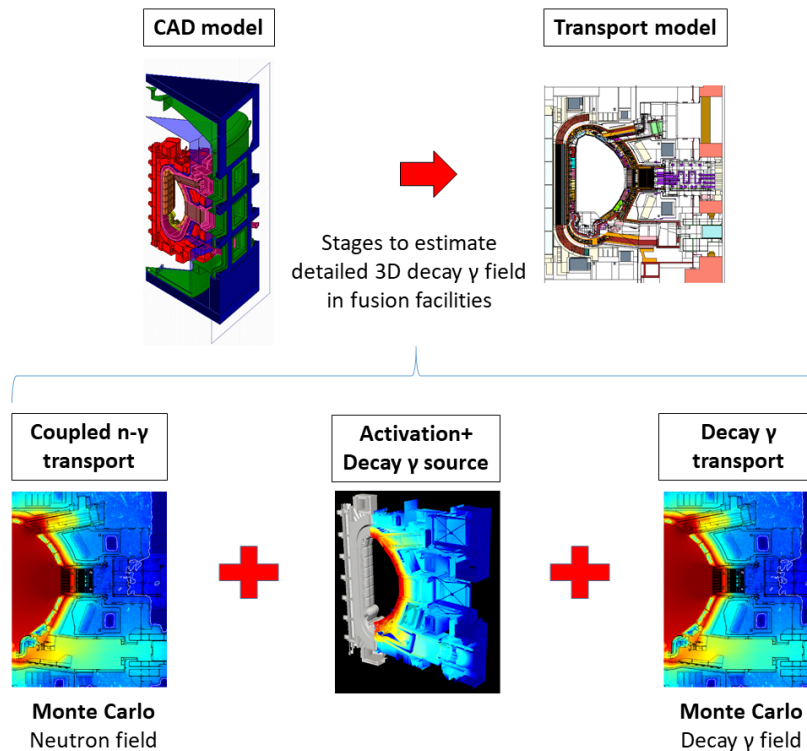


Figure 1.1 Stages to estimate detailed 3D decay gamma field in fusion facilities

Figure 1.1 shows the general stages to estimate the responses associated to the decay gamma field. The first two stages of the scheme[9]–[11], presented at the top of Figure 1.1, correspond to the definition of the relevant fusion facility features. That is, the definition of the physical problem to be analyzed¹.

The following stages of the neutronic analysis correspond to the simulation of the most relevant physical processes² to estimate the decay gamma field and its associated responses. These physical processes can be broken down into three conceptual stages as indicated in Figure 1.1:

¹ It is worth underlining that these steps are out of the frame of this thesis.

² Section 1.1 provides a brief description of the physical processes involved in the decay gamma field calculation.

- i. The estimation of the neutron field.
- ii. The activation of the materials of the facility.
- iii. The estimation of the decay gamma field and the associated responses.

The first stage consists in transporting of the neutron radiation¹ from the source (usually the neutron produced in the plasma) along the complete facility. This step aims to estimate the neutron field which interacts with the materials and induces their activation. This stage is faced using transport codes, which are summarized in section 1.2.1.

The following stage is the neutron activation of the material. This step follows the temporal evolution of the isotopic inventory in each region in order to estimate the Decay Gamma Source (DGS) that is emitted at the time of interest. The methodologies applied to carry out the activation stage are briefly introduced in section 1.2.2.

The last stage is the photon transport, from the DGS, along the complete facility. Consequently, it aims to estimate the decay gamma field and its associated responses. From the computational point of view, this stage is analogous to the first one, because it also consists in transporting the radiation along the geometry. Therefore, it is handled using the same transport codes summarized in section 1.2.1.

Over the last decades, several methodologies, which combine the three stages, have been developed in order to estimate the decay gamma field and its associated responses in the fusion facilities. The most relevant ones are presented in section 1.2.3. It is worth highlighting that the frame of this thesis is the development of new capabilities inside of one of these methodologies.

1.2.1 Transport codes

The transport codes aim to estimate the distribution of the radiation fields and their associated responses. There are two main calculation methods to perform the radiation transport in fusion energy systems [12]: The discrete ordinate [13] (S_N) method and the Monte Carlo [14] (MC) method.

Concerning the S_N transport codes [13] [15], they discretize the space, direction, and energy to solve the radiation transport. These codes provide responses in extended regions with high spatial resolution. The calculation of these responses is fast; however, this method introduces a systematic uncertainty² due to the discretization. Due to this weakness, nowadays the S_N transport codes are not the reference codes in fusion facilities³.

¹ The particle transport also simulates the secondary particles

² They calculate an approximate solution of the transport due to the energy and spatial discretization. In addition, this approach can even lead to unphysical results such as the so-called “ray effect” [97].

³ They are still useful in nuclear analysis of fusion facilities to speed up MC transport simulations [98] [99].

Regarding the MC transport codes [16]–[18], they use a stochastic method based on the simulation of the individual trajectories of a set of source particles and the secondary particles produced by them. The expected radiation field or its effects are derived from the average behaviour of this statistical sample.

The strong point of this calculation method is its capability to simulate high-fidelity 3D geometries without discretizing the space or the energy. For this reason, MC transport codes are considered the most accurate ones of those applied in nuclear analysis of fusion facilities, being the reference codes to the analysis of most of these devices. Note that this thesis is focused on methodologies to estimate the SDR¹ based on MC transport codes.

The MC method introduces a stochastic uncertainty² that can be estimated during the simulation process. This uncertainty decreases as $(NPS)^{-\frac{1}{2}}$, where NPS is the number of source particles simulated. This means that, ideally, we can achieve estimations with satisfactory low (and known) stochastic uncertainty due to the calculation method. However, they can require huge amounts of computational time.

In this sense, one of the worse scenarios to the MC transport code is to determine the radiation field with high energy and spatial resolution in extended material regions. This is because enough particles of different energies must arrive at each point of the region³ to achieve low stochastic uncertainty at all points. However, realistic estimations of the decay gamma field can require this type of simulation⁴ as section 1.2.3 explains. ANNEX A presents an MC neutron transport in JET to contextualize the typical uncertainty level that the MC transport introduces in a realistic case.

It is worth underlining that the stochastic uncertainty due to the MC calculation method is a relevant topic in this thesis.

1.2.2 Activation codes

The activation codes or isotopic inventory codes estimate the temporal evolution of the isotopic inventory of irradiated material. In general, there are two approaches to deal with activation. These approaches or methods are:

- i. General-purpose methods that deal with the complete activation system. That is, this approach considers all possible isotopes, reactions, and decay paths that could happen.

¹ Representative response function associated to the decay gamma field

² Hereinafter, stochastic uncertainty due to the MC method is directly called stochastic uncertainty

³ This requires huge amount of NPS; that is, huge amount of computational time

⁴ It is worth to highlight again that despite of this weakness, MC transport code. are the reference codes for the most relevant fusion projects like ITER[5].

- ii. Methods that consider only the most relevant features of the specific activation case. That is, these methods consider only a few relevant isotopes reactions and decay paths. In addition, they can take into account the specific physical features of the activation case to simplify the mathematical model of the activation.

It is worth highlighting that, the activation step considers the temporal evolution of the neutron flux spectrum as input data. In fusion devices, the neutron flux spectrum is usually considered constant because generally the burn-up of the material and the production of new isotopes is negligible with respect to the original material composition. Therefore, the temporal evolution of the neutron flux only takes into account the intensity of the plasma pulses.

Chapter 3 describes in detail the activation codes and methodologies applied in this thesis.

1.2.3 Coupling transport and activation simulations to the estimation of decay gamma fields and their associated responses

The estimation of the decay gamma fields and their associated responses, such as the SDR, requires the combination of the methodologies presented in sections 1.2.1 and 1.2.2. In the fusion field, the most relevant methodologies that combines these points are Direct 1 Step (D1S) [19] and Rigorous 2 Step (R2S) [20]. The computational steps of these methodologies are described in Figure 1.2.

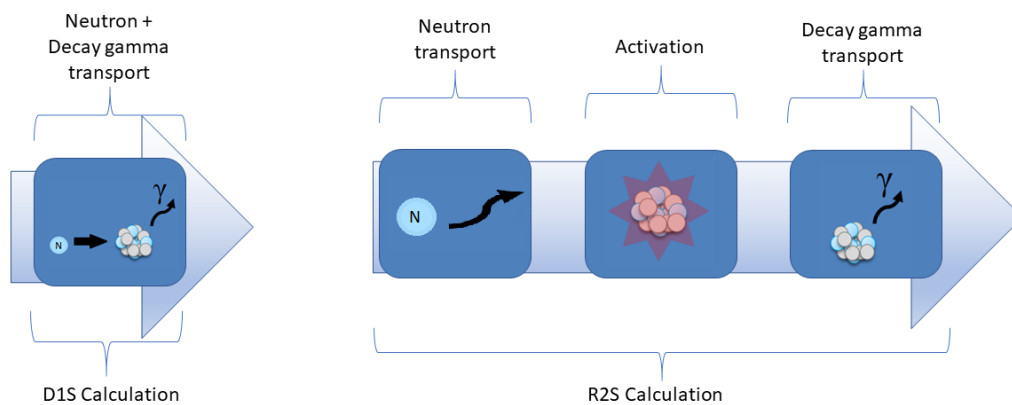


Figure 1.2 Simulation steps in D1S and R2S methodologies

Regarding the D1S methodology, it is an accurate and fast method that calculates the SDR, assuming Single Neutron Interaction and Low Burn-up (SNILB) conditions during the material activation. This hypothesis allows estimating the SDR in only one transport simulation, where the activation is performed during the transport simulation. SNILB conditions, which are described in-depth in section 3.4.2, are commonly met in many practical applications for current fusion facilities. Therefore, D1S method is widely applied in most of the SDR calculations of fusion facilities nowadays.

With respect to the R2S methodology, it calculates the SDR by coupling two transport simulations and one activation calculation, following the physical stages presented in Figure 1.2. The coupling of the programs requires the spatial and energy discretization of the quantities involved¹. In this sense, R2S accuracy is lower than D1S one. In addition, R2S simulation consumes more human and computational resources than D1S simulation. Hence, R2S is generally not used when D1S method can be applied. However, despite this weakness, the application range of R2S methodology is larger than D1S because SNILB hypotheses are not considered during the activation step.

It is worth highlighting that SNILB conditions are not met when neutron fluence is high enough. This is the scenario that is expected in future fusion facilities will be built in the roadmap to the fusion as a commercial energy source (Table 1.1). Under these circumstances, R2S is still the most relevant methodology to estimate the SDR in practical situations, such as nuclear analyses in the first wall of DEMO [21], because D1S method cannot be applied.

In this situation, the development of MC R2S methodology is essential to improve the quality of the neutronic analyses, and consequently the design of these fusion facilities. In this frame, this thesis studies one of the MC R2S weaknesses, which is presented in the following two sections: On one hand, section 1.3 performs a general description of the R2S methodology, paying special attention to the advanced MC R2S. On the other hand, section 1.4 presents the problems related to the calculation of the stochastic uncertainty of the SDR response estimated by MC R2S, which is the main topic of this thesis.

1.3 R2S methodology²

The implementation of R2S methodology is a computational system³, which combines activation and transport codes. The first R2S in the fusion field was introduced in [20] to estimate the responses related to the decay gamma field in ITER. It is described as a coupling of MCNP5.1 [16], as MC transport code, and FISPACT [22], as activation code, following the stages detailed in Figure 1.2. In this R2S, during the neutron transport, the neutron flux spectra are calculated in each cell. Afterward, the activation in these cells is performed with FISPACT producing a decay gamma source (DGS), which is transported to calculate the SDR.

During the development of R2S methodology, several codes have been considered as transport or activation codes in these computational systems. This has resulted in the implementation of MC-based R2S [23]–[25] and S_N -based R2S [26] [27]. As it was discussed in section 1.2.1, the most relevant ones are the MC-based R2S, because they incorporate the most

¹ They are the neutron flux, the activation cross sections and the Decay Gamma Source (DGS)

² Chapter 3 presents a more detailed description of advanced mesh-based MC R2S simulation

³ R2S implementations are computational systems that couple activation and transport code, but hereinafter the R2S implementation will be called codes to simplify the lecture. In the same way, R2S simulation refers to the simulation of the three stages of R2S.

accurate methodology to perform the transport simulations. However, there are still factors that limit the accurateness of these codes, introducing systematic or stochastic uncertainties¹.

Regarding the systematic uncertainties, the most relevant ones are introduced by the spatial and energy discretization, which are considered to couple the transport and activation simulations:

Spatial discretization refers to the finite size where each individual activation simulation is carried out. In the case of the R2S proposed in [20], this discretization is the size of the cells. This method was improved in the so-called mesh-based R2S [23], where the neutron flux is calculated in each element of a mesh superimposed to the geometry. Nowadays, the most advanced R2S² use unstructured meshes [25], or structured meshes with Cell-Under-Voxel (CuV) methodology [24] to define its spatial resolution.

Otherwise, regarding the energy discretization, MC R2S usually requires the neutron flux with fine energy resolution because this affects significantly to the accuracy of the activation step. In addition, MC R2S generally uses energy group-wise to emit the DGS during the photon transport³.

Concerning stochastic uncertainty, the most relevant one is that introduced by the MC method used by the transport codes. This topic was introduced in section 1.2.1, where we argue that this uncertainty can be significant. This is especially relevant in the case of neutron transport because, as was previously commented, achieving good statistical results in extended regions further from the neutron source can be challenging to an MC transport code.

Despite the fact that the MC transport codes can provide the stochastic uncertainty of their responses, the coupling scheme of R2S methodology does not transport the uncertainty of the neutron flux to the SDR [2] [28]. Consequently, the stochastic uncertainty associated with the MC transport radiation⁴ in R2S method is not taken into account in the neutronic analyses. This issue, which is the general topic of this thesis, is discussed in depth in section 1.4.

1.4 The stochastic uncertainty in R2S simulations

The uncertainty of the measure is required to guarantee that, quantities as SDR, are inside of the allowed range. When the SDR uncertainty is unknown, safety factors, which consider the worse possible cases, are applied to ensure that the SDR is kept below a safety level. Options such as additional shielding or remote handling could be considered in order to meet the conditions to operate a nuclear fusion facility. This kind of options increases unnecessarily the

¹ Note that here we are not considering uncertainties due to external input data

² Advanced R2S refers to mesh-based R2S that couples MC transport codes.

³ It is worth noting that these two last discretizations are not intrinsically due to the R2S method, but they are usually considered in most of them.

⁴ MC uncertainty of the photon transport is correctly considered, because it is the last step in R2S

cost of the machine. Otherwise, if the safety conditions cannot be guaranteed, the whole system could be canceled, reducing the scope of the fusion facility.

According to what has been explained in previous sections, MC transport codes, incorporated in the most relevant R2S codes, introduce a stochastic uncertainty due to the calculation method. Despite the fact that the MC codes can provide this uncertainty, the R2S coupling scheme does not allow the neutron flux uncertainty to be transported to the SDR uncertainty. This means that R2S assessments do not supply the uncertainty of the calculation method in the SDR response due to the stochastic uncertainty of the neutron flux [2] [28]. Therefore, the negative effects of the uncertainty are not known.

It is worth highlighting that the uncertainty associated with the MC neutron transport can be relevant due to the features of the neutron transport simulation in R2S¹. Consequently, this problem is considered one of the most relevant issues in R2S methodology. And therefore, important efforts have been dedicated in order to overcome this R2S weakness, developing several methodologies to transport the neutron uncertainty until the SDR response².

The easiest approach considered to estimate the SDR uncertainty due to the MC calculation method was the brute force method³. This method uses the information of a set of R2S clone simulations to estimate the uncertainty. However, it is impractical to estimate the uncertainty in fusion facilities, because each R2S calculation spends a large amount of computational time.

Another approach to estimating the SDR uncertainty in complex R2S simulations was proposed recently. This approach is based on the application of the uncertainty propagation law[29] to the different steps of the R2S simulation. Table 1.2 presents a brief summary of the advantages and weaknesses of the two groups of methodologies, which are briefly described below. The details of these methodologies are presented in Chapter 2.

Table 1.2 Principal advantages and weaknesses of the current methodologies that estimate the MC SDR uncertainty in R2S simulations

	<i>Advantages</i>	<i>Weaknesses</i>
<i>Adjoint based method</i>	<ul style="list-style-type: none"> • Suitable in advanced mesh-based R2S 	<ul style="list-style-type: none"> • Use of external S_N codes • Require SNILB conditions are met
<i>"On fly" method</i>	<ul style="list-style-type: none"> • Do not require extra codes 	<ul style="list-style-type: none"> • Suitable in cell-based R2S • Require SNILB conditions are met

¹ Section 1.2.1 explains these circumstances, while ANNEX A presents a realistic example of a neutron transport simulation in R2S, including the presentation of the neutron flux uncertainty.

² Chapter 2 provides a more detailed state of art of these methodologies

³ This method is also known as the Total Monte Carlo (TMC).

The methodologies based on Multi-Group Consistent Adjoint-Driven Importance Sampling (MS-CADIS) method [30] [31] requires the estimation of the adjoint of the SDR. The estimation of the adjoint, using CADIS methodologies, requires S_N transport codes. Consequently, MC R2S must couple a new code to estimate the uncertainty. In order to improve this weakness, G. Young et al [32] propose an “on-fly” methodology to perform an accurate estimation of the MC uncertainty in R2S calculations using only MC codes¹. However, the methodology is based on cell-based MCNP[16] capabilities. Consequently, it is not suitable for mesh-based R2S where better spatial discretization of the neutron flux is more easily achieved.

In any case, the most important disadvantage of both methods is that they require that SNILB conditions are met in order to transport the uncertainty during the activation step. These assumptions are not inherited from R2S methodology; hence, the estimation of the SDR stochastic uncertainty is more limited than the calculation method. That is, there are practical cases where the SDR uncertainty of the R2S simulation is miscalculated using these existent methods. It is important to highlight again that R2S method is more relevant when SNILB conditions are not met since D1S methods, which are faster and more accurate, cannot be applied. These conditions are expected in the future fusion facilities in the roadmap to commercial plants (see Table 1.1). In fact, these conditions are not met in some specific applications on current fusion facilities in the design phase. For example, the first wall of DEMO already shows applications where these conditions are not met [21].

1.5 Motivation and scope of the thesis

As this chapter explained previously, the estimation of the SDR is vital to the licensing and design of the fusion facilities. Nowadays, this is principally calculated using D1S or R2S computational methodologies based on MC codes.

It is worth highlighting that MC transport codes coupled in D1S or R2S introduce a stochastic uncertainty, which can be estimated. According to the previous chapters, this is one of the most relevant uncertainties in the SDR response due to the calculation method of advanced R2S.

Despite the fact that the MC method allows estimating this uncertainty, the coupling scheme of the R2S codes does usually not propagate the uncertainty of the first MC simulation (neutron transport) to the SDR response. This means that R2S codes do not provide the uncertainty associated with the MC calculation method, which has an important effect on the design of the fusion facility. For this reason, during the last decade, several schemes have been proposed to overcome this issue.

The review of the existing methodologies shows that the current approaches require that SNILB conditions are met to estimate correctly the SDR uncertainty. But precisely when these

¹ It is worth noting that MC methodology is considered more accurate than S_N methodology

conditions are met, the R2S applicability is reduced, because D1S¹ method can be applied. This means that no method can estimate the SDR uncertainty simulated by an R2S code in applications where R2S method is relevant.

In this frame, this thesis aims to develop a methodology that allows estimating the SDR uncertainty due to the stochastic uncertainty from the MC calculation method in R2S. In addition, the methodology proposed in this thesis must achieve the following milestones:

- i. The methodology must be suitable to advance mesh-based R2S like R2S-UNED
- ii. The methodology must not have extra limitations than those inherited from R2S method
- iii. The computational requirements to perform the estimation of the SDR stochastic uncertainty² must be affordable for those cases where R2S-UNED can be applied. Although it requires the use of current supercomputers such as MARCONI[33].

1.6 Outline of the thesis

The last section of this chapter is dedicated to describing the structure followed in this thesis and the chapter's fragmentation.

First of all, Chapter 2 is devoted to presenting the overview of the current methodologies that have been developed to calculate the SDR uncertainty in R2S. That is the current state of the topic on which this thesis is focused.

Afterwards, two chapters are dedicated to describing the methodology implemented in this work: Chapter 3 presents the basis of an MC R2S simulation, focusing on the key points to develop the methodology to transport the neutron uncertainty in R2S. This chapter can be considered an annex if the reader is familiar with R2S. Otherwise, Chapter 4 presents the methodology to transport the neutron uncertainty from a theoretical point of view³.

Chapter 5 describes the implementation of this methodology in R2S-UNED. This chapter also includes the description of the algorithms that have been developed to estimate those inputs required to evaluate the SDR uncertainty due to the MC neutron uncertainty. While Chapter 6 deals with the verification of these algorithms or computational capabilities implemented in R2S-UNED.

Chapter 7 presents the application of the uncertainty module to the ITER benchmark and to the estimation of the air-kerma in the octant 2 of JET. The application of the developed tool

¹ D1S is faster and more accurate than R2S

² Hereinafter the stochastic uncertainty is understood as the stochastic uncertainty due to the MC calculation method applied in R2S

³ Chapter 4 presents the equations that must be evaluated to estimate the SDR uncertainty due to the neutron flux uncertainty in R2S calculations.

required establishing a guideline to apply the methodology. Primarily, this guideline tries to overcome the difficulties related to the estimation of the neutron flux covariance matrix¹, which limits the application range of this methodology. In addition, this chapter also presents the result of the tool application, which allows studying some features of the correlation matrix of the neutron flux.

After that, Chapter 8 presents the summary and conclusions of the thesis. And finally, Chapter 9 describes the ongoing and future work.

¹ The neutron flux covariance matrix is the quantity that represents the neutron flux uncertainty[29]

Chapter 2.

Review of the methodologies to assess the stochastic uncertainty in R2S simulations

This chapter supplies a summary of the state of art of the currently implemented methodologies that can calculate the SDR stochastic uncertainty due to the MC calculation method in R2S simulations. These methodologies can be classified into two different branches:

The first one, described in section 2.1, is the brute force method¹. This method, based on the direct application of MC techniques, is a simple one and consumes a lot of computational resources. Therefore, it does not apply to R2S simulations of fusion facilities due to it requires too much large computational time.

On the other hand, we can find the newest methodologies, which have been proposed to assess the SDR uncertainty, evaluate analytical expressions of this uncertainty. These methodologies, based on the uncertainty propagation law [29], are explained in sections 2.2 and 2.3. These methodologies are suitable only to estimate the stochastic uncertainty of individual tallies, due to the amount of data that must be managed. It is worth noting that the methodology proposed in this thesis belongs to this class.

One of their weak points is that they require the correlation matrix of the neutron flux as input data. But this matrix cannot be calculated in most of the R2S applications in fusion facilities due to its size; therefore, their application range is limited. Nowadays, most of these methods directly assume conservative approximations of this matrix in order to estimate conservative values of SDR uncertainties. However, important efforts are being currently made in order to develop computational methodologies that enable the estimation of this matrix [31], therefore increasing the applicability of all these methods.

Finally, section 2.4 presents a summary and conclusions of the ideas of this chapter.

¹ The brute force method is also called Total Monte Carlo (TMC) method

2.1 Brute force method

This technique consists in simulating a set of clone cases of the complete problem¹, where each clone case is simulated using a different set of random numbers in the MC simulations. The uncertainty of the variable is directly obtained from the set of results, applying the numerical estimator of the standard deviation in the sample of results.

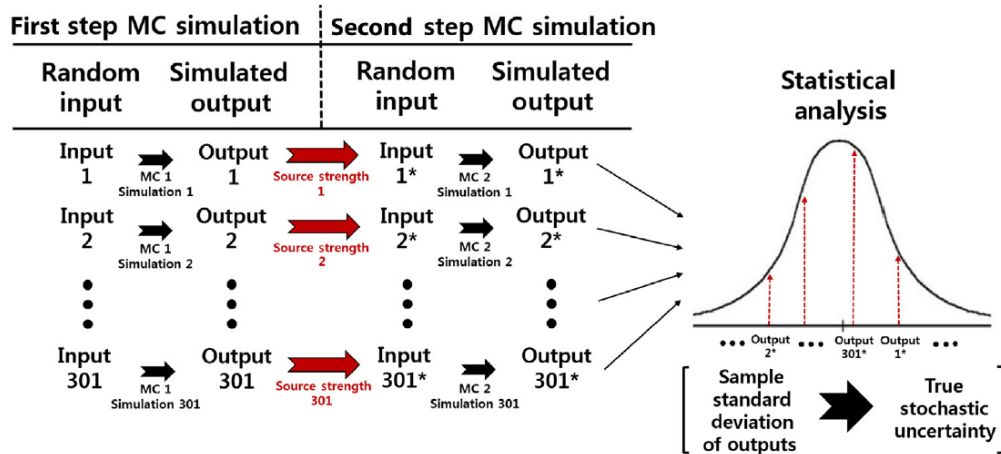


Figure 2.1 Schematic representation of the brute force method for 2MC step simulation [32]

Figure 2.1 shows the scheme of application of the brute force method to estimate the stochastic uncertainty of 2 steps MC simulation like in the case of R2S. This scheme is easily implemented and very accurate, but it spends a large computational time since many clone cases are often needed to obtain an accurate estimation of the uncertainty.

In the particular case of the R2S simulations applied in SDR analysis of fusion facilities, each R2S simulation spends a huge amount of computational time. This means that it is not possible simulating a high number of clone cases. Consequently, this method is not suitable to calculate the uncertainty of the R2S simulations of fusion facilities.

On the contrary, this method can be applied to cases that require low computational time. This is the case of the exercises designed to validate the scheme implemented in this thesis. Therefore, brute force is applied in Chapter 6 and in ANNEX E to validate the method developed in this thesis to calculate the SDR uncertainty in R2S simulations.

¹ In the case of R2S simulation, the complete problem includes the three stages: neutron transport (MC1), activation, and photon transport (MC2)

2.2 Adjoint based Methods

The uncertainty of the SDR estimated with R2S can be expressed according to the uncertainty of each MC simulation, as shown in Equation 2.1. Note that all R2S codes calculate the photon contribution to the uncertainty.

$$\sigma_{SDR}^2 \approx \sigma_{SDR,neutron}^2 + \sigma_{SDR,photon}^2$$

Equation 2.1

The adjoint based method expresses the SDR as a function of the neutron flux and its adjoint, in one (explicit) or two (implicit) steps. Both implicit and explicit methods use Multi-Step Consistent Adjoint Driven Importance Sampling¹ (MS-CADIS [34]) methodology to estimate the adjoint of the neutron flux. This methodology needs the SNILB conditions to be met during the activation step [35].

2.2.1 Explicit adjoint-based method

The explicit implementation, which is presented in [30], expresses the SDR according to Equation 2.2, where $R_{n,i}^e$ is the adjoint of the neutron flux to the SDR².

$$SDR = \sum_{i,e} \phi_i^e R_{n,i}^e$$

Equation 2.2

The neutron flux adjoint is obtained by MS-CADIS method implemented inside of the SCALE [36] package of codes. Using the adjoint of the neutron flux evaluating Equation 2.3.

$$\sigma_{SDR,neutron}^2 = \sum_{i,e} \sum_{i',e'} \left(\frac{\partial SDR}{\partial \phi_i^e} \right) \left(\frac{\partial SDR}{\partial \phi_{i'}^{e'}} \right) cov(\phi_i^e, \phi_{i'}^{e'})$$

Equation 2.3

It is worth noting that the current implementation of this method does not enable the real correlation matrix of the neutron flux to be considered. Instead of this, only superior or inferior limits of the SDR uncertainty can be calculated assuming that the case is completely correlated ($cor(\phi_i^e, \phi_{i'}^{e'}) = 1$) or anticorrelated ($cor(\phi_i^e, \phi_{i'}^{e'}) = -1$).

¹ MS-CADIS is a methodology which calculates the adjoint of the SDR to estimate VR techniques to MC transport codes. However, in this case, MS-CADIS are understood as the calculation method of the adjoint of the SDR.

² Note that the adjoint operator can be also interpreted as the contribution of the “source” per source unit. In this case, the contribution of the neutron flux per unit of neutron flux; that is, the response of one neutron.

2.2.2 Implicit adjoint-based method

The implicit method, implemented in [31], calculates the SDR uncertainty in two steps. The first of them consists in calculating the DGS intensity uncertainty. In order to do that, the uncertainty propagation is applied to Equation 2.4.

$$I_i^g = \sum_e T_{i,e}^g \phi_i^e$$

Equation 2.4

where the coefficient $T_{i,e}^g$ (neutron flux adjoint of the DGS intensity I_i^g) is calculated using the implementation Group-wise Transmutation Consistent Adjoint Driven Importance Sampling¹ (GT-CADIS [35]), where g refers to the energy of the photon. Afterward, the law of uncertainty propagation is applied, enabling the calculation of the DGS uncertainty as shown in Equation 2.5.

$$cov(I_i^g, I_{i'}^{g'}) = \sum_{i,e} \sum_{i',e'} T_{i,e}^g T_{i',e'}^{g'} cov(\phi_i^e, \phi_{i'}^{e'})$$

Equation 2.5

Finally, this uncertainty is propagated to the SDR considering the equation of the DGS intensity adjoint and the law of uncertainty propagation. Both equations are presented in Equation 2.6.

$$SDR = \sum_{i,g} R_{p,i}^g I_i^g \rightarrow \sigma_{SDR,neutron}^2 = \sum_{i,g} \sum_{i',g'} R_{p,i}^g R_{p,i'}^{g'} cov(I_i^g, I_{i'}^{g'})$$

Equation 2.6

where $R_{p,i}^g$ is the DGS intensity adjoint² (I_i^g).

The estimation of the adjoint R_i^g is not explicitly performed; instead, the DGS is emitted modifying³ properly the photon weight. This way the result of the photon transport simulation is directly the uncertainty of the SDR.

¹ GT-CADIS is a specific implementation of MS-CADIS, which uses group-wise activation cross section (like most of R2S codes).

² For the thesis, the adjoint of the DGS intensity is called the photon response function. In addition, the subindex p is omitted $R_i^g = R_{p,i}^g$

³ The MC photon transport directly evaluates Equation 2.6, consequently the adjoint R_i^g is implicitly evaluated. It is worth to highlight that the implemented methodology does not consider the correlation between the DGS intensity. This means that $cov(I_i^g, I_{i'}^{g'}) = 0$ when $i \neq i'$ or $g \neq g'$.

2.3 On-Fly method

In this methodology, presented in [32], the DGS and its uncertainty is directly obtained from the first MC simulation. For that, it is assumed that the DGS is proportional to the neutron flux. Consequently, this method is limited to cases where SNILB conditions are met.

Under these conditions, the SDR uncertainty is calculated according to Equation 2.7. Where the photon response, as well as its uncertainty, are calculated "On-Fly" during the MC photon simulation.

$$SDR = \sum_{i,g} R_i^g I_i^g \rightarrow \sigma_{SDR}^2 \approx \sum_{i,g} \sum_{i',g'} I_i^g I_{i'}^{g'} cov(R_i^g, R_{i'}^{g'}) + R_i^g R_{i'}^{g'} cov(I_i^g, I_{i'}^{g'})$$

Equation 2.7

It is worth noting that this methodology was implemented using cell-based features of R2S. Then, it is not compatible with advanced mesh-based R2S.

2.4 Summary and Conclusions

Currently, the R2S methodologies applied in SDR analysis of the fusion facilities are the MC mesh-based R2S. These R2S couples MC transport codes to calculate the spatial distribution of the neutron field or the decay gamma field. Consequently, the responses estimated by these MC R2S codes have associated an uncertainty due to the stochastic nature of the MC calculation method.

The R2S coupling scheme does not consider the uncertainty of each simulation step. This means that the stochastic uncertainty associated with the neutron flux transport (first MC simulation) is not transported to the SDR uncertainty in R2S simulations. Nowadays, this is one of the most relevant concerns regarding the MC R2S methodology; for this reason, during the last years, several methodologies have been proposed to assess the stochastic uncertainty of the MC R2S simulation. This chapter presents a brief review of the literature of these methodologies in order to contextualize the advances of this thesis:

The most advanced methodologies evaluate analytical expressions of the SDR uncertainty. One common weakness of these methodologies is that they require that SNILB¹ conditions are met during the activation step. Although these conditions are met in many practical cases, the restriction imposed by these conditions to estimate the SDR stochastic uncertainty of the R2S simulation is not inherited from the R2S methodology. In fact, it is important to highlight again

¹ SNILB conditions are explained in section 3.4.2

that R2S method is more relevant when SNILB¹ conditions are not met since D1S² methods, which are faster and more accurate, cannot be applied. These conditions are expected in the future fusion facilities in the roadmap to commercial plants.

The principal topic of this thesis is the development of a methodology that overcomes this difficulty. This topic will be developed in the next chapters according to the outline presented in section 1.6. In particular, the motivation and scope of this thesis are deeply presented in section 1.5.

¹ It is worth underlining that the relevance of these conditions refers at cooling times where the SDR analysis is performed. This depends on the planning of the different fusion facilities.

² D1S is a more accurate and faster methodology than R2S to estimate the SDR that can be applied only if SNILB conditions are met.

Chapter 3.

Transport and activation steps in R2S

This chapter presents the background¹ required to develop the scheme to propagate the neutron flux uncertainty to the SDR in the R2S method. This background deals with three points.

The first one is a detailed description of the advanced mesh-based R2S computational systems, focusing on the equations that describe the different steps of the simulation. These equations are broken down into five calculation steps that are presented in Figure 3.1.

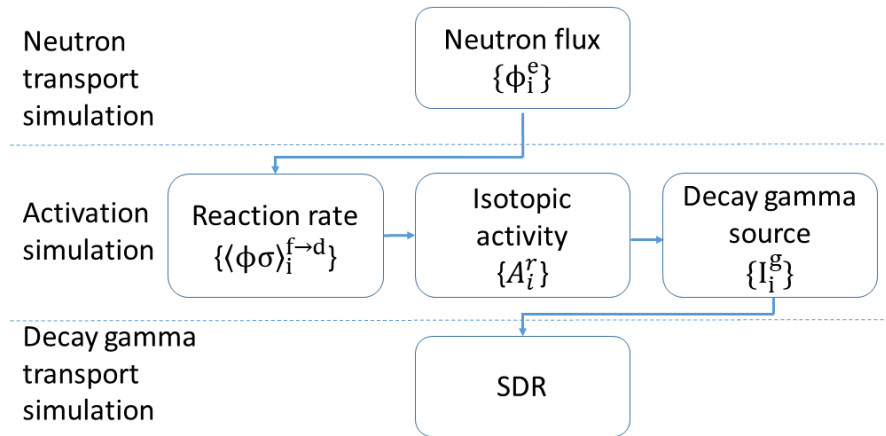


Figure 3.1 Relevant quantities calculated during R2S simulation

Where:

- ϕ_i^e is the spatial distribution (i index) of the neutron flux spectra (e index)
- $\langle \sigma \phi \rangle_i^{f-d}$ is the reaction rate per target isotope², where f is the (target) father isotope and d is the (produced) daughter isotope.
- A_i^r is the activity of radioisotope r , which is relevant to the SDR.
- I_i^g is the number of gammas emitted³ with energy g and in position i .
- SDR is the shutdown dose rate response at a specific point⁴, which is considered during this thesis as the desired response of the R2S simulation.

¹ If the reader is familiar with R2S method, he can skip this chapter

² Hereinafter the reaction rate per target isotope are called reaction rates.

³ Hereinafter the quantity I_i^g is also called DGS intensity

⁴ Actually, the point-like SDR tallies in MC R2S are a mean of the SDR in a small surface or volume

These quantities, shown in Figure 3.1, are presented in three sections, corresponding to each simulation step of R2S-UNED [24].

- i. Neutron transport: the neutron flux is presented in section 3.1*
- ii. Activation: The equations which describe the activation process are described in section 3.2.*
- iii. Photon transport: The SDR is expressed as a function of the DGS intensity in section 3.3*

Concerning the second point of the background, this chapter presents the methods, used in this thesis, to solve the activation step in section 3.4. It is worth noting that they are widely used in several steps during the thesis.

Regarding the last point, section 3.5 presents the derivative of the isotopic activity to the reaction rates¹. According to the proposed methodology to estimate the stochastic uncertainty of the SDR, presented in Chapter 4, these derivatives are required to transport the stochastic uncertainty during the activation step.

Finally, section 3.6 summarizes the content of this chapter.

¹ $\frac{\partial A_i^r}{\partial \langle \sigma \phi \rangle_i^{f-d}}$ During this thesis, they are also called sensitivity coefficients

3.1 Spatial distribution of the neutron flux

The first step of the R2S methodology consists in estimating the spatial distribution of the neutron flux spectra. According to Chapter 1, MC R2S methods discretize both, spatial and energy dimensions of the neutron flux. This means that the neutron flux supplied by MC transport codes is a mean value of the neutron flux inside of the region, and with energy inside of the energy group. This section describes briefly the neutron flux calculated by R2S-UNED [24].

R2S-UNED uses cartesian or cylindrical superimposed structured meshes to perform spatial discretization. The MC transport codes calculate the average of the neutron flux inside of each mesh element¹.

The spectrum of the neutron flux in each mesh element is calculated discretizing the energy. That is, the transport code calculates the average neutron flux in each energy range (bin) used to discretize the energy.

Hereinafter, we refer to the distribution of the neutron flux spectra (set of average neutron flux calculated in each mesh element and inside of the energy range) obtained from the transport code as "neutron flux. These codes calculated the neutron flux ϕ_i^e already integrated into the energy range. Therefore, the units of the neutron flux are $n \cdot cm^{-2} \cdot s^{-1}$.

It is worth highlighting that the transport code of R2S-UNED² calculates the stochastic uncertainty associated to each ϕ_i^e variable. However, they do not calculate the complete uncertainty of the neutron flux, which is the correlation matrix³ of the neutron flux. This capability, described in section 5.1, was introduced in the transport code of R2S-UNED during this thesis.

3.2 Activation step in R2S-UNED

The second computational step in the R2S methodology is the material activation of the facility components. This step calculates the temporal evolution of the isotopic inventory in order to estimate the DGS intensity in each region (defined as a mesh element) at the interest cooling time. Section 3.2.1 presents the first order, linear, Ordinary Differential Equations (ODE) system which describes the material activation.

Otherwise, R2S system requires the discretization of these equations in order to couple the different inputs and outputs of the activation step with the MC transport code. The discretization

¹ R2S-UNED has the Cell-under-Voxel[24] [100] (CuV) capability which improves the spatial resolution. For the purposes of Chapter 3 and Chapter 4, CuV can be considered as a finer mesh.

² The transport code of R2S-UNED is MCNP-R2S, which is a MCNP5 modification. In addition to the R2S required, these modifications includes improvements such as memory optimization[93] among others.

³ The correlation matrix describes the dispersion of the distribution of the quantities, which is usually understood as the uncertainty of these quantities [29] [52]

of these equations is presented in section 3.2.2, according to the R2S-UNED workflow. It is worth mentioning that the resolution of the ODEs system is not presented in this section. This topic will be described in section 3.4.

Before these sections, it is important to introduce the following concepts related to the activation system:

- i. Pathway or chain: Set of isotopes that are connected by reaction or decay paths
- ii. Loop: a subset of isotopes, reactions, and decay paths that connect an isotope with itself
- iii. Linear chain: a pathway that does not contain loops

3.2.1 Mathematical description of the activation step

This section presents the estimation of the DGS intensity during the activation step, following the steps presented in Figure 3.1. That is, calculating the reaction rates, the isotopic activity, and the DGS intensity in consecutive steps.

First, Equation 3.1 defines the reaction rates (first step of the activation stage in Figure 3.1) as a function of two quantities. The first one is the neutron flux density by energy unit ($\varphi_i(E)$). The second one is the pointwise cross section ($\sigma_d^f(E)$) of all the reactions that connects the isotope f with the isotope d.

$$\langle \phi \sigma \rangle_i^{f-d} = \int_E \varphi_i(E) \cdot \sigma_d^f(E) dE$$

Equation 3.1

Afterwards, the temporal evolution of the isotopic inventory is solved, considering the production and burn up of the isotopes by neutron interaction as well as by the disintegration of themselves. Equation 3.2 describes this temporal evolution in region i, as a first order linear Ordinary Differential Equation (ODE) system

$$\frac{dN_i^k(t)}{dt} = \sum_f (\langle \phi \sigma \rangle_i^{f-k} - b_f^k \lambda_f) N_i^f(t) - N_i^k(t) \left(\lambda_k + \sum_d \langle \phi \sigma \rangle_i^{k-d} \right)$$

Equation 3.2

where λ_f is the decay constant of the isotope f and b_f^k is the branching ratio¹ of isotopes that decay from isotope f to the isotope k. The solution of this activation ODE, presented in Equation 3.2, is the concentration of the isotope k at any time t ($N_i^k(t)$), which is expressed in Equation 3.3 as a matrix system.

¹ Hereinafter the branching ratio will be included in the index of the decay constant as $b_f^k \lambda_f = \lambda_f^k$.

$$\frac{dN_i(t)}{dt} = AN_i(t) \Rightarrow N_i(t) = \exp(At) N_i(0)$$

Equation 3.3

where A is a matrix containing the production and disintegration rates of the isotopes, and $N_i(t)$ is the vector containing the concentration of all k isotopes in the region i $N_i^k(t)$. From this quantity, the isotopic activity, which is the second step of the activation stage in Figure 3.1, is estimated by multiplying by the decay constant.

Finally, the DGS intensity is calculated as shown in Equation 3.4.

$$I_i(E_g, t) = \sum_r y_r(E_g) \cdot \lambda_r \cdot N_i^r(t) = \sum_r y_r(E_g) \cdot A_i^r(t)$$

Equation 3.4

where $y_r(E_g)$ is the number of gammas of energy E_g emitted by each isotope disintegration¹. It is worth underlining that the equations of this section were expressed using general energy-dependent functions. The next section introduces the energy discretization which R2S-UNED considers.

3.2.2 Discrete activation equations applied in R2S-UNED

Equation 3.2 describes a first order, linear, ODEs system that depends on the reaction rates presented in Equation 3.1.

The MC transport codes can calculate the reaction rates with point-wise energy resolution, as Equation 3.1. These reaction rates can be read by the activation codes and used to solve the material activation. However, the number of reaction rates that must be calculated to consider all possible paths in the activation case is huge (there are over 33.000 reactions in the EAF library). Consequently, the memory consumption of the simulation avoids performing the MC neutron transport.

A different option to estimate the reaction rates, considered by most of R2S codes², consists in calculating the reaction rate using group-wise cross-sections as shown in Equation 3.5, where σ_e^{f-d} is the group-wise cross section of the neutron reaction from the isotope f to the isotope d³.

¹ The index k (generic isotope) is changed by the index r (relevant radioisotope, subset of the generic isotopes which emits gamma radiation).

² Including R2S-UNED

³ σ_e^{f-d} is the mean of the point-wise cross section in the energy bin e assuming a determinate function to weight the cross section.

$$\langle \phi \sigma \rangle_i^{f-d} = \int_E \varphi_i(E) \cdot \sigma_d^f(E) dE \approx \sum_e \phi_i^e \sigma_e^{f-d}$$

Equation 3.5

This energy discretization of the neutron flux and cross-sections enables all possible activation paths to be considered, although this calculation method is less accurate than using a point-wise cross-section.

Therefore, R2S-UNED solves Equation 3.2 using the reaction rates calculated according to Equation 3.5. In fact, the activation module of R2S-UNED (ACAB) directly supplies the DGS intensity builds as shown in Equation 3.6.

$$I_i^g = \sum_r y_r^g \cdot \lambda_r \cdot N_i^r(t)$$

Equation 3.6

where $y_r^{g,1}$ is the number of gammas emitted by the isotope r whose energy is inside of the energy group g . Consequently, the DGS is defined (and emitted during the photon transport) using energy groups. This approach is found in most of the R2S implementations (as R2S-UNED) because it saves memory describing the DGS [37], in comparison with a DGS described using energy line resolution².

3.3 Photon transport to estimate the SDR

The last step in the common R2S scheme (Figure 3.1) is the transport of the DGS to calculate the SDR. Since the SDR is proportional to the number of photons emitted, the SDR can be expressed as shown in Equation 3.7:

$$SDR(x, y, z) = \sum_i \sum_g I_i^g R_i^g(x, y, z)$$

Equation 3.7

Where the variable R_i^g is the response on the SDR of a photon emitted from position i and energy E , where E is inside of the range of the energy bin g . Hereinafter this quantity is called photon response. The variables x, y, z refer to the point where the SDR is estimated. They remark that the SDR is the estimation in an individual tally.

¹ Actually, ACAB modifies the value y_r^g in order to keep the energy emitted by the isotopes in the group g instead of the number of emitted photons.

² Chapter 4 of this thesis describes the uncertainty propagation considering group-wise energy discretization in both steps (estimation of the reaction rates and DGS emission). However, R2S may be implemented without this energy discretization. The methodology can be easily adapted to this kind of R2S.

Once the mesh¹ where the DGS is calculated, is defined, the photon response is independent of the DGS definition. It only depends on the system configuration during the photon transport (geometry, material composition, etc).

Common R2S implementations do not calculate the photon response since the SDR estimation does not require storing these values. However, they are needed to estimate the SDR uncertainty following the scheme proposed in Chapter 4. Therefore, R2S-UNED was modified to evaluate the contribution to the SDR of all photons emitted from each specific (i,g) Phase Space (PS). From now on, this quantity will be called DGS contribution (t_i^g). The DGS contribution depends on the DGS definition and the system configuration. It is related to the photon response according to Equation 3.8.

$$t_i^g = \frac{R_i^g}{p_i^g}; \quad p_i^g = \frac{I_i^g}{I_T}$$

Equation 3.8

where p_i^g is the probability that the photon was emitted from the position i and energy bin g, and I_T is the total number of photons emitted by the whole DGS.

Although the photon response function is defined over the whole geometry and for all photon energies, the methodology implemented in R2S can only evaluate it on the DGS source PS points where source intensity is not zero. This is not a limitation for the uncertainty evaluation since the methodology only requires the DGS contribution from the regions where the intensity is not zero.

The implementation in R2S-UNED of the calculation of the DGS contribution is briefly described in Chapter 5. It is worth noting that the t_i^g variables are calculated "on-fly" during the MC photon transport; therefore, the uncertainty of this MC transport is associated to these variables. The uncertainty propagation from these variables to the SDR coincides with the SDR uncertainty due to the MC stochastic uncertainty of the photon transport calculation.

3.4 Solving the temporal evolution of the isotopic inventory ODEs system

The first order, linear ODEs system, which represents the activation (see section 3.2), is stiff and sparse [38]; consequently, its resolution can be challenging. For that reason, many numerical solvers were developed to estimate the isotopic inventory of activated materials [22] [39]–[41]. During this thesis, we focused on ACAB [41], which is presented in section 3.4.1. It is worth highlighting that ACAB subroutines are widely used during the thesis.

¹ The spatial and energy discretization

An alternative option to deal with the ODEs system is to simplify the equations. In this regard, SNILB conditions are of especial interest since they are often met in most fusion facilities [42]–[45] and enable the simplification of the ODEs system¹. The assumptions performed when SNILB conditions are met, and the equations that solve the activation step, are presented in section 3.4.2.

3.4.1 ACAB code and solver algorithm

ACAB[41] is the inventory code, used in the UNED, to simulate the inventory temporal evolution of irradiated materials in fusion facilities. In this framework, ACAB has been validated in calculation benchmarks such as the International Atomic Energy Agency (IAEA) Second International Activation Calculation Benchmark Comparison Study [46], where it was considered “suitable and satisfactory” for detailed fusion calculations; and in experimental benchmarks, such as [46] [47].

The ACAB algorithm is based on that of the ORIGEN [48] code. This algorithm consists in solving an ODEs system with constant coefficients for each time step².

In ACAB (and ORIGEN), the ODEs system with constant coefficient is solved in three sequential steps as follows:

- i. The isotopes are classified as long or short according to the rate with which the isotope disappears (diagonal term of the matrix). Afterward, the contribution of short-live isotopes to short or long-live is solved by evaluating the Bateman equations [49].
- ii. The code solves the contribution from long-live isotopes to long-live isotopes by applying the exponential matrix method. The total contribution from short-live to long-live isotopes is properly distributed between the long-live isotopes.
- iii. The algorithm calculates the contribution from long-live isotopes to short-live isotopes considering the last ones in secular equilibrium.

These three steps are carried out in dedicated subroutines in the ACAB code. In this thesis, these subroutines were extracted from ACAB and employed in different parts of the developed programs³.

3.4.2 Single Neutron Interaction and Low Burn-Up (SNILB) conditions

If only single neutron interaction and low burnup conditions are considered, the pathways can be expressed as linear chains according to the ODE Equation 3.9.

¹ The resulting ODEs system is practically uncoupled.

² Note the irradiation scenario introduce temporal dependence in the reaction rates.

³ Hereinafter ACAB solver is understood as the use of these three subroutines, which were originally implemented in ORIGEN[48].

$$\frac{dN^r(t)}{dt} = (\langle\sigma\phi\rangle^{1\rightarrow 2}\delta_r^2 + \lambda_{r-1}^r)N^{r-1}(t) - \lambda_r N^r(t)$$

Equation 3.9

The only single neutron interaction means that only the reaction $\langle\sigma\phi\rangle^{1\rightarrow 2}$ is relevant to the pathway, while the low burnup condition implies that the concentration of the isotope 1 is practically constant ($e^{-\langle\sigma\phi\rangle^{1\rightarrow 2}t_{irr}} \approx 1$).

The solution of this equation is called the Bateman equation [49]. This solution is presented in Equation 3.10.

$$N^r(t) = N^r \cdot e^{-d_r t} + \sum_{k=1}^{r-1} N_k(0) \cdot \left(\prod_{n=k}^{r-1} \frac{a_{n,n-1}}{d_n} \right) \cdot \left(\sum_{j=k}^{r-1} \left(d_j \cdot \frac{e^{-d_j t} - e^{-d_r t}}{d_r - d_j} \cdot \prod_{\substack{n=k \\ n \neq j}}^{r-1} \left(\frac{d_n}{d_n - d_j} \right) \right) \right)$$

Equation 3.10

Where d_i is the i^{th} diagonal value of the matrix A (Equation 3.3), and $a_{n,n-1}$ is the no-diagonal value of the row n .

The reaction rate only appears in the equation when $k=1$, since the neutron collisions with the stable isotope. In addition, the low burning condition means that the reaction rate is small. Consequently, Equation 3.10 is linear with the reaction rate when the SNILB conditions are met.

Commonly, the most relevant isotopes to the study of the SDR in the current fusion facilities are produced by one-step pathways. In addition, another important feature of the activation step is that the intensity of the neutron fluxes varies according to the irradiation scenario. In order to take it into account, the irradiation scenario is discretized in time steps where the neutron power is constant. Afterwards, the ODEs system is solved time step by time step, exactly as ACAB does.

Considering these conditions, the evolution of the concentration of the isotope 2 during the irradiation pulse τ can be expressed with Equation 3.11.

$$N_2(t_\tau) = N_2(t_{\tau-1}) \cdot e^{-\lambda_2(t_\tau - t_{\tau-1})} + N_1 \langle\sigma\phi\rangle^{1\rightarrow 2} P(\tau) \frac{(1 - e^{-\lambda_2(t_\tau - t_{\tau-1})})}{\lambda_2}$$

Equation 3.11

where $\langle\sigma\phi\rangle^{1\rightarrow 2}$ is the reaction rate during the first pulse, and $P(\tau)$ is the relative increment of the neutron source intensity during the pulse τ . If the whole irradiation scenario is taken into account, the concentration can be expressed as in Equation 3.12.

$$N_2(t) = N_2(0) \cdot e^{-\lambda_2 t} + N_1 \langle\sigma\phi\rangle^{1\rightarrow 2} \frac{\alpha(t)}{\lambda_2}$$

Equation 3.12

3.5 Derivative of the isotopic concentration to the reaction rates

This section presents the derivative of the isotopic concentration to the reaction rates. They are also called sensitivity coefficients of the isotopic concentration to the reaction rates per target isotope. But hereinafter, they will be referred to as sensitivity coefficients since there are no more explicit derivatives in the equations used in this thesis.

The estimation of the sensitivity coefficients is a required step for the estimation of the SDR uncertainty. Although some activation codes include the capability to calculate them, this is not the case for ACAB¹; therefore, this capability was implemented in ACAB during the thesis.

The bibliography [50]–[53] contains several useful approaches to calculate the sensitivity coefficients. In this thesis, they are calculated using a direct method [53]. That is, solving the ODEs system that describes the temporal evolution of the sensitivity coefficients. This ODEs system, which can be obtained performing the appropriate derivative to Equation 3.2, is expressed in Equation 3.13.

$$\frac{d}{dt} \frac{\partial N_i(t)}{\partial \langle \phi \sigma \rangle^{f \rightarrow d}} = \sum_j (\langle \phi \sigma \rangle^{j \rightarrow i} + \lambda_j^i) \frac{\partial N_j}{\partial \langle \phi \sigma \rangle^{f \rightarrow d}} - \left(\lambda_i + \sum_k \langle \phi \sigma \rangle^{i \rightarrow k} \right) \frac{\partial N_i}{\partial \langle \phi \sigma \rangle^{f \rightarrow d}} + \sum_j \delta_j^f \delta_i^d N_j - \sum_k \delta_i^f \delta_k^d N_i$$

Equation 3.13

The ODEs system of the sensitivity coefficients and isotopic concentration is also stiff and sparse due to the similarity to the activation system. Consequently, the same solvers used to calculate the activation may be also applied to estimate the sensitivity coefficients; in our case, using ACAB subroutines as explained in section 5.5.

In addition, when the SNILB conditions are considered, Equation 3.13 can be also simplified. The sensitivity coefficient of the second isotope is expressed as shown in Equation 3.14. This solution was also implemented as seen in section 5.5.

$$\frac{\partial N_2}{\partial \langle \sigma \phi \rangle^{1 \rightarrow 2}} = N_1 \frac{\alpha(t)}{\lambda_2}$$

Equation 3.14

¹ Activation module of R2S-UNED

3.6 Summary and Conclusions

This section presents the background required to derive and implement the equations to estimate the SDR uncertainty in MC R2S simulations, which will be depicted in Chapter 4.

This background includes three topics: Firstly, a detailed description of the MC mesh-based R2S method. Secondly, the methods used to solve the activation step. And thirdly, the definition of the sensitivity coefficients.

Regarding the activation step of the R2S method, it is presented using two procedures. Both of them were considered during the implementation of the algorithm in Chapter 5.

- I. The ODEs activation system is presented without the assumption of any hypothesis in the ODEs activation system. This option describes the activation ODEs system just like R2S method deals with it.
- II. The ODEs activation system is presented assuming that SINLB conditions are met. This hypothesis simplifies the ODEs system, and consequently, the different activation simulations are speed up.

Consequently, for each type (I or II) of ODEs system, a specific solver was developed:

- I. The first one is a general-purpose solver, based on the isolated subroutines used by ACAB and ORIGEN, to deal with the same type of ODEs systems. This solver is called ACAB solver during the following chapters.
- II. The second one is a specific solver valid only when SNILB conditions are met. This solver is faster than the general-purpose solver.

Chapter 4.

Analytical expressions to assess the stochastic uncertainty in R2S simulations

This chapter presents the equations that allow propagating¹ the stochastic uncertainty of the MC calculation method used in R2S-UNED until the SDR response. Principally, the propagation process consists in to apply the uncertainty propagation law, presented in section 5.1, to the equations that describe the R2S simulation (presented in Chapter 3). The propagation process is divided into three stages:

- i. The neutron flux uncertainty is transported to the DGS intensity. This stage, which is described in section 4.2, considers only the stochastic uncertainty from the neutron transport simulation.*
- ii. The uncertainty of the DGS contribution is transported to the photon response. This stage, which is described in section 4.3, considers only the stochastic uncertainty from the photon transport simulation.*
- iii. The uncertainties of the DGS intensity and photon response are combined to estimate the stochastic uncertainty of the SDR due to both MC simulations performed in the R2S calculation. This stage is explained in section 4.4.*

Finally, section 4.5 presents the summary and conclusions of this chapter.

¹ It is worth underlining that the uncertainty to be propagated is assumed known in this chapter

4.1 Uncertainty propagation law

The uncertainty propagation law [29] enables the covariance¹ of a set of functions² $\{y_a\}$, which depends on a set of variables $\{x_v\}$, to be obtained as a function of the covariance of the variables $\{x_v\}$. Equation 4.1 presents this law.

$$cov(y_a, y_b) = \sum_v \sum_\mu \frac{\partial y_a}{\partial x_v} \frac{\partial y_b}{\partial x_\mu} cov(x_v, x_\mu)$$

Equation 4.1

This law is based on a first order Taylor series of the functions $\{y_a\}$ and on the covariance definition. This implies that the uncertainty of the $\{y_a\}$ variables, calculated using Equation 4.1, is only an approximation when $\{y_a\}$ are not linear functions of $\{x_v\}$. Note that this approach is valid only when the propagated uncertainty, represented by $cov(x_v, x_\mu)$, is small enough³.

4.2 Uncertainty of the Decay Gamma Source intensity

This section aims to derive the equations that calculate the DGS intensity uncertainty due to the neutron flux uncertainty. These equations were obtained applying the uncertainty propagation law (Equation 4.1) to the equations presented in 3.2.2⁴.

The first equation from section 3.2.2 is Equation 3.5, which describes the reaction rates. Identifying the variables of this equation with those of the expression Equation 4.1, we have: $y_a = \{\langle \phi \sigma \rangle_i^{f-d}\}$, where i is the position and $f-d$ is father-daughter isotopes, and $x_b = \{\phi_i^e\}$ ⁵, where e is the neutron energy bin. Therefore, the derivative required in Equation 4.1 to estimate the uncertainty of the reaction rate is shown in Equation 4.2

$$\frac{\partial y_a}{\partial x_v} = \frac{\partial \langle \phi \sigma \rangle_i^{f-d}}{\partial \phi_i^e} = \frac{\partial}{\partial \phi_i^e} \sum_\varepsilon \sigma_\varepsilon^{f-d} \phi_i^\varepsilon = \sum_\varepsilon \sigma_\varepsilon^{f-d} \delta_\varepsilon^e = \sigma_e^{f-d}$$

Equation 4.2

Hence, the uncertainty of the reaction rates can be estimated using Equation 4.3⁶.

¹ Note that the covariance matrix, which represents the uncertainty of the quantities, is considered known during this chapter.

² Note that a function that depends on a random variable is also a random variable

³ This condition is usually met

⁴ Consequently, the equations presented in this chapter can be used to transport any neutron uncertainty, independently of its origin (nuclear data, neutron source definition, etc).

⁵ Note that, therefore, the index a and b represent the pair of indexes $(f - d, i)$ and (e, i) respectively

⁶ If the reaction rates are directly calculated using MC codes, the input uncertainty is the result of this step, instead of the covariance matrix of the neutron flux (see section 3.2.2)

$$cov\left(\langle\phi\sigma\rangle_i^{f-d}, \langle\phi\sigma\rangle_{i'}^{f'-d'}\right) = \sum_e \sum_{e'} \sigma_e^{f-d} \sigma_{e'}^{f'-d'} cov\left(\phi_i^e, \phi_{i'}^{e'}\right)$$

Equation 4.3

Following section 3.2.2, the next quantity to estimate the DGS intensity is the isotopic concentration. In this case, the variable identification, in Equation 4.1, is: $y_\alpha = \{N_i^r\}$, and $x_\nu = \{\langle\phi\sigma\rangle_i^{f-d}\}$, where r is the relevant radioisotope contributing to the SDR.

In this case, we did not find simple analytical expressions that define the isotopic concentration as a function of the reaction rates. However, they can be calculated, as section 3.5 shows. Therefore, the isotopic concentration uncertainty is presented in Equation 4.4, as a function of the sensitivity coefficients, which are considered known or calculable¹.

$$cov\left(N_i^r, N_{i'}^{r'}\right) = \sum_{\bar{f}-d} \sum_{\bar{f}'-d'} \frac{\partial N_i^r}{\partial \langle\phi\sigma\rangle_i^{f-d}} \frac{\partial N_{i'}^{r'}}{\partial \langle\phi\sigma\rangle_{i'}^{f'-d'}} cov\left(\langle\phi\sigma\rangle_i^{f-d}, \langle\phi\sigma\rangle_{i'}^{f'-d'}\right)$$

Equation 4.4

Finally, the last step of section 3.2.2 to estimate the DGS intensity is the evaluation of Equation 3.6. In this case, the identification of the variables, in Equation 4.1, is: $y_\alpha = \{I_i^g\}$, and $x_\nu = \{N_i^k\}$, where k is a generic isotope, and g is the photon energy group². Thus, the corresponding derivative required in Equation 4.1 to estimate the uncertainty of the DGS intensity is presented in Equation 4.5.

$$\frac{\partial y_\alpha}{\partial x_\nu} = \frac{\partial I_i^g}{\partial N_i^k} = \frac{\partial}{\partial N_i^k} \sum_k y_k^g \lambda_k N_i^k = \sum_k y_k^g \lambda_k \delta_r^k = y_r^g \lambda_r$$

Equation 4.5

Then, Equation 4.6 expresses the uncertainty of the DGS intensity as a result of the application of the law of uncertainty propagation.

$$cov\left(I_i^g, I_{i'}^{g'}\right) = \sum_{k_r} \sum_{k_r'} y_{k_r}^g y_{k_r'}^{g'} \lambda_{k_r} \lambda_{k_r'} cov\left(N_i^r, N_{i'}^{r'}\right)$$

Equation 4.6

As a summary of this section, the uncertainty of the neutron flux can be transported up to the uncertainty of the DGS intensity³ using Equation 4.3, Equation 4.4, and Equation 4.6.

¹ The implemented method to calculate the sensitivity coefficients is presented in section 5.5

² The meaning of g changes if the DGS is emitted with point-wise resolution (section 3.2.2)

³ All quantities resulting from the activation step are also functions of the isotopic concentration. Therefore, we can estimate their uncertainty applying the uncertainty propagation law, just like this section.

As commented previously, this section considers that the uncertainty is only associated to the neutron flux. However, the same method can be used to consider the uncertainty in the cross-sections¹.

When neutron flux and cross-section are considered not correlated, the uncertainty of the reaction rates can be expressed as in Equation 4.7:

$$cov\left(\langle\phi\sigma\rangle_i^{f-d}, \langle\phi\sigma\rangle_{i'}^{f'-d'}\right) = \sum_e \sum_{e'} \sigma_e^{f-d} \sigma_{e'}^{f'-d'} cov\left(\phi_i^e, \phi_{i'}^{e'}\right) + \phi_i^e \phi_{i'}^{e'} cov\left(\sigma_e^{f-d}, \sigma_{e'}^{f'-d'}\right)$$

Equation 4.7

In cases where the correlation between flux and cross-section can exist, as when the burn up is considered during the neutron transport [54], this must be also considered when the uncertainty propagation law is applied. However, this example is not an application case of R2S methodology, because common R2S simulation does not consider changes in the material composition during irradiation which can affect the neutron flux.

4.3 Uncertainty of the photon response

This section aims to assess the uncertainty of the photon response defined, in Equation 4.8

$$R_i^{g*} = \frac{t_i^g(p_i^*)}{p_i^{g*}}$$

Equation 4.8

where p_i^{g*} is the probability that a photon was emitted from a position i and an energy group g .

As commented in section 3.3, the photon response does not depend on the photon source. This means that any arbitrary DGS can be used to calculate these coefficients. This is remarked using the symbol $*$. Consequently, the photon response function does not introduce uncertainty related to the DGS. The photon response uncertainty is associated only with the MC uncertainty introduced by the photon transport simulation, via the DGS contribution (t_i^g).

Concerning the diagonal terms of the DGS contribution covariance matrix, they can be evaluated using the numerical estimator of the covariance matrix[29] shown in Equation 4.9. It is worth noting that the MC transport codes evaluate this expression to estimate the MC uncertainty of their responses. Therefore, these terms of the DGS contribution covariance matrix can be directly evaluated during the photon transport simulation.

¹ It is worth to underline that the cross section uncertainty can be as important or more than the stochastic uncertainty due to the calculation methods of the neutron flux [101].

$$var(t_i^g) = \frac{\overline{(t_{hi}^g)^2} - (\bar{t}_{hi}^g)^2}{NPS}$$

Equation 4.9

Regarding the no diagonal terms of the DGS contribution covariance matrix can be directly calculated using the output of the photon transport, that is, using the mean value of each DGS contribution. This is because only one photon is emitted from each photon history. Hence, one photon history cannot contribute from to different phase space. Therefore¹, $\overline{t_{hi}^g t_{hi'}^{g'}} = 0$, and subsequently, the covariance[29] between each two different DGS contributions can be computed as Equation 4.10 shows.

$$cov(t_i^g, t_{i'}^{g'}) = \frac{\overline{t_{hi}^g t_{hi'}^{g'}} - \bar{t}_{hi}^g \bar{t}_{hi'}^{g'}}{NPS} = -\frac{\bar{t}_{hi}^g \bar{t}_{hi'}^{g'}}{NPS} \quad \forall i \neq i' \cup g \neq g'$$

Equation 4.10

This uncertainty is propagated to the photon response applying the uncertainty propagation law (Equation 4.1) to Equation 4.8, considering p_i^{g*} as constants. In this case, the variable assignation is $\{y_a\} = \{R_i^g\}$ and $\{x_v\} = \{t_i^g\}$. In consequence, the stochastic uncertainty of the photon response is estimated as shown in Equation 4.11. This equation considers the definition

$$p_i^{g*} = \frac{I_i^{g*}}{I_t^*}$$

$$cov(R_i^g, R_{i'}^{g'}) = \frac{I_t^* \cdot I_t^*}{I_i^{g*} \cdot I_{i'}^{g'*}} cov(t_i^g, t_{i'}^{g'})$$

Equation 4.11

4.4 Uncertainty of the SDR

Finally, the last step is to propagate the uncertainty from the DGS intensity and the photon response to the SDR uncertainty. Instead of applying the uncertainty propagation law to calculate the SDR uncertainty, it is calculated using the definition of variance presented in Equation 4.12.

$$\begin{aligned} var(SDR) &= \overline{SDR^2} - (\overline{SDR})^2 = \sum_{i,g} \sum_{i',g'} \overline{I_i^g R_i^g I_{i'}^{g'} R_{i'}^{g'}} - \sum_{i,g} \sum_{i',g'} \overline{I_i^g R_i^g} \overline{I_{i'}^{g'} R_{i'}^{g'}} \\ &= \sum_{i,g} \sum_{i',g'} \left(\overline{I_i^g R_i^g I_{i'}^{g'} R_{i'}^{g'}} - \overline{I_i^g R_i^g} \overline{I_{i'}^{g'} R_{i'}^{g'}} \right) \end{aligned}$$

Equation 4.12

¹ Notice that the subindex h refers to the variable of the DGS contribution of one history, while t_i^g is the numeric mean of the DGS contribution calculated with NPS histories.

Chapter 4

Analytical expressions to assess the stochastic uncertainty in R2S

This expression is manipulated considering that photon simulation is independent of the neutron simulation. That is, considering the condition is expressed in Equation 4.13.

$$\text{cov}(R_i^g, I_{i'}^{g'}) = 0 = \overline{R_i^g I_{i'}^{g'}} - \overline{R_i^g} \cdot \overline{I_{i'}^{g'}} \quad \forall i, g, i', g'$$

Equation 4.13

The SDR uncertainty can be expressed as Equation 4.14 shows, combining Equation 4.12, Equation 4.13 as well as the definition of correlation[29].

$$\begin{aligned} \text{var}(SDR) &= \sum_{i,g} \sum_{i',g'} \left(\overline{I_i^g I_{i'}^{g'}} \cdot \overline{R_i^g R_{i'}^{g'}} - \overline{R_i^g} \cdot \overline{I_i^g} \cdot \overline{R_{i'}^{g'}} \cdot \overline{I_{i'}^{g'}} \right) \\ &= \sum_{i,i'} \sum_{g,g'} I_i^g I_{i'}^{g'} \text{cov}(R_i^g, R_{i'}^{g'}) + R_i^g R_{i'}^{g'} \text{cov}(I_i^g, I_{i'}^{g'}) + \text{cov}(I_i^g, I_{i'}^{g'}) \text{cov}(R_i^g, R_{i'}^{g'}) \end{aligned}$$

Equation 4.14

The evaluation of Equation 4.14 requires that the DGS intensity and photon response covariance matrixes are known. These quantities can be assessed following the equations detailed in section 4.2 and section 4.3 respectively.

Regarding the different terms of Equation 4.14, it is worth underlining that:

- i. The term $\sum_{i,i'} \sum_{g,g'} I_i^g I_{i'}^{g'} \text{cov}(R_i^g, R_{i'}^{g'})$ is the uncertainty supplied by the MC transport code during the photon transport, as said in section 4.3.
- ii. The terms $\text{cov}(I_i^g, I_{i'}^{g'}) \text{cov}(R_i^g, R_{i'}^{g'})$ can usually be considered negligible with respect to the terms where the photon response or the DGS intensity appears. This is because this term is a correction¹ of the uncertainty propagation law (see section 4.1), which is relevant only when the propagated uncertainties are huge.

¹ Superior order of the Taylor series.

4.5 Summary and Conclusions

This section presents the equations that can be evaluated to calculate the SDR uncertainty of individual tallies in R2S calculations. That is, this chapter provides the theoretical basis to calculate the SDR uncertainty in R2S. They are divided into three conceptual steps:

- I. The first step propagates the uncertainty from the neutron flux to the DGS intensity. It is worth highlighting that the covariance of the neutron flux can represent any kind of neutron uncertainty¹. During this thesis, it represents the stochastic uncertainty of the MC neutron transport.
- II. The second step propagates the photon transport uncertainty from the DGS contribution to the photon response. In this step, the DGS contribution uncertainty is directly obtained from the output of the photon transport simulation.
- III. Finally, the third step combines the uncertainties of the DGS intensity and the photon response in order to get the SDR uncertainty of the R2S calculation.

It is worth highlighting that this scheme is suitable to estimate the uncertainty of SDR individual tallies. That is, to the SDR estimated in a point². However, it cannot apply to the estimation of SDR maps (a great number of SDR tallies) because the evaluation of each SDR uncertainty requires the management of a huge amount of data. Therefore it is not viable to provide all the data required to estimate the uncertainty of an SDR map in the same calculation. This point is also discussed in Chapter 5.

¹ For example, it can represent the uncertainty due to the transport cross-section uncertainty, neutron source definition uncertainty

² Actually, the point-like SDR tallies in MC R2S are a mean of the SDR in a surface or volume defined by the user

Chapter 5.

Implementation of the methodology to estimate the SDR uncertainty in R2S-UNED

Chapter 3 and Chapter 4 established the theoretical basis to calculate the MC uncertainty of an individual SDR tally. In this section, we present the computational implementation of this theory in R2S-UNED. The practical implementation of any computational algorithm requires answering two questions, which in this case are:

- i. Is all input data required to evaluate the SDR uncertainty available?*
- ii. Can the evaluation of the SDR uncertainty be performed in an acceptable time, taking into account the currently available computational resources?*

With respect to the first question, a review of the equations presented in Chapter 4 shows that the evaluation of the SDR uncertainty requires additional data to those calculated in a common R2S-UNED simulation. Specifically, R2S-UNED does not provide the covariance matrix of the neutron flux, the DGS contribution, and the sensitivity coefficients, which are required to estimate the SDR uncertainty.

Consequently, the implementation of the methodology to estimate the SDR uncertainty must also include the required modifications of R2S-UNED in order to calculate these input data.

Concerning the second question, the number of operations required to evaluate the SDR uncertainty, and consequently, the time spent in to do it, is influenced principally by¹:

- i. The number of mesh elements ($\sim 10^5$)*
- ii. The number of radioisotopes (~ 1000)*
- iii. The number of reactions considered in the activation step (~ 33000)*
- iv. The number of group-wise energy groups (neutron (~ 100) and photon (~ 20))*

These numbers suggest that the calculation can require a lot of time. However, most of these variables (regions, isotopes, reactions) do practically not affect the SDR estimated in the desired point. Therefore, they can also be neglected during the estimation of stochastic uncertainty.

¹ The estimated number of these quantities is based on the experience of the common R2S calculation carried out in UNED. But it depends on the application and the user

In this sense, we implemented filters of the most relevant quantities (regions, radioisotopes, and reactions) according to their contribution to the SDR. This way, we reduce the time required to estimate the SDR uncertainty.

*Table 5.1 Computational stages in an R2S simulation including the uncertainty estimation. The table highlights: i) * Mandatory new input data to estimate the SDR uncertainty. ii) ** Optional new input data to estimate the SDR uncertainty*

Computational Step	Input data	Process/stages	Output data
1. <i>MCNP-R2S</i>	<ul style="list-style-type: none"> MCNP input data¹ 	Neutron transport	<ul style="list-style-type: none"> Neutron flux The covariance matrix of the neutron flux
2. <i>Activation module</i>	<ul style="list-style-type: none"> Material definition Activation libraries Neutron flux Irradiation scenario 	Material Activation	<ul style="list-style-type: none"> DGS intensity Activation summary
3. <i>MCNP-R2S</i>	<ul style="list-style-type: none"> MCNP input data DGS intensity 	Photon transport	<ul style="list-style-type: none"> SDR DGS contribution
4. <i>Uncertainty module</i>	<ul style="list-style-type: none"> DGS intensity DGS contribution* Activation summary** 	Filtering	<ul style="list-style-type: none"> Relevant positions Relevant isotopes Relevant reactions
	<ul style="list-style-type: none"> Irradiation scenario Relevant positions, isotopes, and reactions* Activation summary** 	Estimation of the sensitivity coefficients	<ul style="list-style-type: none"> Sensitivity coefficients
	<ul style="list-style-type: none"> Neutron flux DGS intensity DGS contribution* The covariance matrix of the neutron flux** 	Estimation of the Uncertainty	<ul style="list-style-type: none"> Reaction rate uncertainty Isotopic activity uncertainty DGS intensity uncertainty SDR uncertainty

Taking into account these points and the scheme presented in Chapter 4, we amplify the computational steps of the R2S simulation. Table 5.1 presents a detailed scheme of the workflow implemented to estimate the SDR uncertainty with R2S-UNED. The newly implemented features in R2S-UNED are described below. Note that they are classified by the computational step.

¹ MCNP input data includes geometry, material definition, nuclear data and neutron source when the DGS is not available.

i. Neutron flux transport:

- ❖ MCNP-R2S code was modified to estimate the correlation matrix of the neutron flux. The implemented calculation method of this matrix is presented in section 5.1.

ii. Activation step:

- ❖ The future estimation of the sensitivity coefficients and the filters will require the use of data calculated during the activation step. This step can write a summary of the activation in order to avoid the repetition of this computational step. However, writing this file requires more time than the repetition of the activation calculation. Therefore, this step is optional. The content and purpose of this optional file¹ are presented in section 5.2.

iii. Photon transport:

- ❖ MCNP-R2S code was modified to get the DGS contribution. The modification is explained in section 5.3

iv. Uncertainty module of R2S-UNED:

- ❖ This module calculates the contribution of the regions, radioisotopes, or pathways to the SDR. These contributions are used to filter the regions, radioisotopes, and pathways considered to estimate the SDR uncertainty, saving computational time. These filtering steps are explained in section 5.4.
- ❖ Estimation of the sensitivity coefficients: The implementation included in R2S-UNED to calculate them is presented in section 5.5
- ❖ Estimation of the uncertainty in the different steps: reaction rates, activity, DGS, and SDR. The implementation of the calculation scheme in the R2S-UNED workflow is explained in sections 5.6 and 5.7

Finally, a summary and conclusions of this chapter are presented in section 5.8.

It is worth commenting that all steps of the workflow presented in Table 5.1 support MPI in order to reduce the time required to perform the calculation, including the implementation of the evaluation of the SDR uncertainty.

¹ It is worth noting that writing the file requires more time than simulate the activation. Therefore, the use of the file is optional

5.1 Estimation of the stochastic neutron uncertainty due to the MC transport code

The numerical estimation of the neutron flux covariance [29] is performed by computing its numerical definition inside of the MC transport code. This definition is presented in Equation 5.1.

$$cov(\phi_i^e, \phi_{i'}^{e'}) = \frac{1}{NPS} \left(\frac{1}{NPS} \sum_{h=1}^{NPS} \phi_{h,i}^e \phi_{h,i'}^{e'} - \frac{1}{NPS} \left(\sum_{h=1}^{NPS} \phi_{h,i}^e \right) \cdot \frac{1}{NPS} \left(\sum_{h=1}^{NPS} \phi_{h,i'}^{e'} \right) \right)$$

Equation 5.1

where ϕ_i^e is the neutron flux in the region i and energy bin e , NPS is the number of simulated histories during the neutron transport to estimate ϕ_i^e , and $\phi_{h,i}^e$ is the neutron flux in the region i and energy bin e of the neutron history h .

Concerning the method applicability, typical R2S simulations¹ usually consider about 175 groups of energy and meshes with around $\sim 10^5$ spatial elements. According to Equation 5.2², the size of this matrix would be 1225 TB. Consequently, the covariance matrix of the neutron flux cannot be directly calculated by this methodology in most of the common applications.

$$RAM = \text{elemet size} \cdot \#_{elements} = \text{elemet size} \cdot \left(\frac{\#_{energy\ groups}^2 \cdot \#_{regions}^2}{2} + \frac{\#_{energy\ groups} \cdot \#_{regions}}{2} \right)$$

Equation 5.2

It is worth highlighting that the tool implemented during the thesis requires the neutron flux covariance matrix to estimate the actual³ stochastic SDR uncertainty⁴. Consequently, this issue, related to the neutron flux covariance estimation, limits the tool's applicability.

In this sense, three possible options can be studied in order to overcome this issue.

- i. At this time, teams are studying the features of the covariance matrix [31]. These studios aim to develop a methodology to estimate the neutron correlation using the currently available computational resources.
- ii. R2S-UNED new features, which will be presented during this chapter, provide data useful to optimize or redefine the simulation. Thus, the R2S calculation can be adapted to the RAM computational requirements imposed by the size of the neutron flux covariance estimation. It is worth mentioning that this thesis studies the option

¹ Common R2S applications in neutronic analysis of fusion facilities (see ANNEX A)

² Equation 5.2 estimates the size required to store the covariance matrix of the neutron flux, where $\#$ is "number of" and *elemet size* is 8 Byte.

³ If the neutron flux covariance matrix is not available, the tool can still estimate an approach of the uncertainty (see section 5.7).

⁴ It is worth underlining that this problem is common to most sophisticated methodologies to estimate the SDR uncertainty.

to redefine the R2S simulation, obtaining different guidelines or methodologies to calculate the SDR uncertainty using R2S-UNED. More details of these methodologies and the results obtained applying them are presented in Chapter 7.

- iii. The SDR uncertainty can be estimated during the neutron transport simulation without the need of storing the neutron flux covariance matrix. Otherwise, this method will increase the computational time of the neutron transport simulation. The study of this method is one of the future works proposed after this thesis.

Regarding the details of the implementation in R2S-UNED of the estimation of the covariance matrix of the neutron flux, it is worth mentioning how the spatial discretization is considered:

According to Chapter 3, R2S-UNED uses the CuV method to discretize the geometry during the neutron transport. However, this method increases the number of regions used to discretize the space¹, and consequently the size of the neutron flux covariance matrix.

On the contrary, other mesh-based R2S methodologies calculate the mean flux in the whole mesh element. This method uses less RAM than CuV method. Otherwise, it can miscalculate the SDR when the mesh element lies over void and material, where unrealistic increased neutron fluxes can be associated to the neighbouring material regions.

Considering these points, we decided to use a mixed approach. The neutron flux is estimated in the whole mesh element. But only the contribution from the relevant material regions is taken into account. That is, the contributions to the neutron flux are filtered by material, avoiding contributions from the void or no activated cells. Although it is an approximation to the actual calculation uncertainty, this approach is enough, considering the accuracy required to estimate the SDR uncertainty².

5.2 Activation summary

The activation summary file, whose content is explained in section 5.2.1, is an optional file that contains data calculated during the activation step. This file aims to speed up the execution of the uncertainty module of R2S-UNED.

Despite the usage of this data actually speeds up the uncertainty module simulation, the time spent in the complete R2S simulation³ is increased. This is because the time spent building the file is greater than the time required to repeat the activation step. The performance analysis of the activation step presented in 5.2.2 demonstrates this conclusion. Due to this result, the

¹ The method divides the mesh element in the cells inside of the voxel, increasing the number of regions

² One example of this is presented in ANNEX E.

³ Neutron transport, activation, photon transport, and uncertainty estimation

activation process can be repeated during the execution of the uncertainty module of R2S-UNED instead of reading the data of this file.

5.2.1 Contents of the activation summary file

This file contains three types of data required to speed up the execution of the uncertainty module of R2S-UNED. These quantities, and their usage in the uncertainty module of R2S-UNED, are described below.

I. Isotopic concentration at the interest time

The isotopic concentration at the interest time is required data to estimate the most relevant isotopes. This filter is described in 5.4.1.

II. Activation matrix of the ODEs system

The activation matrix of the ODEs system contains the reaction rates¹ and decay constants of the isotopes. They are required for estimating the relevant reactions, which produce the isotopes and the sensitivity coefficients. The description of the calculation of these quantities is detailed in sections 5.4.3 and 5.5, respectively.

III. Existent isotopes during the activation step

This information contains those isotopes whose concentration was nonzero during, at least, one of the times of the irradiation scenario. This means that this array contains all the isotopes that are produced during the material activation.

This information is useful to speed up the definition of reduced activation systems² [41]. This definition process is carried out to perform two different tasks: i) The estimation of the relevance of the reaction rates and ii) the estimation of the sensitivity coefficients. The description of the calculation of these quantities is detailed in sections 5.4.3 and 5.5, respectively.

It is worth highlighting that if the activation summary file is not used, the activation step is repeated before performing these two tasks. Consequently, the array of the existent isotopes is re-estimated and therefore is still used, saving the computational time in any case.

5.2.2 Consuming time during the activation step

The R2S-UNED version at the beginning of the thesis was based on distributing ACAB[41] activation cases in the different CPUs. That means that an ACAB simulation (with the corresponding library data lecture and preprocessing) is executed by the activation of each material region, and afterwards, the outputs of all ACAB simulations are merged to produce the

¹ Note that the reaction rates depend on the time. The file contains the reaction rates of the first temporal step. During the next time steps, they are rescaled according to the irradiation scenario.

² A reduced activation system is defined as the ODE system that describes only the activation of a small set of elements and pathways.

DGS. Therefore, it was not optimized to perform the activation step of the R2S simulation and neither to estimate the new required quantities, such as the sensitivity coefficients or the relevance of the reaction rates. For that reason, the activation module of R2S was re-programmed during the thesis.

The new version was verified by comparing the results obtained in JET [55] with those calculated using the old version. The results show an excellent agreement between them, validating the *new* R2S-UNED version. However, this section is focused on the comparison of the performance of the different activation versions. Their execution time was measured in the activation of the mesh 3 in JET simulation described in section 7.2. This mesh contains 48.856 voxels, which were activated using the same 200 CPUs of our cluster¹. The results are presented in Table 5.2.

Table 5.2 Time consumption of the different versions of the activation module of R2S-UNED

Code version	Output data	Time (h:min:s)
<i>Old version</i>	DGS	3:58:57
	DGS and summary activation file	4:41:44
<i>New version</i>	DGS	0:16:23
	DGS and summary activation file	2:27:50

The results of Table 5.2 show that the time required to compute and store the summary (~40 minutes in the best implementation) file is greater than the time spent performing the material activation (~15 minutes²). Consequently, the activation step was also implemented in the uncertainty module of R2S-UNED.

5.3 Estimation of the DGS contribution during the photon transport

A new capability was implemented in R2S-UNED in order to evaluate the DGS contribution³. This capability calculates the DGS contribution to the SDR of the regions of the DGS (defined by a superimposed mesh over the geometry) with energy resolution (defined by an energy group-wise structure, i.e. energy bins).

The implemented method to estimate the DGS contribution is as follows. When a photon is emitted from the DGS, its position and energy are stored. Then, if this photon history contributes

¹ Our cluster is currently composed by 1000 processor Intel(R) Xeon(R) Silver 4210 CPU @ 2.20GHz

² It is worth underlining that this time is also representative of the worst time spent repeating the activation calculation in the uncertainty module of R2S-UNED. Because it uses the same code, but most cases are not repeated.

³ This capability was already implemented in MCNP-R2S before the begin of the thesis

to the SDR tally, its contribution is scored in the contribution mesh-tally, in the position and energy bin corresponding to the position and energy of the emitted photon.

It is worth highlighting that the application of the uncertainty module of R2S-UNED requires the use of the same spatial and energy binning for the estimation of both the DGS and the DGS contribution. In addition, the implementation of the DGS contribution does not support the CuV format. This means that the CuV capability cannot be used to estimate the SDR uncertainty.

5.4 Filtering steps applied to speed up the estimation of the SDR uncertainty

Three filters were implemented in order to reduce the computational time spent in estimating the SDR uncertainty. These filters define the regions, isotopes, and reactions considered in the R2S-UNED calculation to estimate the SDR uncertainty. This means that they define the ranges of the sums in Equation 4.3, Equation 4.4, Equation 4.6, and Equation 4.14, implemented in the uncertainty module of R2S-UNED.

The spatial filter is presented in section 5.4.1, the radioactive isotope filter is shown in 5.4.2, while the filters of the reactions, which produce these radioactive isotopes, are described in 5.4.3.

5.4.1 Spatial contribution of the DGS to the SDR

The spatial contribution is estimated by summing the contributions of all energy bins of the DGS contribution. It is defined from the definition of the SDR in Equation 5.3.

$$SDR = \sum_i \sum_g R_i^g I_i^g \rightarrow C_{region}(i) = \sum_g R_i^g I_i^g = \sum_g t_i^g$$

Equation 5.3

Where C represents the contribution, the index i refers to the region, and the index g refers to the photon energy group.

The filtering, in the uncertainty module of R2S-UNED, is applied as follows: i) The contribution of each region $C_{region}(i)$ is estimated. ii) The regions are sorted according to this quantity. iii) The regions are considered until the filter condition is overcome.

5.4.2 Isotopic contribution to the SDR

The isotopic contribution ($C_{isot}(r, i)$) from a radioisotope r in a region i to the SDR is derived from the definition of SDR. The SDR mathematical expression, which depends on the isotopic contribution, can be deduced from Equation 3.6 and Equation 3.7. It is expressed in Equation 5.4.

$$SDR = \sum_i \sum_r \left(\sum_g R_i^g y_r^g \lambda_r \right) N_i^r = \sum_i \sum_r C_i^r N_i^r = \sum_i \sum_r C_{Isot}(r, i)$$

Equation 5.4

Consequently, the isotopic contribution of the isotope r can be obtained from Equation 5.4 as Equation 5.5 shows.

$$C_{Isot}(r, i) = \sum_g R_i^g y_r^g \lambda_r N_i^r$$

Equation 5.5

This filtering, in the uncertainty module of R2S-UNED, is applied as follows: i) For each relevant region (see section 5.4.1), the isotopic contribution $C_{Isot}(r, i)$ is estimated. ii) In each region, the isotopes are sorted according to this contribution. iii) In each region, the isotopes are considered until the filter condition is overcome.

5.4.3 Pathway contribution to the production of the relevant isotopes

The contribution of a reaction rate to the SDR cannot be defined [35]. For this reason, we can define the pathway¹ contribution to the production of a radioisotope, because we can estimate the concentration of the isotope r according to Equation 5.6².

$$N_i^r = \sum_{pathways} P_{p,i}^r$$

Equation 5.6

where $P_{p,i}^r$ is the contribution of the pathway p to the isotope r in the region i.

Once the relevant pathways are filtered³ according to their contribution, the relevant reaction rates are defined as those reactions which belong to some of these pathways.

This approach to filtering the relevant reactions is not directly applicable in R2S-UNED because ACAB code cannot estimate the pathway contribution to the isotope production. Therefore, two different approaches were implemented during the thesis in order to identify the pathways and quantify their contribution to the isotopic contribution.

The simplest one considers that the activation system meets the SNILB conditions, simplifying the activation ODEs system. In particular, we consider that the pathways are linear chains of one

¹ The pathway is a set of isotopes, reactions, and decay paths. It was defined in section 3.2

² Note that the contribution of a pathway does not affect the other contributions

³ It is the last filter applied in the uncertainty module of R2S-UNED. Therefore, it is only applied to find the pathways (reactions) contributing to the most relevant isotopes in the most relevant positions.

step¹. Consequently, the pathways are directly identified from the activation ODEs system, as section 5.4.3.1 shows.

The other one considers the complete activation system. Hence, more complete types of pathways can be detected and analyzed. The methodology implemented to detect the pathways and quantify their contribution to the isotopic concentration, in general activation systems, is presented in section 5.4.3.2.

5.4.3.1 SNILB approach

According to the explained in section 3.4.2, the concentration of an isotope produced by one-step reaction can be expressed as shown in Equation 5.7 when the initial concentration of this isotope is zero.

$$N_r = \frac{\alpha_r(t)}{\lambda_r} \sum_f N_f \langle \phi \sigma \rangle^{f \rightarrow r}$$

Equation 5.7

Therefore, the pathways that produce the relevant isotopes are directly identified from the isotope fathers in the initial material ($N_f \neq 0$). These pathways are sorted according to their contribution to the r isotope concentration (proportional to $N_f \langle \phi \sigma \rangle^{f \rightarrow r}$). Afterwards, the pathways (reactions) are considered, in order, until the filter condition is overcome.

It is worth underlining that our experience in important fusion facilities, such as JET and ITER [56], shows that two-step chains where the second step is produced by decay are also relevant in these installations. Most of them meet the condition of Equation 5.8, which means that the excited state of the isotope r decays almost immediately compared with the lifetime of the isotope r, in a linear chain of isotopes $f \rightarrow r^* \rightarrow r$

$$\frac{\lambda_r}{\lambda_{r^*}} \ll 1$$

Equation 5.8

According to the Bateman equations (Equation 3.10), the concentration of the isotope r of this chain can be expressed as Equation 5.9 shows.

$$N_r = N_f \cdot \left(\frac{\langle \phi \sigma \rangle^{f \rightarrow r^*} (e^{-\langle \phi \sigma \rangle^{f \rightarrow r^*} t} - e^{-\lambda_r t})}{\lambda_r - \langle \phi \sigma \rangle^{f \rightarrow r^*}} \frac{\lambda_{r^*}}{\lambda_{r^*} - \lambda_r} + \frac{\lambda_{r^*} (e^{-\lambda_{r^*} t} - e^{-\lambda_r t})}{\lambda_r - \lambda_{r^*}} \frac{\langle \phi \sigma \rangle^{f \rightarrow \lambda_{r^*}}}{\langle \phi \sigma \rangle^{f \rightarrow \lambda_{r^*}} - \lambda_{r^*}} \right)$$

Equation 5.9

¹ Our experience in fusion facilities shows that these chains are most relevant in most of the SDR analyses.

If *low burning* conditions¹ and Equation 5.8 are considered in Equation 5.9, the concentration of the isotope r can be expressed according to Equation 5.10

$$N_r = \frac{N_f \langle \phi \sigma \rangle^{f \rightarrow r^*}}{\lambda_r} (1 - e^{-\lambda_r t})$$

Equation 5.10

Note that this is the same expression that those used to estimate the concentration of r in a linear chain $f \rightarrow r$ when SNILB conditions are met, but produced by the reaction rate $\langle \phi \sigma \rangle^{f \rightarrow r^*}$. Consequently, in order to consider these two-step chains, the reaction rate $\langle \phi \sigma \rangle^{f \rightarrow r^*}$ is assigned to produce the isotope r instead of r^* .

Note that, due to this approach, the isotope r^* is not produced. Therefore, isotopes r and r^* cannot be relevant at the same time. Nevertheless², the contribution of this isotope is expected small, since its concentration is always insignificant in these circumstances compared with the relevant isotope r , as Equation 5.11 shows.

$$N_r \gg N_{r^*} = N_f \frac{\langle \phi \sigma \rangle^{f \rightarrow r^*}}{\lambda_{r^*}} (1 - e^{-\lambda_{r^*} t})$$

Equation 5.11

5.4.3.2 General activation

In the case of general activation, we can define different methodologies to detect and quantify the pathways:

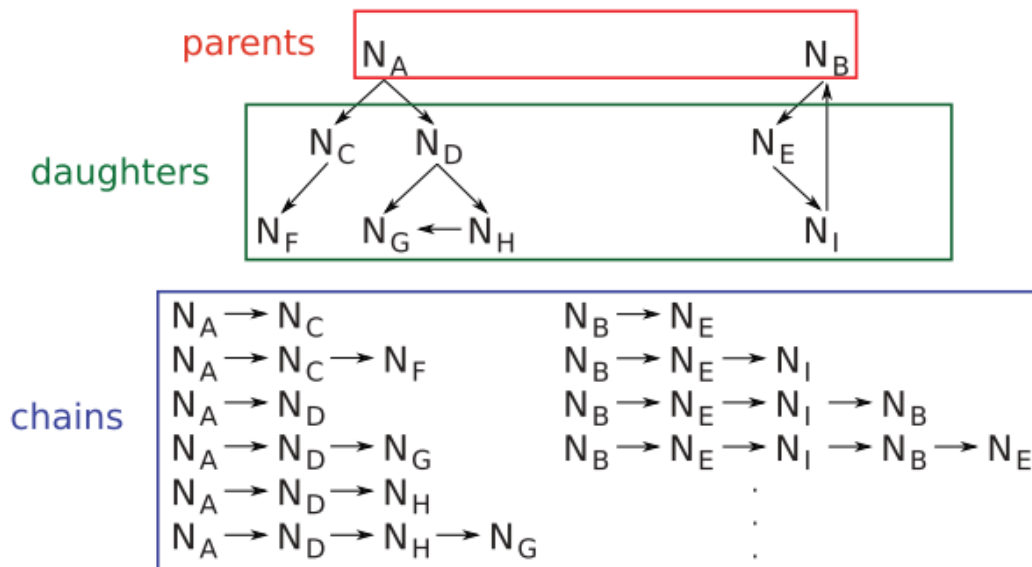


Figure 5.1 Independent linear chain decomposition in solvers based on linear chain solvers [35]

¹ They were introduced in section 3.4.2

² Even if both isotopes were relevant, we can use the general mode instead of SNILB approach

The first one, which is depicted in Figure 5.1, consists in to break down the activation case in linear chains, including the loops. Afterwards, they solve each pathway to estimate their contribution to producing the isotope. It is worth noting that codes, such as Alara or Actys-Go [39] [40], directly use this workflow to estimate the isotopic inventory. That is, they estimate the pathway contribution while they estimate the isotopic concentration.

The second methodology is as follows: They define the possible (more generic) pathway to evaluate, which connects an existent isotope with the relevant isotope. Afterwards, they estimate the contribution of this pathway¹ (evaluating the reduced activation system).

In the last years, FISPACT [40] has incorporated the capability to perform this pathway evaluation. In this thesis, we implemented a similar methodology to that used by FISPACT [57] [58].

In our implementation, the user must define that type of pathways are considered. The considered pathway definitions are presented below.

- i. Linear chains
- ii. Linear chains with loops
 - o Only loops with metastable states
 - o General loops
- iii. General contribution from the nonzero initial concentration isotope (not implemented, since it considers so many reactions)

Note that this development aims to filter the relevant pathways to the relevant isotope. Consequently, the definition must be the simplest one that detects all relevant reactions that produce the isotope. For example; the pathways do not include loops if they do significantly not affect to the concentration of the isotope.

In cases where the loops are considered, no relevant reactions can be included because the contribution of the loop itself is not quantified. The evaluation of the pathway removing the loop would indicate if it is worth considering the reactions of the loop in the calculation. However, it is worth underlining the activation of SDR analysis usually can be described by linear chains with very few exceptions² named in the literature [59]–[61]. For this reason, this improvement of the filter process was not implemented.

¹ Note that the loops are inside of the pathway instead of being detailed in several pathways. Consequently, this approach provides less information. Nevertheless, this application does not require this level of detail.

² Usually, loops with metastable (decay) isotope. Pathways with loops were added to cover these exceptions.

Concerning the implementation of the algorithm, the implemented scheme can be depicted as Figure 5.2 shows. The scheme includes the introduction of loops since it is the most complete workflow.

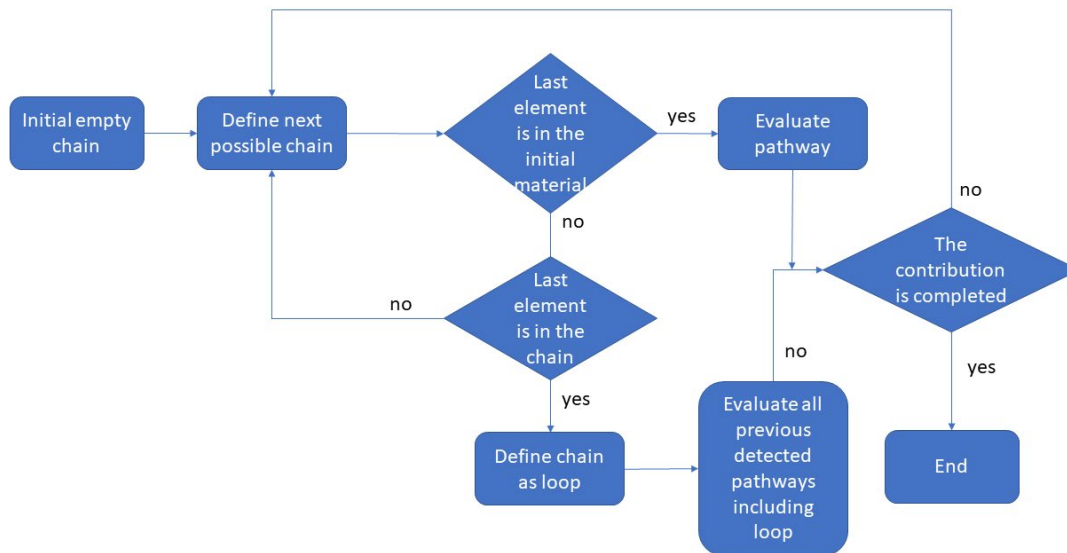


Figure 5.2 Algorithm scheme used to find the contributing pathways to the relevant isotope

The initial possible chain is the relevant isotope its-self. Afterwards, the possible chains are built following all the father isotopes until i) the incorporated isotope is an initial material or ii) the incorporated isotope defines a loop.

As mentioned above, the pathway contribution is evaluated from the concentration of the relevant isotope in the reduced system. Specifically, the relative contribution is defined as $\frac{N_{reduced}^r}{N^r}$, where $N_{reduced}^r$ is the isotopic concentration of the r isotope estimated in the reduced system, while N^r is the concentration of the r isotope in the complete activation system.

Regarding the scheme to define the possible chains, they are built following all the fathers of the isotope. The order to build these chains is to try all possible chains of a determinate length before trying possible larger chains. Thus, short-length pathways, like those expected in the fusion facilities, are found first.

Figure 5.3¹ presents an example of the algorithm. In this example, we are looking for the relevant pathways contributing to the production of isotope 1. In addition, the initial material is composed by the isotopes 2, 3, 6, and 8.

¹ Note that the loop is described in the scheme as a linear chain. Similar to the case of Figure 5.1

The first possible chain is isotope 1. But as it is not part of the initial material, this pathway is not evaluated. Afterwards, the algorithm looks for inside the fathers of the isotope 1.

The next possible chain is the 2-1. As 2 is part of the initial material, the contribution of the pathway 2-1 is evaluated. Afterwards, the algorithm looks for the next chain. It is the 3-1, which is the same as the case 2-1. The next possible chain is 4-1, but 4 is not part of the initial material (no evaluated).

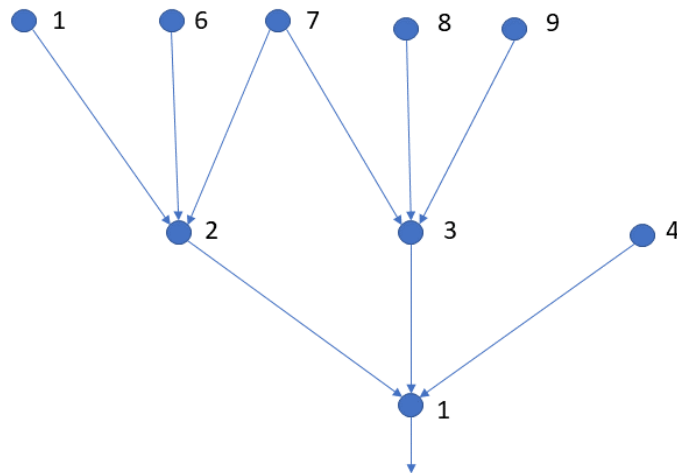


Figure 5.3 Visual tree for the nuclei 1. Points represent the isotope while the lines joint the father with the daughter isotope (the arrow indicates the daughter isotope).

Since there are no more fathers of the isotope 1, grandfathers of 1 are considered. Then, the next possible chain is 1-2-1. This chain is a loop. Consequently, the algorithm also re-evaluates the previous pathways that contain one of the loop isotopes¹. In this case, as isotope 1 is in all pathways, all they are re-evaluated.

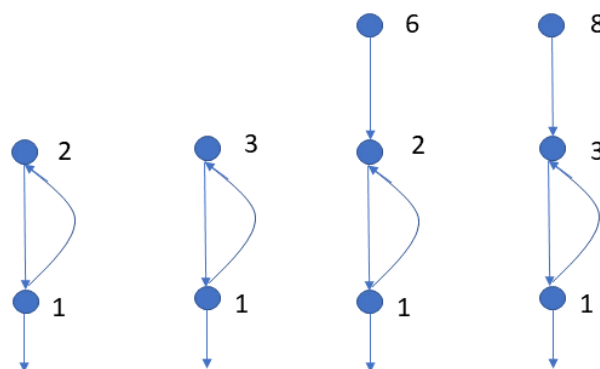


Figure 5.4 Detected pathways in the example of Figure 5.3

¹ It is worth highlighting again that the user chooses if the algorithm considers the loops or not.

According to this scheme, the subsequent chains are 6-2-1, 7-2-1, 7-3-1, and 8-3-1. Where the contribution of the chains 6-2-1 and 8-3-1¹ are evaluated considering the loop 1-2-1. The chain 9-3-1 is not evaluated since the total contribution to the isotope 1 was already detected. Figure 5.4 summarizes the detected pathways.

If these contributions do not complete the concentration of the isotope 1, the algorithm continues searching. In this example, the algorithm tries the fathers of isotopes 6, 7, 8, and 9. The fathers of isotope 1 are not considered because it is a loop.

5.5 Estimation of the sensitivity coefficients

The sensitivity coefficients, in this thesis, are the derivatives of the concentration to the reaction rates. The equations, which describe these coefficients (Equation 5.12), can be obtained by performing the proper derivative to Equation 3.2.

$$\frac{d}{dt} \frac{\partial N_{x,i}(t)}{\partial \langle \phi \sigma \rangle_x^{f \rightarrow d}} = \sum_j (\langle \phi \sigma \rangle_x^{j \rightarrow i} + \lambda_j^i) \frac{\partial N_{x,j}}{\partial \langle \phi \sigma \rangle_x^{f \rightarrow d}} - \left(\lambda_i + \sum_k \langle \phi \sigma \rangle_x^{i \rightarrow k} \right) \frac{\partial N_{x,i}}{\partial \langle \phi \sigma \rangle_x^{f \rightarrow d}} + \sum_j \delta_j^f \delta_i^d N_{x,j} - \sum_k \delta_i^f \delta_k^d N_{x,i}$$

Equation 5.12

ACAB code does not directly estimate these coefficients. For that, we develop two different methods² to evaluate them. The first implemented method simplifies the activation system, but it is useful only when SNILB conditions are met. The second method can deal with general activation systems. Note that the election of the solver is related to the method chosen to filter the isotopes (see section 5.4.3). These two methods implemented to estimate the sensitivity coefficients are described in sections 5.5.1 and 5.5.2.

5.5.1 SNILB method

This solver estimates the sensitivity coefficients of one-step linear chains where the SNILB conditions are met. According to the explained in section 3.5, we can evaluate the sensitivity coefficients when the SNILB conditions are met using Equation 5.13.

$$\frac{\partial N_r}{\partial \langle \sigma \phi \rangle^{f \rightarrow r}} = N_f \frac{\alpha_r(t)}{\lambda_r}$$

Equation 5.13

¹ Note that in these evaluations, the initial concentration of isotopes 2 and 3 is zero since there are not detected as initial materials. The contribution of materials 2 and 3 was already evaluated in the chains 2-1 and 3-1

² A general review of methodologies to estimate the sensitivity coefficients can be found in [50].

It is worth highlighting that several two steps pathways, where the second step is a decay path, are also relevant, and the algorithm can consider them[56]. The conditions met to consider these pathways were already presented in section 5.4.3.1.

5.5.2 General activation system

The method implemented to deal with the general activation system, hereafter called general solver, consists in solving the ODEs system presented in Equation 5.12. In this thesis, we use the ACAB solver to solve this system. Note that ACAB was widely tested solving activation ODE systems (see section 3.4.1).

It is worth highlighting that the subroutines of ACAB solver have an outset to the concentration. Thus, ACAB guarantees that the isotopic concentration is not negative, avoiding numerical errors. For the sensitivity coefficients calculation, these outset were removed since the sensitivity coefficients can be negatives.

The review performed to ACAB code [62] indicates that the different subroutines should work properly. However, the ACAB solver has not been deeply tested for these conditions. In addition, the modification can affect to ACAB solver's accuracy, as shown during the validation of the tool, presented in Chapter 6.

Regarding the practical application of the method, it solves the ODEs system that contains all sensitivity coefficients related to the production of each radioisotope at only one simulation. Note that the filter information is already used to reduce the ODEs system only to the contributing pathways. Therefore, the ODEs system (Equation 5.12) usually contains around no more than 10 equations.

5.6 Saving format of the sensitivity coefficient data. "P1C" coefficients

Chapter 4 shows how the SDR statistical uncertainty in R2S can be estimated. Especially, Equation 4.3, Equation 4.4, Equation 4.6, and Equation 4.14 show how the neutron flux uncertainty can be considered in the SDR uncertainty. These equations, which require the sensitivity coefficients to be evaluated, can be manipulated affecting the possible relevant output as well as the calculation time used to estimate the SDR uncertainty.

The sequential evaluation of these equations, which only needs the sensitivity coefficients, enables the evaluation of the uncertainty of the reaction rates, isotopic concentration, DGS intensity, and SDR response. However, each one of the evaluations has a double summation over each variable of the equation. Therefore, this implementation can be relatively slow.

If Equation 4.3 is introduced in Equation 4.4, the uncertainty of the isotopic concentration can be calculated according to Equation 5.14.

$$\begin{aligned} cov(N_i^r, N_{i'}^{r'}) &= \sum_e \sum_{e'} \left(\sum_{f-d} \sigma_e^{f-d} \frac{\partial N_i^r}{\partial \langle \phi \sigma \rangle_i^{f-d}} \right) \left(\sum_{f'-d'} \sigma_{e'}^{f'-d'} \frac{\partial N_{i'}^{r'}}{\partial \langle \phi \sigma \rangle_{i'}^{f'-d'}} \right) cov(\phi_i^e, \phi_{i'}^{e'}) \\ cov(N_i^r, N_{i'}^{r'}) &= \sum_e \sum_{e'} P_1 C 1_i^{e,r} \cdot P_1 C 1_{i'}^{e',r'} cov(\phi_i^e, \phi_{i'}^{e'}) \end{aligned}$$

Equation 5.14

Notice that the calculation of the coefficients¹ $P_1 C 1_i^e$ requires only one sum over its variables to be assessed. On the contrary, the covariance of the concentrations is estimated without calculating the covariance of the reaction rates. Then, the calculation of the SDR uncertainty is speeded up at the expense of obtaining less useful information during the uncertainty module application.

This can be repeated by introducing Equation 5.14 in Equation 4.6

$$\begin{aligned} cov(I_i^g, I_{i'}^{g'}) &= \sum_e \sum_{e'} \left(\sum_r P_1 C 1_i^{e,r} y_r^g \lambda_r \right) \cdot \left(\sum_{r'} P_1 C 1_{i'}^{e',r'} y_{r'}^{g'} \lambda_{r'} \right) cov(\phi_i^e, \phi_{i'}^{e'}) \\ cov(I_i^g, I_{i'}^{g'}) &= \sum_e \sum_{e'} P_1 C 2_i^{e,g} \cdot P_1 C 2_{i'}^{e',g'} cov(\phi_i^e, \phi_{i'}^{e'}) \end{aligned}$$

Equation 5.15

In this case, presented in Equation 5.15, the uncertainty of the isotopic concentration cannot be obtained, since the DGS intensity uncertainty is calculated directly from the neutron flux uncertainty.

Again, we can introduce Equation 5.15 in Equation 4.14. We present the expression of the SDR uncertainty in Equation 5.16, where the last term, which is negligible, is eliminated.

$$\sigma_{SDR}^2 = \sum_e \sum_{e'} \left(\sum_g P_1 C 2_i^{e,g} R_i^g \right) \cdot \left(\sum_{g'} P_1 C 2_{i'}^{e',g'} R_{i'}^{g'} \right) cov(\phi_i^e, \phi_{i'}^{e'}) + \sigma_{photon}^2 + O(2)$$

Equation 5.16

The simulation time of the cases where the uncertainty module was applied was not excessively high. Consequently, some of the P₁C were not implemented. Table 5.3 summarizes the coefficients that can be stored during phase 1 in order to evaluate the SDR uncertainty during phase 2 of the uncertainty module of R2S-UNED.

¹ This name means Phase 1 Coefficients The notation is related to the subroutine names and the workflow of them in the specific implementation of the uncertainty module of R2S-UNED.

Table 5.3 Definition of the phase 1 coefficients (P_1C)

P_1C	Term	Enables the uncertainty calculation	Implemented
P_1C0	$\frac{\partial N_i^r}{\partial \langle \phi \sigma \rangle_i^{f-d}}$	<ul style="list-style-type: none"> • Reaction rate • Activity • DGS • SDR 	Yes
P_1C1	$\left(\sum_{f-d} P_1C0_i^{r,f-d} \sigma_e^{f-d} \right)$	<ul style="list-style-type: none"> • Activity • DGS • SDR 	Yes
P_1C2	$\left(\sum_r P_1C1_i^{e,r} y_r^g \lambda_r \right)$	<ul style="list-style-type: none"> • DGS • SDR 	No
P_1C3	$\left(\sum_g P_1C2_i^{e,g} R_i^g \right)$	<ul style="list-style-type: none"> • SDR 	No

5.7 Estimation of the stochastic uncertainty in R2S-UNED

The uncertainty module of R2S-UNED calculates the stochastic uncertainty of the relevant reaction rates, isotopic activity, DGS, and SDR, as section 5.6 explains. The accurate estimation of these uncertainties requires the covariance matrix of the neutron flux. However, the estimation of this matrix is limited by the size of the matrix, as remarked in section 5.1. That is, by the number of spatial regions and the number of energy groups used to describe the neutron flux.

For these cases, where the covariance matrix of the neutron flux cannot be estimated, the uncertainty module of R2S-UNED presupposes the correlation matrix¹ of the neutron flux. Therefore, three additional calculation methods were implemented, according to the assumptions considered with respect to the correlation matrix of the neutron flux.

- i. Completely correlated: The correlation of the neutron flux is considered 1 between all pairs of elements. Consequently, this option is a superior limit of the uncertainty.
- ii. Completely anticorrelated: The correlation of the neutron flux is considered -1 between all pairs of different elements. Consequently, this option is an inferior limit of the uncertainty.
- iii. Uncorrelated: All no diagonal elements of the neutron flux correlation matrix are 0. This option only is adequate when the neutron flux is actually uncorrelated.

¹ The correlation of the variables a and b is defined as $\rho_{a,b} = \frac{cov(a,b)}{\sigma_a \sigma_b}$ [29]

When the SDR uncertainty is calculated¹, the result is split in six different terms, expressed from Equation 5.17 to Equation 5.22.

$$TT_{diag} = \sum_i \sum_g I_i^{g^2} \sigma_{R_i^g}^2$$

Equation 5.17

$$TT_{No_{diag}} = \sum_{i,i'} \sum_{g,g'} I_i^g I_{i'}^{g'} cov(R_i^g, R_{i'}^{g'}) \quad \forall i \neq i' \cap \forall g \neq g'$$

Equation 5.18

$$SS_{diag} = \sum_i \sum_g R_i^{g^2} \sigma_{I_i^g}^2$$

Equation 5.19

$$SS_{No_{diag}} = \sum_{i,i'} \sum_{g,g'} R_i^g R_{i'}^{g'} cov(I_i^g, I_{i'}^{g'}) \quad \forall i \neq i' \cap \forall g \neq g'$$

Equation 5.20

$$ST_{diag} = \sum_i \sum_g \sigma_{R_i^g}^2 \sigma_{I_i^g}^2$$

Equation 5.21

$$ST_{No_{diag}} = \sum_{i,i'} \sum_{g,g'} cov(I_i^g, I_{i'}^{g'}) cov(R_i^g, R_{i'}^{g'}) \quad \forall i \neq i' \cap \forall g \neq g'$$

Equation 5.22

The term TT refers to the uncertainty due to photon transport. That is; the stochastic uncertainty introduced during the MC photon simulation.

The SS terms describe the contribution of the DGS intensity uncertainty to the SDR uncertainty, where the DGS intensity uncertainty comes from the neutron flux uncertainty; that is, from the MC neutron transport simulation.

Finally, the ST term is a second-order term, which takes into account both uncertainties. In most cases, this term is negligible, as shown in Chapter 4.

In addition, these terms are also divided into i) The contribution of the diagonal terms of the correlation matrixes of the photon response and DGS intensity, and ii) The contribution of the no diagonal terms of the correlation matrixes of the photon response and DGS intensity.

¹ Using any of these assumptions or the actual covariance matrix of the neutron flux.

5.8 Summary and conclusions

This section presents the implementation in R2S-UNED of the computational scheme¹ to estimate the SDR uncertainty. This implementation required introducing new features to R2S-UNED, which can be divided into three groups:

I. Estimation of the input data

R2S-UNED common workflow cannot provide all input data required to estimate the SDR stochastic uncertainty. Consequently, it was modified to calculate: i) the covariance matrix of the neutron flux, ii) the derivate of the isotopic concentration to the reaction rates (sensitivity coefficients) iii) the DGS contribution to the SDR².

It is worth highlighting that the estimation of the covariance matrix is limited to cases where the superimposed mesh is relatively small. Otherwise, the size of this matrix is excessively high to be computed.

II. The filtering of relevant quantities according to their contribution to the SDR

The computational time required to estimate the SDR stochastic uncertainty depends on the number of regions, radioisotopes, and reactions considered during the R2S calculation. Consequently, to optimize the simulation, the calculation is reduced to estimate the uncertainty of the SDR coming from the most contributing regions, radioisotopes, and reactions.

It is worth underlining that this information is valuable itself to the analysis of the fusion facilities. Because during this process, the contribution of the different regions and radioisotopes to the SDR is computed. In addition, the reactions are filtered based on the production pathways of the relevant radioisotopes. Consequently, we also developed an algorithm that i) finds the pathways producing the relevant radioisotopes and ii) quantifies their relevance to the SDR.

III. Estimation of the SDR uncertainty

The last implemented feature is the evaluation of the SDR uncertainty. From this point, it is worth mentioning that different calculation modes were implemented in order to provide useful information when the covariance matrix of the neutron flux cannot be obtained. That is; when the actual uncertainty of the R2S calculation cannot be estimated.

These calculation modes are based on assuming the neutron flux is completely correlated, uncorrelated, or anti-correlated. The most relevant one is the completely correlated assumption since it is a superior limit of the SDR uncertainty. That is, it is the most conservative assumption.

¹ All the steps of the scheme are summarized in Table 5.1.

² This work was already implemented in R2S-UNED before the thesis

Chapter 6.

Verification of the developments in R2S-UNED

The previous chapter details the implementation of the uncertainty module of R2S-UNED and those modifications of R2S-UNED needed to obtain all data used to calculate the SDR uncertainty. This chapter presents the verification of all these new steps, summarized in Table 5.1. Below we briefly describe the verification exercises carried out with this purpose for each developed step.

i. Correlation matrix of the neutron flux (section 5.1):

The neutron flux correlation matrix estimated using the developed methodology is compared with those processed by NumPy class of python. Section 6.1 presents a comparison of the results of both methods.

ii. Isotopic contribution to the tally (section 5.4.2):

Section 6.2 presents an R2S simulation whose photon transport is carried out in a complete void material geometry. Consequently, the photon flux in the tally is proportional to the source activity. The verification exercise consisted in comparing the isotopic contribution of the R2S simulation with the activation calculation (calculated with ACAB). The results are also presented in section 6.2.

iii. The most relevant pathways (section 5.4.3):

Two exercises were performed to verify this algorithm. The first one is the detailed analysis of a random small ODE. This exercise aimed to verify that all pathways are detected according to the expected working of the code. The second exercise was a comparison of the pathway contribution calculated by the new and the previous methodology. Both exercises are presented in section 6.3.

iv. Derivative of the isotopic concentration with respect to the reaction rate per target isotope (section 5.5):

R2S-UNED uncertainty module includes two solvers to calculate the sensitivity coefficients. Section 6.4 presents the exercises used to verify each solver. For that, the values provided by them were compared with those calculated with other methods based on activation solvers or python libraries.

v. *Stochastic uncertainty of the SDR calculated with R2S method (Chapter 5):*

R2S-UNED calculates the uncertainty of the reaction rates, isotopic activity, DGS, and the SDR uncertainty due to the MC calculation method. The exercise used to validate all these estimations is presented in Section 6.5. This exercise consists in comparing the uncertainty calculated with R2S-UNED with the uncertainty calculated using the Brute Force method (see Chapter 2). Part of this validation was published in [63].

Finally, section 6.6 presents a summary of the results obtained in this chapter.

6.1 Verification of the algorithm that calculates the neutron flux correlation matrix in R2S-UNED

This section aimed to verify the implementation of the estimation of the correlation matrix of the neutron flux.

The verification of this capability consisted in comparing the results calculated by i) the algorithm implemented in MCNP-R2S, and ii) an algorithm that uses the *NumPy* class [64] of python [65] to process the neutron flux of each history, which was obtained from MCNP-R2S. Note that we assume that the python algorithm works properly since *NumPy* class has been widely tested.

Table 6.1 Definition of SS316LN-IG

Natural element	Weight (%)	Natural element	Weight (%)
B	0.001	Mn	1.8
C	0.0297	Fe	64.8643
N	0.07	Co	0.03
Si	0.5	Ni	12.25
P	0.025	Cu	0.3
S	0.01	Nb	0.01
Ti	0.1	Mo	2.5

The neutron simulation consisted in a box of $1 \times 1 \times 2 \text{ cm}^3$ of SS316LN-IG steel (Table 6.1). The spatial discretization divides the space in a homogeneous $2 \times 2 \times 2$ mesh. The boundaries of the energy resolution of the neutron flux are 0, 0.1, 1.0, and 2.0 MeV. The neutron flux source is uniformly emitted in Z-axis over the 1 cm^2 face. The energy spectrum is sampled with the same probability in each energy bin of the neutron flux (corresponding to the VITAMINJ[66] energy structure, where the group width is not homogeneous), and inside of each bin, the energy is sampled uniformly. The sampled spectrum correspond to those presented in Figure 6.1.

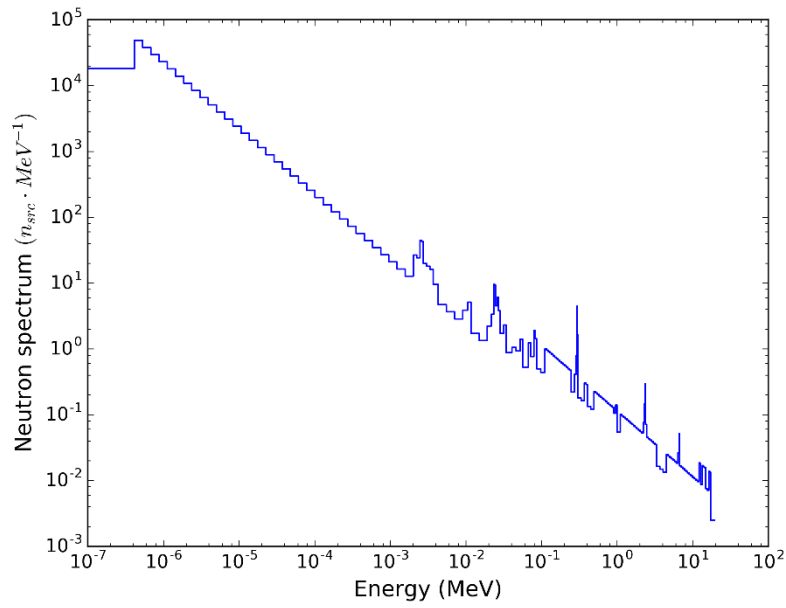


Figure 6.1 Neutron source spectrum

Figure 6.2 presents the relative difference of the correlation of the neutron flux, where the X -axis is a dummy index that represents each pair of neutron flux variables (pair of positions and energy bins). This figure shows that the differences are negligible.

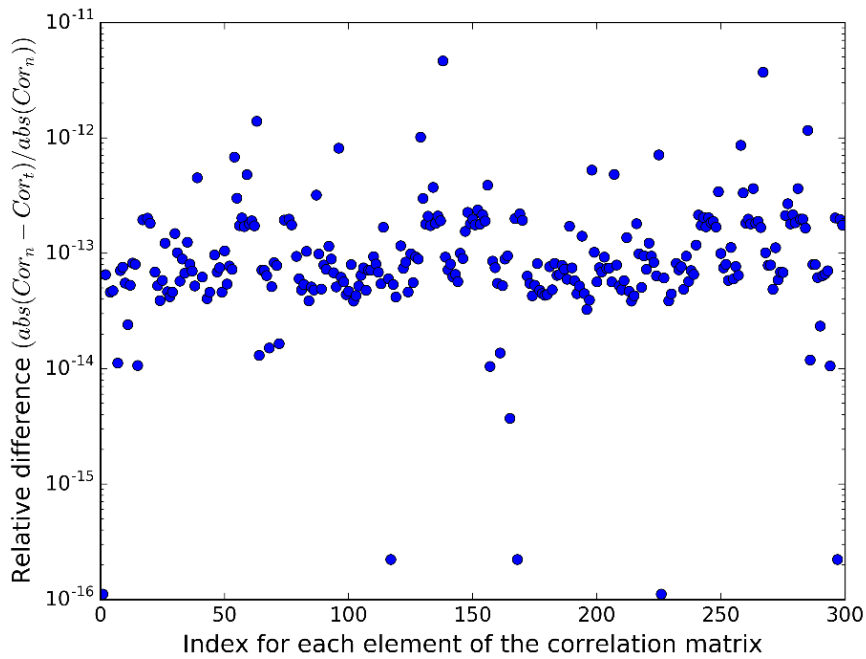


Figure 6.2 Relative difference of the correlation (Cor) calculated using NumPy library (n) or the solver of the transport code (t) of R2S-UNED

6.2 Verification of the algorithm that calculates the isotopic contribution in R2S-UNED

This exercise aims to verify that the isotopic contribution to the SDR, calculated with R2S-UNED uncertainty module, is correct. For that, this section presents an exercise whose response from the R2S simulation is proportional to the number of gamma emitted by the DGS. Therefore we can compare the isotopic contribution from the material activation (relative number of gamma emitted by each isotope) with isotopic contribution calculated by R2S-UNED transporting the DGS (see section 5.4.2).

The exercise consists in the irradiation of a SS316LN-IG steel (Table 6.1) slab whose dimensions are $1 \times 1 \times 0.1 \text{ cm}^3$. The steel slab is wrapped by a void spherical cell. The neutron source is uniformly emitted in Z-axis over the 1 cm^2 face. The neutron source spectrum is sampled with the same probability in each group of the VitaminJ structure [66]. That is, it is sampled according to the spectrum shown in Figure 6.1. The irradiation scenario consists in 10^7 seconds of irradiation and 10^6 seconds of cooling time with an intensity of 1 neutron per second.

The DGS generated in the slab is transported in the same geometry, but removing the material of the slab¹. In this exercise, the photon flux is measured in the void spherical cell. Due to the fact that there are not any attenuation between the source and the response, the photon flux is proportional to the number of gammas emitted by the DGS.

This exercise was performed using R2S-UNED. 10^8 neutron histories were run during the neutron transport, and 10^9 photon histories were run during the photon transport. It is worth noting that the neutron uncertainty does not affect the comparison, because exactly the same uncertainty is introduced in both estimations (activation step and R2S-UNED). However, the stochastic uncertainty of the photon transport only affects the R2S-UNED estimation, and therefore it must be taken into account. In this case, the uncertainty is small enough to be negligible ($<0.5\%$). During the R2S activation step the library containing the photon spectrum was modified deleting all low-energy photons. This way, we guarantee that the energy cut-off of the MCNP-R2S does not kill any photon, which was taken into account during the activation step.

Table 6.2 shows the comparison of the isotopic contribution, calculated from the complete R2S simulation or from the activation step. The results of both estimations are in excellent agreement. Consequently, the R2S-UNED estimation of the isotopic contribution to the tally is adequate.

¹ This means that the photon simulation is performed in a void geometry.

Table 6.2 Contribution to the photon flux calculated from the isotopic activity using R2S-UNED activation solver or from R2S-UNED uncertainty module

<i>Isotope</i>	<i>Activity (Bq)</i>	<i>Yield (γBq⁻¹)</i>	<i>Contribution calculated from the activation step (%)</i>	<i>Contribution calculated from R2S-UNED simulation (%)</i>
<i>Co⁵⁸</i>	$4.56 \cdot 10^{-5}$	1.5692	68.32	68.32
<i>Mn⁵⁴</i>	$8.48 \cdot 10^{-6}$	1.2545	9.71	9.71
<i>Co⁵⁷</i>	$7.89 \cdot 10^{-6}$	1.6270	8.61	8.61
<i>Ta¹⁸²</i>	$2.25 \cdot 10^{-6}$	3.7848	5.84	5.84
<i>Cr⁵¹</i>	$4.06 \cdot 10^{-5}$	0.3251	4.53	4.53
<i>Co⁶⁰</i>	$3.87 \cdot 10^{-7}$	1.9986	0.98	0.98
<i>Fe⁵⁹</i>	$5.82 \cdot 10^{-7}$	1.0406	0.74	0.74
<i>Tc^{99m}</i>	$3.96 \cdot 10^{-7}$	0.9688	0.45	0.45
<i>Nb^{92m}</i>	$1.44 \cdot 10^{-7}$	1.7163	0.31	0.31
<i>Mo⁹⁹</i>	$4.09 \cdot 10^{-7}$	0.3344	0.18	0.18
<i>Nb⁹¹</i>	1.3610^{-7}	0.6975	0.10	0.10
<i>Nb⁹⁵</i>	$7.06 \cdot 10^{-7}$	0.9996	0.10	0.10
<i>Sc⁴⁶</i>	$1.95 \cdot 10^{-8}$	1.9997	0.05	0.05
<i>Ni⁵⁷</i>	$7.74 \cdot 10^{-9}$	2.2286	0.02	0.02

6.3 Verification and validation of the algorithm that calculates the contributing production pathways in R2S-UNED

This section aims to verify the implementation of the method to evaluate the importance of the pathways that produce the relevant isotopes¹. For that, two exercises were performed:

The first one consists in analyzing a simple matrix to follow systematically the algorithm which detects the pathways. This exercise aims to verify that the pathways are found according to the expected working of the algorithm. The results of this exercise are presented in section 6.3.1.

The second exercise compares the method depicted in section 5.4.3.2 with a “hand-made” methodology used to calculate the contribution of the pathways with ACAB. This comparison, described in section 6.3.2, is carried out in a ITER exercise analyzed in previous works [67] [68].

¹ We refer to the method, introduced in section 5.4.3.2, that deals with general activation systems.

In addition to its application during the thesis, the method was also successfully applied to find the most relevant chains in ITER [56] [69].

It is worth highlighting that in all its practical applications of JET, ITER, and DEMO, no relevant loops were found in the pathways that produce the most relevant isotopes. This suggests that the implemented method is enough for most of the practical applications where R2S-UNED is used. Other studies also support this idea [59]–[61], with very few exceptions named in them. Nevertheless, the implemented module can consider them when they are relevant.

6.3.1 Estimation of the pathway contributions in a simple matrix

This study aims to show that the different pathways are correctly detected, and the contribution is always less or equal to 100%. During this exercise, we consider that the ACAB evaluation is correct. Therefore, the estimation of the pathway contribution is also correct.

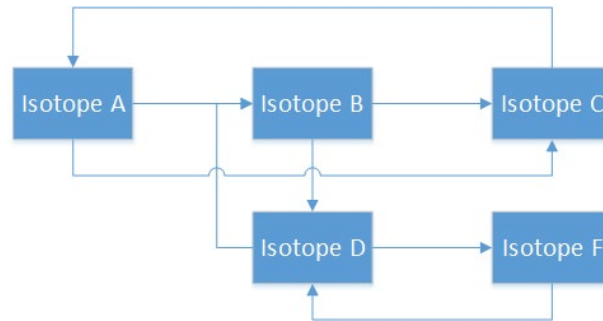


Figure 6.3 Scheme of the activation case for verifying the algorithm to look for the relevant pathways

The studied case is shown in Figure 6.3, where the isotope C is the relevant isotope to our “activation system”. The transition matrix, which represents the activation system of Figure 6.3, was generated randomly. This matrix is shown in Equation 6.1, where the order of the isotopes was assigned according to the alphabetic order.

$$\text{General case: } \hat{A} = \begin{pmatrix} -1.532 & 0.000 & 0.522 & 0.000 & 0.000 \\ 0.839 & -0.780 & 0.000 & 0.710 & 0.000 \\ 0.693 & 0.409 & -0.522 & 0.000 & 0.000 \\ 0.000 & 0.371 & 0.000 & -1.298 & 0.980 \\ 0.000 & 0.000 & 0.000 & 0.588 & -0.980 \end{pmatrix}$$

Equation 6.1

This case was analyzed using the three different pathway definitions, which are:

- i. Linear chains
- ii. Linear chains with loops¹
 - Only loops with metastable estates
 - General loops

¹ The algorithm only considers the loops if it contains an isotope which belongs to the considered linear chain between the relevant isotope and the initial material isotope.

iii. General contribution from the nonzero initial concentration isotope¹

For the linear chain mode, the found pathways are the linear chains A-C and A-B-C. The matrix of the ODEs system that represents these pathways are presented in Equation 6.2

$$\begin{aligned} \text{Linear chain 1: } \hat{A} &= \begin{pmatrix} -1.532 & 0 \\ 0.693 & -0.522 \end{pmatrix} \\ \text{Linear chain 2: } \hat{A} &= \begin{pmatrix} -1.532 & 0 & 0 \\ 0.839 & -0.780 & 0 \\ 0 & 0.409 & -0.522 \end{pmatrix} \end{aligned}$$

Equation 6.2

The linear chains and loops mode found two linear chains and the correspondent loops. That is the loops that contain at least one isotope of the linear chain. These systems are represented in Equation 6.3

$$\begin{aligned} \text{Linear chain and loops 1: } \hat{A} &= \begin{pmatrix} -1.532 & 0.522 \\ 0.693 & -0.522 \end{pmatrix} \\ \text{Linear chain and loops 2: } \hat{A} &= \begin{pmatrix} -1.532 & 0 & 0.522 & 0 \\ 0.839 & -0.780 & 0 & 0.710 \\ 0 & 0.409 & -0.522 & 0 \\ 0 & 0.371 & 0 & -1.298 \end{pmatrix} \end{aligned}$$

Equation 6.3

Finally, the last mode found the matrix of Equation 6.4.

$$\text{Contribution case: } \hat{A} = \begin{pmatrix} -1.532 & 0 & 0.522 & 0 \\ 0.839 & -0.780 & 0 & 0.710 \\ 0.693 & 0.409 & -0.522 & 0 \\ 0 & 0.371 & 0 & -1.298 \end{pmatrix}$$

Equation 6.4

The contribution of the different presented pathways and the loops found is presented in Table 6.3.

This table shows that the algorithm finds the corresponding pathways. Only the loop which contains the isotope F was not found due to the loop definition². In addition, when a new loop is considered, the pathway contribution is increased, as expected (missing isotopes are re-incorporated via the loop). The results of this exercise indicate that the algorithm finds the possible pathways properly.

¹ This method was not included in the module of uncertainty of R2S-UNED developed in the thesis, since it considers excessive reactions. Consequently, it does not filter the most important reactions.

² Note that the loop D-F is not taken into account since any of these isotopes belongs to the principal chain

Table 6.3 Pathways detected by the method according to the search option

Mode	Loops	Principal path	Contribution (%) ¹
Linear Chains	-	Path 1: A → C	75.529
		Path 2: A → B → C	21.805
		Total	94.334
Linear Chains and loops	. C → A. B ↔ D	Path 1: A → C	76.907
		Path 2: A → B → C	21.870
		Total	98.777
All contribution	. C → A. B ↔ D	A → C A → B → C	99.998

6.3.2 Verification and Validation of the pathway contribution calculation method in ITER

This section compares the contribution of the pathways calculated using the developed method², with a previous method (hereinafter it will be called elimination method) used at UNED to quantify the pathway. The methods are compared in ITER activation environment³ [67] [68].

The elimination method works as follow:

- i. The complete ODE⁴ system is solved. This result is the reference isotopic concentration
- ii. The studied reaction is deleted from the activation library
- iii. The new ODEs system is solved.
- iv. The relative loss of concentration is associated to the importance of the reaction.

The method described in section 5.4.3.2 estimates the importance of the pathways in the production of a radioisotope. However, the elimination method directly gets the importance of the different reactions. The pathway contribution is derived from the importance of the reactions which compose the pathway.

It is worth noting that the total importance defined by this method can be different to one⁵ (even higher than one) due to the influence of a reaction in the rest of the pathways. Consequently, this method has some limitations to its general application:

¹ Due to the features of the proposed ODEs system, ACAB code guarantee the error of the isotopic concentration is about 10⁻⁶ the result [102].

² We refer to the method, introduced in section 5.4.3.2, which deals with general activation systems.

³ These works were performed, using the previous algorithm, before this thesis.

⁴ These activation ODEs systems were solved using ACAB code

⁵ As section 5.4.3.2 comments, the reaction contribution cannot be defined.

- i. The burn-up cannot be considered: Since the reaction is deleted before the calculation, the loss of isotope due to the reaction is not properly considered during the temporal evolution of the isotopic inventory.
- ii. One reaction can belong to more than one pathway, then, careful analysis must be done to determine the contribution of the rest of the reactions.

In this thesis, we take advantage of the works [67] [68], which use the elimination method methodology to detect the most relevant reactions in SDR analysis performed in ITER environment, in order to a future investigation of the quality of these cross-sections. For that, they evaluate the activation of common materials located in the port interspace (PI) and port cell (PC) at the relevant times to the maintenance activities in both areas (at 1 day in the PI and 12 days in the PC). These regions are shown in Figure 6.4.

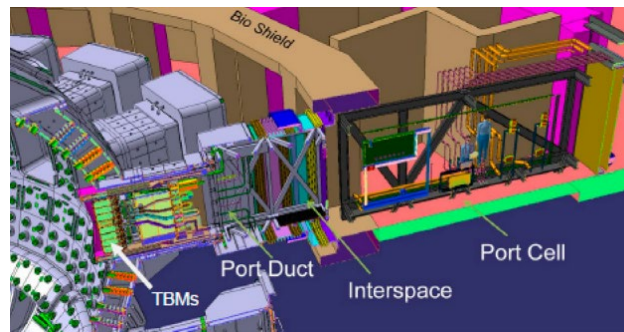


Figure 6.4 ITER Port Cell (PC) and Port Interspace (PI) areas [67].

The neutron flux calculated in both regions are shown in Figure 6.5, and the SA-2 irradiation scenario was considered to perform the material activation [70].

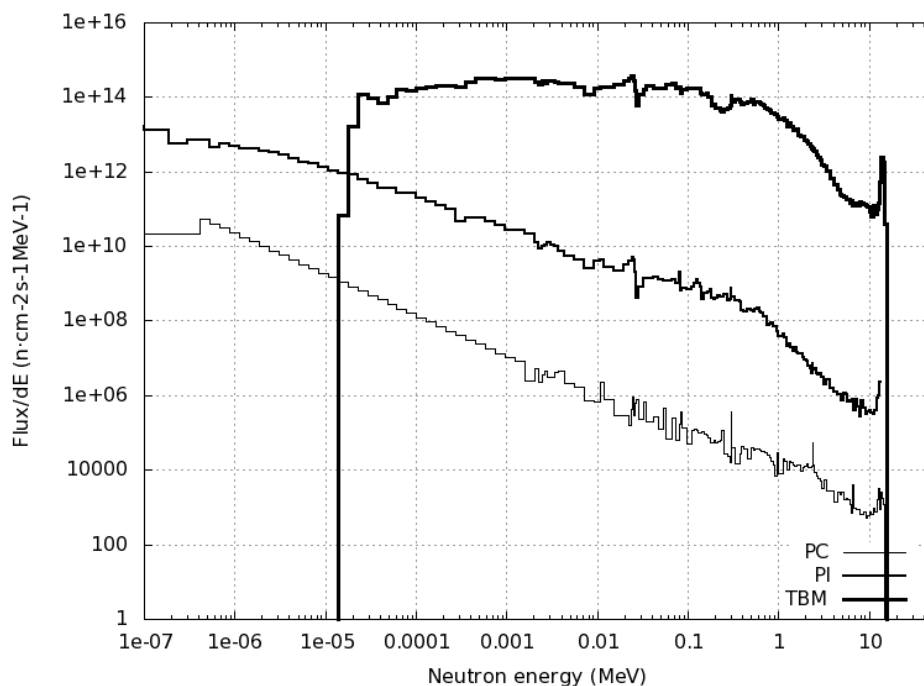


Figure 6.5 Neutron flux used for activation calculation [67]

Chapter 6
Verification of the developments in R2S-UNED

Since this ITER application meets SNILB conditions, the elimination method is suitable for this specific application. Consequently, we can use this exercise, presented in [67] [68], to validate our implementation.

The results calculated applying the elimination method¹ were obtained from the literature[67] [68]. Tables from Table 6.4 to Table 6.8 present those calculated obtained from the elimination method and the new method (implemented in *Achains* program²). All results provided by *Achains* are in excellent agreement with the results obtained from the literature.

Table 6.4 Pathways for radionuclides of interest from ACAB+EAF-2007 activation simulation for conventional concrete.

Major radionuclide	Cooling time (days)	Relevant pathways and contribution (%)	
		Literature	<i>Achains</i>
²⁴ Na	1	²³ Na(n,g) ²⁴ Na (99.6)	²³ Na(n, γ) ²⁴ Na (70.5)
			³ Na(n, γM) ^{24m} Na(γ) ²⁴ Na (29.1)

Table 6.5 Pathways for radionuclides of interest from ACAB+EAF-2007 activation simulation for barite concrete.

Major radionuclide	Cooling time (days)	Relevant pathways and contribution (%)		
		Literature	<i>Achains</i>	
²⁴ Na	1	²⁴ Mg(n,p) ²⁴ Na (33.6)	²⁴ Mg(n,p) ²⁴ Na (23.3)	
			²⁴ Mg(n,p_s) ^{24m} Na (γ) ²⁴ Na (10.4)	
			²⁷ Al(n,α) ²⁴ Na (66.3)	²⁷ Al(n, α) ²⁴ Na (45.8)
			²⁷ Al(n,a_s) ^{24m} Na (γ) ²⁴ Na (20.5)	
⁵⁴ Mn	1	⁵⁴ Fe(n,p) ⁵⁴ Mn (100)	⁵⁴ Fe(n,p) ⁵⁴ Mn (100)	
⁵⁹ Fe	1	⁵⁸ Fe(n,g) ⁵⁹ Fe (100)	⁵⁸ Fe(n, γ) ⁵⁹ Fe (100)	
¹³¹ Ba	1	¹³⁰ Ba(n,g) ¹³¹ Ba (99.9)	¹³⁰ Ba(n, γ) ¹³¹ Ba (74.9)	
			¹³⁰ Ba(n, γM) ^{131m} Ba (γ) ¹³¹ Ba (25.0)	
¹³³ Ba	1	¹³² Ba(n,g) ¹³³ Ba (97.1)	¹³² Ba(n, γ) ¹³³ Ba (89.3)	
			¹³² Ba(n,g) ^{133m} Ba (γ) ¹³³ Ba (7.8)	
			¹³⁴ Ba(n,2n) ¹³³ Ba (2.7)	¹³⁴ Ba(n,2n) ¹³³ Ba (1.5)
			¹³⁴ Ba(n,2n) ^{133m} Ba (γ) ¹³³ Ba (1.4)	
^{135m} Ba	1	¹³⁴ Ba(n,g) ^{135m} Ba (58.6)	¹³⁴ Ba(n, γ) ^{135m} Ba (58.6)	
			¹³⁵ Ba(n,n') ^{135m} Ba (32.5)	¹³⁵ Ba(n,n') ^{135m} Ba (32.5)
			¹³⁶ Ba(n,2n) ^{135m} Ba (8.9)	¹³⁶ Ba(n,2n) ^{135m} Ba (8.9)

¹ In the results of the elimination method, two-step pathways, which meet the conditions presented in section 5.4.3.1, were considered inside of the direct pathway. In *Achains*, these details are depicted.

² The methodology proposed to detect pathways and quantify their contribution was implemented was also implemented to individual activation calculations. In this framework, out of R2S method, the code where this methodology was implemented is called *Achains*.

Table 6.6 Pathways for radionuclides of interest from ACAB+EAF-2007 activation simulation for L2N concrete.

Major radionuclide	Cooling time (days)	Relevant pathways and contribution (%)	
		Literature	Achains
⁵⁴ Mn	12	⁵⁴ Fe (n,p) ⁵⁴ Mn (94.3)	⁵⁴ Fe (n,p) ⁵⁴ Mn (94.3)
		⁵⁵ Mn (n,2n) ⁵⁴ Mn (5.7)	⁵⁵ Mn (n,2n) ⁵⁴ Mn (5.7)
⁵⁹ Fe	12	⁵⁸ Fe(n,g) ⁵⁹ Fe (98.8)	⁵⁸ Fe(n, γ) ⁵⁹ Fe (98.8)
		⁵⁹ Co(n,p) ⁵⁹ Fe (1.2)	⁵⁹ Co(n,p) ⁵⁹ Fe (1.2)
⁶⁰ Co	12	⁵⁹ Co(n,g) ⁶⁰ Co (100)	⁵⁹ Co(n, γ) ⁶⁰ Co (55.6)
			⁵⁹ Co(n,g_m) ^{60m} Co(γ) ⁶⁰ Co (44.4)
¹³⁴ Cs	12	¹³³ Cs(n,g) ¹³⁴ Cs (100)	¹³³ Cs(n, γ) ¹³⁴ Cs (90.9)
			¹³³ Cs(n,g) ^{134m} Cs(γ) ¹³⁴ Cs (9.1)
¹⁵² Eu	12	¹⁵¹ Eu(n,g) ¹⁵² Eu (100)	¹⁵¹ Eu(n, γ) ¹⁵² Eu (99.9)
¹⁵⁴ Eu	12	¹⁵³ Eu(n,g) ¹⁵⁴ Eu (100)	¹⁵³ Eu(n, γ) ¹⁵⁴ Eu (98.4)
			¹⁵³ Eu(n, γ) ^{154m} Eu(γ) ¹⁵⁴ Eu (1.6)
¹⁶⁰ Tb	12	¹⁵⁹ Tb(n,g) ¹⁶⁰ Tb (100)	¹⁵⁹ Tb(n, γ) ¹⁶⁰ Tb (100)

Table 6.7 Pathways for radionuclides of interest from ACAB+EAF-2007 activation simulation for Cu.

Major radionuclide	Cooling time (days)	Relevant pathways and contribution (%)	
		Literature	Achains
⁶⁴ Cu	1	⁶³ Cu(n,g) ⁶⁴ Cu (100)	⁶³ Cu(n, γ) ⁶⁴ Cu (100)
⁶⁰ Co	12	⁶³ Cu(n,a) ⁶⁰ Co (100)	⁶³ Cu(n, γ) ⁶⁰ Co (74.3)
			⁶³ Cu(n, γM) ^{60m} Co(γ) ⁶⁰ Co (25.7)
^{110m} Ag	12	¹⁰⁹ Ag(n,g) ^{110m} Ag (100)	¹⁰⁹ Ag(n, γM) ^{110m} Ag(100)

Table 6.8 Pathways for radionuclides of interest from ACAB+EAF-2007 activation simulation for W.

Major radionuclide	Cooling time (days)	Relevant pathways and contribution (%)	
		Literature	Achains
^{182}Ta	12		$^{182}\text{W}(n,p) \ ^{182}\text{Ta}(92.7)$
			$^{182}\text{W}(n,p \text{ N}) \ ^{182\text{s}}\text{Ta}(\gamma) \ ^{182\text{m}}\text{Ta}(\gamma)$
			$^{182}\text{Ta}(2.9)$
			$^{182}\text{W}(n,p) \ (98.3)$
			$^{182}\text{W}(n,p_M) \ ^{182\text{m}}\text{Ta}(\gamma) \ ^{182}\text{Ta}(2.7)$
			$^{183}\text{W}(n,D) \ ^{182\text{m}}\text{Ta}(\gamma) \ ^{182}\text{Ta}(0.6)$
			$^{183}\text{W}(n,D) \ (1.2) \ ^{182}\text{Ta}$
			$^{183}\text{W}(n,np) \ ^{182\text{m}}\text{Ta}(\gamma) \ ^{182}\text{Ta}(0.3)$
			$^{183}\text{W}(n,D) \ ^{182}\text{Ta}(0.6)$
			$^{183}\text{W}(n,np) \ ^{182}\text{Ta}(0.1)$
^{181}W	12		$^{180}\text{W}(n,g) \ ^{181}\text{W} (50.6)$
			$^{180}\text{W}(n, \gamma) \ ^{181}\text{W} (50.6)$
			$^{182}\text{W}(n,2n) \ ^{181}\text{W} (49.4)$
^{187}W	1		$^{186}\text{W}(n,g) \ ^{187}\text{W} (100)$
	12		$^{186}\text{W}(n, \gamma) \ ^{187}\text{W} (100)$

6.4 Verification of the algorithm that calculates the derivatives of the concentration to the reaction rates per target isotope in R2S-UNED

This section is divided into two subsections; each one deals with the verification of one of the solvers, implemented in the uncertainty module of R2S-UNED, to calculate the sensitivity coefficients (see section 5.5). Section 6.4.1 verifies the appropriate working of the solvers when SNILB conditions are met, while section 6.4.2 deals with the verification of the general-purpose solver.

6.4.1 Verification of the algorithm when SNILB conditions are met

This section verifies the specific solver to SNILB conditions as well as the general-purpose solver when SNILB conditions are met. For that, the results of the implemented solvers¹ are compared with those derived from the activation calculation of two verified activation codes:

¹ Note that the approach to consider 2 step pathways (see section 5.4.3.1) using the SNILB solver, was also considered during the application of the general-purpose solver. This way, both codes detect exactly the same pathways

- i. `d1stime.py`: It is a verified python script that calculates the correction factor (associated with the irradiation scenario) in D1S-UNED simulations. This coefficient allows directly evaluating the sensitivity coefficient (see Equation 3.14)
- ii. ACAB solver¹: It is used to calculate the isotopic concentration at the time of interest. Assuming no initial concentration of the relevant radioisotope $N_2(0) = 0$, the sensitivity coefficient (Equation 3.14) can be calculated by dividing the isotopic concentration calculated by ACAB (Equation 3.12) by the corresponding reaction rate.

Table 6.9 Mixture material

Isotope	Atoms (%)	Isotope	Atoms (%)
Cu⁶³	25	Mn⁵⁵	25
Co⁵⁹	25	Cr⁵²	25

The activation case, where these methods were compared, consists in the irradiation of $2 \cdot 10^{22}$ atoms of the material described in Table 6.9. The neutron spectrum was sampled according to Figure 6.1. The irradiation scenario used was the SA-2² [70], which is commonly assumed in ITER analyses.

Table 6.10 Derivative of the isotopic concentration with respect to the reaction rate per target isotope (at·s)

Reaction	D1S-time.py	ACAB solver	SNILB solver	General solver
<i>Co⁵⁹-Co⁶⁰</i>	$8.20649 \cdot 10^{30}$	$8.20649 \cdot 10^{30}$	$8.20662 \cdot 10^{30}$	$8.20662 \cdot 10^{30}$
<i>Co⁵⁹-Co⁵⁸</i>	$6.07310 \cdot 10^{29}$	$6.07310 \cdot 10^{29}$	$6.07320 \cdot 10^{29}$	$6.07320 \cdot 10^{29}$
<i>Cr⁵²-Cr⁵¹</i>	$2.01288 \cdot 10^{29}$	$2.01288 \cdot 10^{29}$	$2.01292 \cdot 10^{29}$	$2.01292 \cdot 10^{29}$
<i>Cu⁶³-Cu⁶⁴</i>	$1.58515 \cdot 10^{21}$	$1.58515 \cdot 10^{21}$	$1.58517 \cdot 10^{21}$	$1.58521 \cdot 10^{21}$
<i>Mn⁵⁵-Mn⁵⁴</i>	$2.23108 \cdot 10^{30}$	$2.23108 \cdot 10^{30}$	$2.23111 \cdot 10^{30}$	$2.23111 \cdot 10^{30}$

Table 6.10 shows the results of the four methods are in excellent agreement. The difference is due to the decay constant value. In the case of D1S-time.py and ACAB solver, the decay constants are read directly from the EAF decay library. However, the uncertainty module of R2S read this data from the DECAY.dat³ library (specific library used by ACAB code [41]).

¹ ACAB solver refers to the three subroutines used in ACAB to solve the ODEs system, which were originally implemented in ORIGEN[48]. See section 3.4.1

² The scenario is complicated enough because this has several sets of pulses of different intensities. Then it can be considered as representative of any other scenario used.

³ DECAY.dat library contains also EAF data but with fewer significant digits than the EAF decay library.

6.4.2 Verification of the general-purpose algorithm

This section verifies the estimation of the derivatives of the isotopic concentration to the reaction rates when the SNILB conditions are not met. For that, two different cases are performed. The first one consists in a two-isotope case where the burn-up is important. The second case verifies the derivatives of several reactions of pathways where the Single Neutron Interaction is not met.

The verification consists in the comparison of numerical derivatives, with the results obtained by the general-purpose solver of R2S-UNED uncertainty module. The numerical derivative¹ code couples the *ScyPy* [71] python library with the ACAB and Euler ODEs solvers to calculate linear chains.

It is worth highlighting that Euler solver was also implemented as the ODEs solver of the general-purpose algorithm². Thus, we can distinguish if the possible differences are due to the implemented methodology, or to the accuracy of the ODEs solver used to carry out the estimation of the sensitivity coefficients.

6.4.2.1 Verification of the estimation of the sensitivity coefficients when the burn up is relevant

This case consists in the activation of the chain A-B where the initial concentration of A is 10^{10} isotopes and there is no initial concentration of B. B is an unstable isotope whose decay constant is 10^{-6} s^{-1} . The reaction rate between A-B is $2 \cdot 10^{-6} \text{ reaction} \cdot \text{s}^{-1} \cdot \text{at}^{-1}$, and the irradiation scenario consisted in an irradiation of 10^7 seconds and a cooling time of 10^6 seconds.

Table 6.11 Derivatives of the concentration with respect to the reaction rate (at·s) when the burn up is extremely important

Numerical derivative (Euler)	Numerical derivative (ACAB)	Complete ODEs system (ACAB)	Complete ODEs system (EULER)
$-1.666 \cdot 10^{11}$	$-1.669 \cdot 10^{11}$	$-1.622 \cdot 10^{11}$	$-1.669 \cdot 10^{11}$

The results of the case, presented in Table 6.11, show an excellent agreement between all the methodologies and the analytical solution ($-1.669 \cdot 10^{11} \text{ at} \cdot \text{s}$). The complete ODEs system solved by ACAB shows a slight difference from the other solutions. However, the difference is small enough to its effect in the SDR uncertainty was negligible if this kind of error would happen using the uncertainty module of R2S-UNED. Nevertheless, it suggests that ACAB solver performance must be evaluated. This error can be due to the detected problems of ACAB [62] or to ACAB modification (see section 5.5).

¹ This method was not used to estimate the sensitivity coefficient in R2S-UNED because it is slower than implemented one calculating all the required derivatives.

² The final implementation of the general-purpose solver in R2S-UNED does not consider Euler since it is slower and requires the election of the time step in order to control the accuracy of the solver.

6.4.2.2 *Verification of the estimation of the sensitivity coefficients when the pathways are linear chains of more than one reaction*

This exercise evaluates the derivatives of the most important reactions that produce Ta¹⁸² from pure tungsten¹ in the activation exercise described in Table 6.12. Where the irradiation scenario consisted in an irradiation of 10⁷ seconds and a cooling time of 10⁶ seconds.

Table 6.12 Relevant data to define the activation system to produce ¹⁸²Ta

<i>Variable</i>	<i>Value</i>
<i>¹⁸²W initial concentration</i>	1.649·10 ²¹ Atoms
<i>¹⁸⁰W initial concentration</i>	7.469·10 ¹⁸ Atoms
<i>¹⁸³W initial concentration</i>	8.909·10 ²⁰ Atoms
<i>¹⁸²W- ¹⁸²Ta reaction rate</i>	3.609·10 ⁻¹⁴ reactions/s/atoms
<i>¹⁸²W- ¹⁸¹W reaction rate</i>	1.771·10 ⁻¹¹ reactions/s/atoms
<i>¹⁸⁰W- ¹⁸¹W reaction rate</i>	7.426·10 ⁻¹⁰ reactions/s/atoms
<i>¹⁸³W- ^{182m}Ta reaction rate</i>	3.514·10 ⁻¹⁵ reactions/s/atoms
<i>¹⁸³W- ¹⁸¹W reaction rate</i>	1.677·10 ⁻¹² reactions/s/atoms
<i>¹⁸²W- ^{182s}Ta reaction rate</i>	1.133·10 ⁻¹⁵ reactions/s/atoms
<i>¹⁸¹Ta - ¹⁸²Ta reaction rate</i>	1.474·10 ⁻⁹ reactions/s/atoms

The exercise was solved with the numerical and general solvers. Table 6.13² presents the results of this exercise.

It is worth highlighting that the implementation of the numerical derivative only enables linear chains to be solved. Then, if one reaction belongs to more than one pathway, the derivative of the concentration due to this reaction is the sum of the derivative of each pathway³. On the contrary, the general-purpose solver implemented in R2S-UNED uncertainty module solves all the system that produces the relevant isotope in only one calculation. Consequently, its results are directly the complete derivative of the isotopic concentration with respect to the corresponding reaction rate per target isotope.

¹ This activation exercise contains one of the most common pathway of more than one step found in SDR analysis of fusion facilities [21].

² Despite of the ODEs system was also solved using Euler solver, only ACAB solver results are presented because both solvers provides exactly the same result.

³ This is due to the isotope concentration can be expressed as the sum of the isotopic concentrations of all the pathways that produce this isotope.

Table 6.13 Derivatives of the isotopic concentration of tantalum 182 with respect to the reactions. The reactions are represented in bold font.

Chain and reaction	Numeric derivative (at·s)	complete system (at·s)
$^{182}\text{W} - ^{182}\text{Ta}$	$1.10618 \cdot 10^{28}$	$1.10606 \cdot 10^{28}$
$^{182}\text{W} - ^{181}\text{W} - ^{181}\text{Ta} - ^{182}\text{Ta}$	$1.79605 \cdot 10^{25}$	$1.79581 \cdot 10^{25}$
$^{180}\text{W} - ^{181}\text{W} - ^{181}\text{Ta} - ^{182}\text{Ta}$	$8.10221 \cdot 10^{22}$	$8.10221 \cdot 10^{22}$
$^{183}\text{W} - ^{182\text{m}}\text{Ta} - ^{182}\text{Ta}$	$5.97549 \cdot 10^{27}$	$5.97543 \cdot 10^{27}$
$^{183}\text{W} - ^{181}\text{W} - ^{181}\text{Ta} - ^{182}\text{Ta}$	$9.70292 \cdot 10^{24}$	$9.70280 \cdot 10^{24}$
$^{182}\text{W} - ^{182\text{s}}\text{Ta} - ^{182\text{m}}\text{Ta} - ^{182}\text{Ta}$	$1.10629 \cdot 10^{28}$	$1.10612 \cdot 10^{28}$
$^{182}\text{W} - ^{181}\text{W} - ^{181}\text{Ta} - ^{182}\text{Ta}$	$2.14880 \cdot 10^{23}$	-
$^{180}\text{W} - ^{181}\text{W} - ^{181}\text{Ta} - ^{182}\text{Ta}$	$4.07374 \cdot 10^{22}$	-
$^{183}\text{W} - ^{181}\text{W} - ^{181}\text{Ta} - ^{182}\text{Ta}$	$1.09925 \cdot 10^{22}$	-
Suma: $^{181}\text{Ta} - ^{182}\text{Ta}$	$2.66609 \cdot 10^{23}$	$2.66609 \cdot 10^{23}$

The results calculated by both methods present an excellent agreement. Consequently, the implementation of the ACAB solver to calculate the derivatives can be considered correct.

6.5 Verification of the algorithm that transports the stochastic uncertainty in the neutron flux until the SDR uncertainty

The exercise aims to validate each step of the SDR uncertainty calculation in a simple R2S example in order to make all the steps involved traceable. This R2S simulation must be suitable to calculate the stochastic SDR uncertainty using the R2S-UNED uncertainty module. In addition, the R2S simulation must allow applying the brute force method in order to compare the results of both approaches. This means that:

- i. R2S simulation must be fast to run a high enough number of clone cases to estimate the SDR uncertainty using the brute force method.
- ii. The number of mesh elements must be small enough to estimate the correlation matrix.

In addition, the exercise must verify both calculation modes of the uncertainty module of R2S-UNED. They are the faster and simpler mode which is useful when SNILB conditions are met (sections 5.4.3.1 and 5.5.1), and the more complete method to deal with a general activation case (sections 5.4.3.2 and 5.5.2).

Considering these points, we define an R2S exercise to validate the algorithms. It consisted in the activation of a small slab in order to measure the photon flux in the surrounding of the

slab¹. The dimensions of the slab are 1 cm² of surface and 0.1 cm of thickness. Neutrons uniformly irradiated this slab² for 10⁷ seconds, followed by 10⁶ seconds of cooling time. The source energy spectrum was defined according to the Vitamin-J group structure with equal emission probability for each group. This spectrum is shown in Figure 6.1.

Concerning the library data used in the R2S transport simulations, the neutron transport used FENDL3.1 [72] library while the photon transport used MCPLIB04[73] library. Regarding the activation, the EAF2007 [74] library with Vitamin-J [66] group structure and flat weighting function were considered to estimate the reaction rates³. The DGS was described in three energy groups, whose boundaries are 0.0, 1.0, 5.0 and 20.0 MeV.

About the material and irradiation scenario, they change between the simulation where SNILB⁴ conditions are met or the general activation case as follows:

For the SNILB case, the material was natural nickel, while the irradiation scenario consisted in 10⁷ seconds of irradiation and 10⁶ seconds of cooling time with an intensity of 1n/s. These conditions guarantee that SNILB conditions are met. This case is detailed in section 6.5.1.

For the general activation case, the material was natural tungsten, which was irradiated with an intensity of 10¹⁴ n/s. The irradiation scenario consisted in 10⁷ seconds of irradiation and 10⁶ seconds of cooling time. These conditions are enough to produce relevant isotopes by pathways that do not meet SNILB conditions. The results of this exercise are presented in section 6.5.2.

It is worth noticing that the general activation case was repeated, considering only the pathways producing Ta¹⁸². This way, the relevance of the pathways, which do not meet SNILB conditions, is increased⁵.

6.5.1 Verification of the uncertainty estimation when SNILB conditions are met

This section describes the uncertainty of the R2S simulation of the nickel slab. The R2S-UNED simulation was completely run⁶, including the uncertainty module, according to the earlier R2S simulation description. The relevant input parameters of R2S-UNED uncertainty module are detailed in Table 6.14.

¹ The proposed exercise is similar to the exercise described in section 6.1.

² The slab is irradiated according to the Z-axis, perpendicular to the face of 1cm²

³ Therefore, the neutron flux was also calculated using Vitamin-J energy group structure.

⁴ The results of this verification case of the tool were published in [63].

⁵ It is worth highlighting that the estimation of the stochastic R2S uncertainty, without any additional limitation during the activation step, was one of the aims of the thesis.

⁶ Neutron and photon transport were run up to 10⁶ source histories were simulated

Table 6.14 Relevant parameters of the R2S-UNED uncertainty module in the nickel slab simulation

<i>Parameters</i>	<i>Value</i>
<i>Spatial filter</i>	100%
<i>Isotopic Filter</i>	99.8%
<i>Reaction Filter</i>	99.9%
<i>Solver</i>	SNILB
<i>Two step chains by immediately decay</i>	Ni ⁵⁷ -Co ⁵⁷ Co ^{58m} -Co ⁵⁸ Co ^{60m} -Co ⁶⁰

The R2S simulation was carried out to estimate the most relevant isotopes and reactions. The brute force simulation calculates only the most relevant isotopes and reactions previously detected. The results of the most relevant isotopes and reactions are presented in Table 6.15.

Table 6.15 Isotope contribution to the photon flux and pathways that produce them

<i>Isotope</i>	<i>Photon flux contribution</i>	<i>Pathway</i>	<i>Contribution to the isotope production</i>
<i>Co⁶⁰</i>	0.18%	Ni ⁶⁰ -Co ⁶⁰	99.24%
		Ni ⁶¹ -Co ⁶⁰	0.74%
<i>Co⁵⁸</i>	97.50%	Ni ⁵⁸ -Co ⁵⁸	99.99%
<i>Co⁵⁷</i>	2.20%	Ni ⁵⁸ -Co ⁵⁷	100%

Consequently, the covariance matrix of the reaction rates, activity, DGS intensity, and photon flux were calculated considering only these relevant pathways. The estimation was carried out using R2S-UNED and the brute force method (1000 R2S cases).

The uncertainty of these quantities was calculated using two different spatial discretizations; 1 mesh element and 6 mesh elements. The 1 mesh element allows following each detail of the calculation, while the 6 mesh elements case allows verifying the correlation between different regions¹. Subsections 6.5.1.1 and 6.5.1.2 present these cases.

6.5.1.1 1-Voxel case

The correlation of the neutron flux is presented in Figure 6.6. In this figure, all the correlations below 0.01 are printed in white colour. The figure shows that the neutron flux is almost not correlated, as it was expected because the slab is small, and the neutrons do almost not suffer interactions with the material. The standard deviation of the neutron flux is close to 1.5% in each bin.

¹ The code uses different subroutines to deal with the uncertainty of a mesh than to deal with the uncertainty between two correlated regions

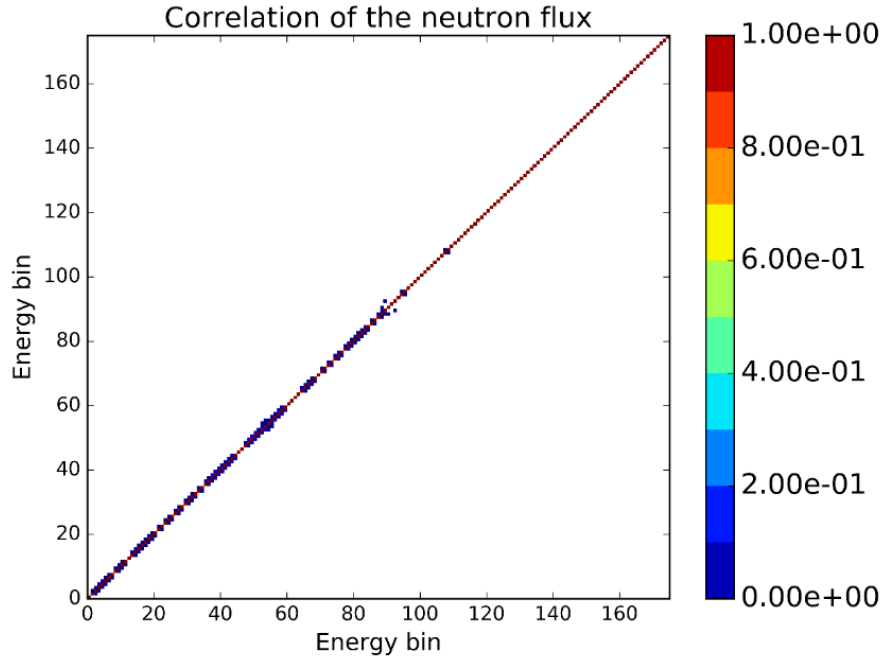


Figure 6.6 Neutron flux correlation

The uncertainty¹² of the reaction rates, which is the first step, is presented in Table 6.16 and Figure 6.7.

Table 6.16 Reaction rate and its uncertainty estimated using the brute force of a set of cases or the R2S-UNED uncertainty module in a particular case

Reaction	Mean reaction rate (s^{-1})	Brute force uncertainty (s^{-1})	Particular reaction rate (s^{-1})	Estimated uncertainty (s^{-1})
$N^{58}-Co^{58}$	$1.095 \cdot 10^{-25}$	$2.07 \cdot 10^{-28}$	$1.097 \cdot 10^{-25}$	$2.09 \cdot 10^{-28}$
$N^{58}-Co^{57}$	$4.703 \cdot 10^{-26}$	$1.70 \cdot 10^{-28}$	$4.718 \cdot 10^{-26}$	$1.74 \cdot 10^{-28}$
$N^{60}-Co^{60}$	$1.623 \cdot 10^{-26}$	$4.10 \cdot 10^{-29}$	$1.634 \cdot 10^{-26}$	$4.12 \cdot 10^{-29}$
$N^{61}-Co^{60}$	$2.823 \cdot 10^{-27}$	$1.46 \cdot 10^{-29}$	$2.836 \cdot 10^{-27}$	$1.51 \cdot 10^{-29}$
	$\begin{pmatrix} 1.0 & 0.270 & 0.705 & 0.089 \\ 0.270 & 1.0 & 0.723 & 0.842 \\ 0.705 & 0.723 & 1.0 & 0.362 \\ 0.089 & 0.842 & 0.362 & 1.0 \end{pmatrix}$		$\begin{pmatrix} 1.0 & 0.250 & 0.719 & 0.068 \\ 0.250 & 1.0 & 0.692 & 0.844 \\ 0.719 & 0.692 & 1.0 & 0.350 \\ 0.068 & 0.844 & 0.350 & 1.0 \end{pmatrix}$	

Figure 6.7 Correlation of the reaction rate calculated by brute force (left) or by R2S-UNED uncertainty module (right)

¹ During this section, the different quantities uncertainty is represented by the standard deviation of the quantities and the correlation matrix.

² R2S-UNED uses the calculated covariance matrix of the neutron flux.

The next calculation step of R2S-UNED uncertainty module is to estimate the uncertainty of the isotopic activity. For that, the covariance matrix of the reaction rates is properly multiplied by the sensitivity coefficients, which are presented in Table 6.17.

Table 6.17 Sensitivity coefficients of the most relevant reactions in the activation of the Nickel

$\frac{\lambda_{Co^{58}} \cdot \partial N^{Co^{58}}}{\partial(\sigma\phi)_{Ni^{58}-Co^{58}}}$	$\frac{\lambda_{Co^{57}} \cdot \partial N^{Co^{57}}}{\partial(\sigma\phi)_{Ni^{58}-Co^{57}}}$	$\frac{\lambda_{Co^{60}} \cdot \partial N^{Co^{60}}}{\partial(\sigma\phi)_{Ni^{60}-Co^{60}}}$	$\frac{\lambda_{Co^{60}} \cdot \partial N^{Co^{60}}}{\partial(\sigma\phi)_{Ni^{61}-Co^{60}}}$	
$3.761845 \cdot 10^{21}$	$1.542852 \cdot 10^{21}$	$9.734889 \cdot 10^{19}$	$4.232077 \cdot 10^{18}$	Bq·s·reaction ⁻¹

Table 6.18 and Figure 6.8 show the values of the activity and its uncertainty calculated using the brute force method or the R2S-UNED uncertainty module.

Table 6.18 Isotopic activity and its uncertainty estimated using the brute force of a set of cases or the R2S-UNED uncertainty module in a particular case

Activity	Mean activity (Bq)	Brute force uncertainty (Bq)	Particular case activity (Bq)	Estimated uncertainty (Bq)
Co ⁵⁸	$4.169 \cdot 10^{-4}$	$7.86 \cdot 10^{-7}$	$4.176 \cdot 10^{-4}$	$7.84 \cdot 10^{-7}$
Co ⁵⁷	$7.280 \cdot 10^{-5}$	$2.62 \cdot 10^{-7}$	$7.303 \cdot 10^{-5}$	$2.67 \cdot 10^{-7}$
Co ⁶⁰	$1.596 \cdot 10^{-6}$	$4.01 \cdot 10^{-9}$	$1.601 \cdot 10^{-6}$	$4.01 \cdot 10^{-9}$

$$\begin{pmatrix} 1.0 & 0.271 & 0.721 \\ 0.271 & 1.0 & 0.714 \\ 0.721 & 0.714 & 1.0 \end{pmatrix} \quad \begin{pmatrix} 1.0 & 0.250 & 0.717 \\ 0.250 & 1.0 & 0.702 \\ 0.717 & 0.702 & 1.0 \end{pmatrix}$$

Figure 6.8 Correlation of the isotopic activity calculated by brute force (left) or by R2S-UNED uncertainty module (right)

According to the scheme of uncertainty propagation presented in Chapter 4, the next calculated quantity is the intensity of the DGS. This calculation is performed by multiplying properly the covariance of the isotopic activity by the number of gammas produced by the isotope in each energy group, which are supplied in Table 6.19.

Table 6.19 Gammas per disintegration emitted in the Nickel slab by the relevant isotopes to the photon flux¹

Photon energy group	Co57	Co58	Co60
0-1 MeV	$0.2504 (\gamma \cdot Bq^{-1})$	$1.934 (\gamma \cdot Bq^{-1})$	$1.793 \cdot 10^{-4} (\gamma \cdot Bq^{-1})$
1-5 MeV	$0.0000 (\gamma \cdot Bq^{-1})$	$2.898 \cdot 10^{-3} (\gamma \cdot Bq^{-1})$	$0.8345 (\gamma \cdot Bq^{-1})$

¹ Note that R2S modifies the number of gammas in order to emit the same energy.

Table 6.20 and Figure 6.9 present the DGS intensity and its uncertainty.

Table 6.20 DGS intensity and its uncertainty estimated using the brute force method or the R2S-UNED uncertainty module

<i>Energy bin</i>	<i>Mean gamma source intensity</i>	<i>Brute force uncertainty</i>	<i>Particular case</i>	<i>Estimated uncertainty</i>
<i>0-1 MeV</i>	$8.253 \cdot 10^{-4} (s^{-1})$	$1.54 \cdot 10^{-6} (s^{-1})$	$8.267 \cdot 10^{-4} (s^{-1})$	$1.54 \cdot 10^{-6} (s^{-1})$
<i>1-5 MeV</i>	$2.773 \cdot 10^{-6} (s^{-1})$	$5.76 \cdot 10^{-9} (s^{-1})$	$2.779 \cdot 10^{-6} (s^{-1})$	$5.22 \cdot 10^{-9} (s^{-1})$

$$\begin{pmatrix} 1.0 & 0.882 \\ 0.882 & 1.0 \end{pmatrix} \quad \begin{pmatrix} 1.0 & 0.908 \\ 0.908 & 1.0 \end{pmatrix}$$

Figure 6.9 Correlation matrix of the DGS intensity

In order to estimate the R2S response uncertainty, we require the DGS contribution presented in Table 6.21.

Table 6.21 Contribution of the DGS intensity to the photon flux emitted from the Nickel slab and its uncertainty, where γ_s^{-1} is per photon source

<i>Energy bin</i>	<i>PS element contribution</i>	<i>MC Uncertainty</i>
<i>0-1 MeV</i>	$8.79 (\gamma \cdot cm^{-2} \cdot \gamma_s^{-1})$	$0.03 (\gamma \cdot cm^{-2} \cdot \gamma_s^{-1})$
<i>1-5 MeV</i>	$2.86 \cdot 10^{-2} (\gamma \cdot cm^{-2} \cdot \gamma_s^{-1})$	$5 \cdot 10^{-4} (\gamma \cdot cm^{-2} \cdot \gamma_s^{-1})$

Table 6.22 presents the uncertainty of the total DGS and the photon flux, which is the last step of the uncertainty propagation scheme implemented in the R2S-UNED uncertainty module. It is worth noting that the SDR relative uncertainty (0.2%) is almost 10 times lower than the uncertainty of each neutron flux (1.5%).

Table 6.22 Total source factor and photon flux emitted from the Nickel slab and its uncertainties estimated using the brute force of a set of cases or the R2S-UNED uncertainty module in a particular case

	<i>Mean magnitude</i>	<i>Brute force uncertainty</i>	<i>Particular case</i>	<i>Estimated uncertainty</i>
<i>Total source factor</i> $(\gamma \cdot s^{-1})$	$8.281 \cdot 10^{-4}$	$1.54 \cdot 10^{-6}$	$8.295 \cdot 10^{-4}$	$1.54 \cdot 10^{-6}$
<i>Photon flux</i> $(\gamma \cdot s^{-1} \cdot cm^{-2})$	$7.568 \cdot 10^{-2}$	$1.42 \cdot 10^{-4}$	$7.554 \cdot 10^{-2}$	$1.42 \cdot 10^{-4}$

As a summary of the results presented during this section, they show the correct data operation step by step, according to the equations presented in Chapter 4. In addition, these results also show the correct prediction of the uncertainty of the R2S simulation, because they are in good agreement with the results of the brute force method.

6.5.1.2 6-Voxels case

The neutron flux uncertainty was calculated using MCNP-R2S in a rectangular mesh of $1 \times 2 \times 3^1$ covering the slab. The standard deviation of the neutron flux is close to 1.5% in each energy bin of each position. The correlation of the neutron flux is presented in Figure 6.10. In this figure, the increasing of the voxel index corresponds, first at moving in Z-axis, and afterwards in Y-axes. Note that the Z-axis was the irradiation direction.

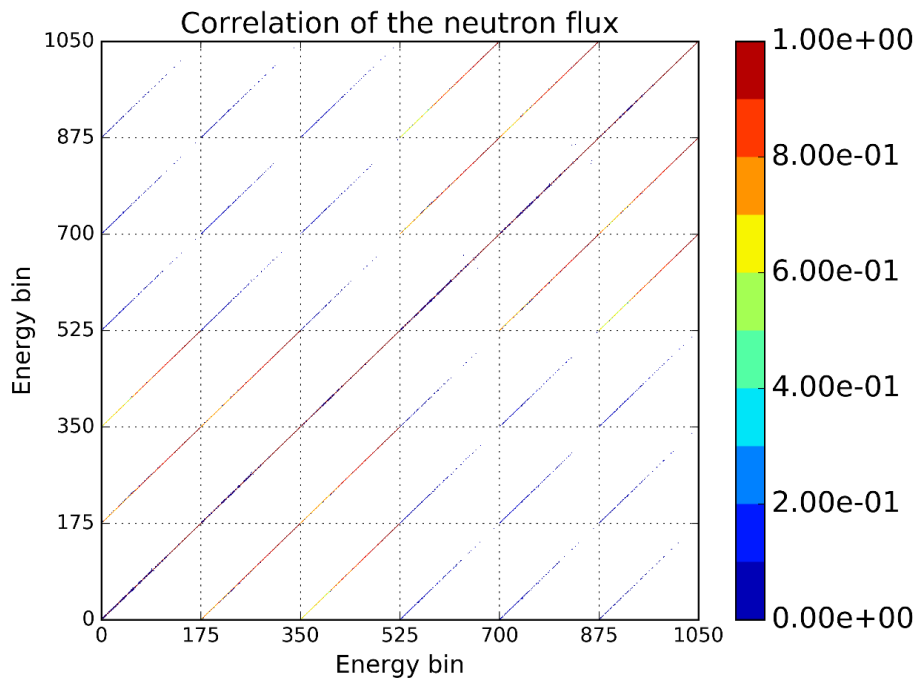


Figure 6.10 Correlation of the 6-voxel neutron flux

As expected, the voxels connected according to z-direction are correlated. According to the voxels are further away, the correlation decreases. In addition, the correlation between the voxels according to the y-direction also exists. Principally this is seen at low energy, possibly because there are more interactions. These interactions stray from the neutron trajectory and weakly correlate the nearest voxels. This correlation also decreases with the distance. Equivalent and more detailed results² were obtained in [31].

Due to the size of the correlation matrix of the different quantities, only the uncertainty of the activity, DGS intensity³, and photon flux are calculated and compared with the brute force results. The uncertainty of the uncorrelated case is also calculated. The estimation aims to show how the correlation of the case affects the uncertainty in this case⁴.

¹

² More materials with different thickness and structured meshes were studied.

³ The activity and DGS intensity results provided are integrated over all the slabs.

⁴ Note that the neutron flux is almost uncorrelated, as shown in Figure 6.9.

Table 6.23 presents the uncertainty of the activity in the whole nickel slab.

Table 6.23 Isotopic activity in the nickel slab and its uncertainty estimated using the brute force of a set of cases or the R2S-UNED uncertainty module in a particular case

<i>Activity</i>	<i>Mean activity (Bq)</i>	<i>Brute force uncertainty (Bq)</i>	<i>Particular activity (Bq)</i>	<i>Estimated uncertainty (Bq)</i>	<i>Uncertainty uncorrelated neutron flux (Bq)</i>
Co^{58}	$4.169 \cdot 10^{-4}$	$8.07 \cdot 10^{-7}$	$4.161 \cdot 10^{-4}$	$7.79 \cdot 10^{-7}$	$5.11 \cdot 10^{-7}$
Co^{57}	$7.281 \cdot 10^{-5}$	$2.60 \cdot 10^{-7}$	$7.227 \cdot 10^{-5}$	$2.65 \cdot 10^{-7}$	$1.59 \cdot 10^{-7}$
Co^{60}	$1.597 \cdot 10^{-6}$	$3.98 \cdot 10^{-9}$	$1.587 \cdot 10^{-6}$	$3.98 \cdot 10^{-9}$	$2.48 \cdot 10^{-9}$

Table 6.24 shows the uncertainty of the total photons per second emitted by the source and the uncertainty of the photon flux.

Table 6.24 Total source factor and photon flux and its uncertainties estimated using the brute force of a set of cases or the R2S-UNED uncertainty module in a particular case

	<i>Mean magnitude</i>	<i>Brute force uncertainty</i>	<i>Particular case</i>	<i>Estimated uncertainty</i>	<i>Uncertainty uncorrelated neutron flux</i>
<i>Total source factor</i> ($\gamma \cdot s^{-1}$)	$8.281 \cdot 10^{-4}$	$1.58 \cdot 10^{-6}$	$8.264 \cdot 10^{-4}$	$1.53 \cdot 10^{-6}$	$1.005 \cdot 10^{-6}$
<i>Photon flux</i> ($\gamma \cdot s^{-1} \cdot cm^{-2}$)	$7.574 \cdot 10^{-2}$	$1.48 \cdot 10^{-4}$	$7.557 \cdot 10^{-2}$	$1.42 \cdot 10^{-4}$	$9.536 \cdot 10^{-5}$

The results show a good agreement between both methodologies. The uncertainty of the R2S cases presented in this section and section 6.5.1.1 are practically the same¹. Consequently, in this case, the uncertainty of the individual elements of the neutron flux (1.5%) is notably superior to the response uncertainty (0.2%).

Regarding the comparison between the uncorrelated case and the real correlated case, it shows that the effects of the correlation are small but appreciable and are correctly taken into account.

¹ Note that the simulations are practically the same. The uncertainty due to the spatial discretization is negligible in this simulation.

6.5.2 Verification of the uncertainty estimation using the general-purpose method

This section aims to demonstrate that the uncertainty of the quantities is correctly estimated when the SNILB conditions are not met. For that, the material and irradiation conditions were changed. The new conditions consist in irradiating natural tungsten with the same spectrum (Figure 6.1) and a neutron intensity of $10^{14} \text{ n}\cdot\text{s}^{-1}$. The irradiation scenario also consists in 10^7 seconds of irradiation and 10^6 seconds of cooling. The mesh covering the slab has only one mesh element¹.

The most relevant pathways, which produce the most relevant isotopes, were calculated in order to verify that the SNILB conditions are not met. These results are presented in² Table 6.25.

Table 6.25 Pathways produced in the tungsten slab

Isotope	Contribution to the photon flux (%)	Pathways	Contribution to the production (%)
^{187}W	17.97	$^{186}\text{W}(n,G) ^{187}\text{W}$	100%
^{182}Ta	2.70	$^{182}\text{W}(n,P) ^{182}\text{Ta}$	45.63%
		$^{182}\text{W}(n,2n) ^{181}\text{W}(\beta^+) ^{181}\text{Ta} (n,\gamma) ^{182}\text{Ta}$	37.90%
		$^{180}\text{W}(n,\gamma) ^{181}\text{W}(\beta^+) ^{181}\text{Ta} (n,\gamma) ^{182}\text{Ta}$	7.07%
		$^{183}\text{W}(n,D-m) ^{182m}\text{Ta} (n,\gamma) ^{182}\text{Ta}$	2.40%
		$^{183}\text{W}(n,nP-m) ^{182m}\text{Ta} (n,\gamma) ^{182}\text{Ta}$	1.94%
		$^{183}\text{W}(n,3n) ^{181}\text{W}(\beta^+) ^{181}\text{Ta} (n,\gamma) ^{182}\text{Ta}$	1.43%
		$^{182}\text{W}(n,P-s) ^{182s}\text{Ta}(\gamma) ^{182m}\text{Ta} (\gamma) ^{182}\text{Ta}$	1.34%
		$^{183}\text{W}(n,D) ^{182}\text{Ta}$	1.32%
		$^{183}\text{W}(n,nP) ^{182}\text{Ta}$	
		$^{182}\text{W}(n,P-m) ^{182m}\text{Ta} (\gamma) ^{182}\text{Ta}$	
^{181}W	75.34	$^{182}\text{W}(n,2n) ^{181}\text{W}$	80.73%
		$^{180}\text{W}(n,\gamma) ^{181}\text{W}$	15.08%
		$^{183}\text{W}(n,3n) ^{181}\text{W}$	4.13%
^{188}Re	1.52	$^{186}\text{W}(n,3\gamma) ^{187}\text{W}(n,\gamma) ^{188}\text{W}(\beta^-) ^{188}\text{Re}$	99.96%
^{181}Hf	0.60	$^{184}\text{W}(n,A) ^{181}\text{Hf}$	99.63%

¹ The 6 mesh element case (presented in section 6.5.1.2) was also performed, but they do not provide additional valuable information. For that reason, these results are not detailed in this thesis.

² Isotopes that contribute less than 0.5% are not presented

Due to the high number of reactions and isotopes, the complete correlation matrix of the different quantities is not presented. Therefore, this section only compares the uncertainty of the activity, DGS intensity, and photon flux¹.

The R2S-UNED uncertainty simulation is carried out considering the input parameters presented in Table 6.26. Where both, the general purpose² and the SNILB solvers, are used.

Table 6.26 Input parameter of uncertainty module of R2S-UNED considered running the uncertainty module of R2S-UNED in the tungsten slab simulation

Parameters	Value
<i>Spatial filter</i>	100%
<i>Isotopic Filter</i>	99.0%
<i>Reaction Filter</i>	99.9%
<i>Solver</i>	General-purpose and SNILB
<i>Max number of elements in the chain</i>	7
<i>Two-step chains by immediately decay</i>	None

The results are presented in Table 6.27 and Table 6.28. Only the activity of Ta¹⁸² and Re¹⁸⁸ shows differences between SNILB or not SNILB conditions as was expected according to the production pathways presented in Table 6.25. The difference in the uncertainty of the photon flux is small because the importance of these isotopes in the photon flux is not excessively large. However, the difference is enough to show the correct working.

Table 6.27 Isotopic activity and its uncertainty estimated using the brute force of a set of cases or the R2S-UNED uncertainty module in a particular case

<i>Isotope</i>	<i>Activity</i>	<i>SNILB uncertainty</i>	<i>General uncertainty</i>	<i>Brute force activity</i>	<i>Brute force uncertainty</i>
<i>W181</i>	$1.625 \cdot 10^{10}$	$4.79 \cdot 10^7$	$4.73 \cdot 10^7$	$1.63 \cdot 10^{10}$	$4.66 \cdot 10^7$
<i>W187</i>	$3.616 \cdot 10^8$	$4.78 \cdot 10^6$	$4.74 \cdot 10^6$	$3.65 \cdot 10^8$	$4.80 \cdot 10^6$
<i>Ta182</i>	$5.654 \cdot 10^7$	$1.32 \cdot 10^5$	$2.81 \cdot 10^5$	$5.71 \cdot 10^7$	$2.80 \cdot 10^5$
<i>Re188</i>	$2.563 \cdot 10^8$	0.00	$4.79 \cdot 10^6$	$2.64 \cdot 10^8$	$4.96 \cdot 10^6$
<i>Hf181</i>	$1.011 \cdot 10^7$	$4.45 \cdot 10^4$	$4.42 \cdot 10^4$	$1.02 \cdot 10^7$	$4.37 \cdot 10^4$

¹ Note that the neutron flux uncertainty and the propagation to this uncertainty to the reaction rates is similar to those presented in section 6.5.1

² Note that the development and validation of this calculation mode was one of the aims of this thesis

Chapter 6
Verification of the developments in R2S-UNED

Table 6.28 Total source factor and photon flux and its uncertainties estimated using the brute force of a set of cases or the R2S-UNED uncertainty module in a particular case

	<i>Mean magnitude</i>	<i>Brute force uncertainty</i>	<i>Particular case</i>	<i>Estimated uncertainty</i>	<i>SNILB uncertainty</i>
<i>Total source factor ($\gamma \cdot s^{-1}$)</i>	$1.776 \cdot 10^9$	$6.38 \cdot 10^6$	$1.767 \cdot 10^9$	$6.26 \cdot 10^6$	$5.99 \cdot 10^6$
<i>Photon flux ($\gamma \cdot s^{-1} \cdot cm^{-2}$)</i>	$1.247 \cdot 10^{11}$	$4.57 \cdot 10^8$	$1.241 \cdot 10^{11}$	$4.47 \cdot 10^8$	$4.27 \cdot 10^8$

In order to increase the importance of the no SNILB pathways, this exercise was repeated modifying the libraries¹ used by R2S-UNED. Thus, only the Ta¹⁸² contributes to the photon flux, and consequently, the relative contribution of the no SNILB pathways is increased. The uncertainty of this R2S simulation was also calculated using R2S-UNED and the brute force method. The uncertainty of the Ta¹⁸² activity is the same as in the complete R2S simulation. The uncertainty of the DGS and the photon flux are presented in Table 6.29. In this case, and the previous ones, the uncertainty calculated by both methodologies is in excellent agreement.

Table 6.29 Total source factor and photon flux and its uncertainties estimated using the brute force of a set of cases or the R2S-UNED uncertainty module in a particular case of the R2S simulation where only tantalum 182 is considered

	<i>Mean magnitude</i>	<i>Brute force uncertainty</i>	<i>Particular case</i>	<i>Estimated uncertainty</i>	<i>SNILB uncertainty</i>
<i>Total source factor ($\gamma \cdot s^{-1}$)</i>	$3.791 \cdot 10^7$	$1.89 \cdot 10^5$	$3.751 \cdot 10^7$	$1.85 \cdot 10^5$	$5.99 \cdot 10^4$
<i>Photon flux ($\gamma \cdot s^{-1} \cdot cm^{-2}$)</i>	$3.365 \cdot 10^9$	$1.68 \cdot 10^7$	$3.328 \cdot 10^9$	$1.65 \cdot 10^7$	$7.92 \cdot 10^6$

¹ The photon spectrum of the other isotopes was deleted from data of the library file

6.6 Summary and conclusions

The implementation of the scheme to propagate the stochastic neutron flux uncertainty to the SDR required the development of new capabilities in R2S-UNED, as Chapter 5 presents. This chapter includes the verification exercises that were performed to certify the correct working of these capabilities, one by one:

- I. Correlation matrix of the neutron flux
- II. Isotopic contribution
- III. The most relevant pathways
- IV. Derivative of the isotopic concentration with respect to the reaction rates
- V. Uncertainty calculation of the isotopic activity, DGS, and SDR uncertainty due to the neutron flux uncertainty in an R2S simulation

In general, the verification of each step consisted in comparing the results obtained by the developed method with those obtained with alternative validated methods or programs. The results show that all the capabilities were correctly implemented. Consequently, R2S-UNED can estimate the SDR uncertainty due to the MC calculation method used during the transport simulation.

It is especially remarkable the verification of the SDR uncertainty estimation when SINBL conditions are not met because it was one of the aims of this thesis. It is worth underlining that this capability distinguishes the uncertainty module of R2S-UNED from the other methodologies already implemented¹.

Otherwise, it is worth highlighting the discrepancy found validating the estimation of the sensitivity coefficients. These discrepancies were found when the burn-up is extremely important. Therefore, the solver properly works in the relevant activation conditions to the R2S-UNED application. The discrepancies were identified as a miscalculation of ACAB solver. This result could motivate the research of the adequate use of ACAB² to estimate the derivatives or the search for a better ODE solver. Nevertheless, the error introduced in the calculated cases has almost no effect on the SDR uncertainty in any case calculated during the thesis.

¹ A review of these methodologies was presented in Chapter 2

² Definition of adequate time step in order to the resulting ODEs to the time step was correctly solved. Or other techniques that guarantee the accuracy of ACAB solver.

Chapter 7.

Application of the uncertainty module of R2S-UNED

One of the thesis aims was that the developed methodology can be used in general R2S-UNED applications. This chapter deals with this aim by applying the new R2S-UNED features in relevant computational examples. Specifically, R2S-UNED was used to estimate the SDR uncertainty in the SDR computational benchmark of ITER and the air-kerma estimation in the detector of the JET octant 2. As we comment below, each application has a different degree of realism and difficulty¹.

The ITER benchmark was designed to reproduce the relevant features of an ITER port to the computational estimation of the SDR. This means that the model includes radiation streaming and realistic materials but using extremely simple geometry. This simple geometry makes the exercise highly traceable. Therefore, neutronic teams use this benchmark as a touchstone for any computational advance in computation methodologies to estimate SDR in fusion applications. This fact enables the actual uncertainty of the R2S simulation to be estimated using R2S-UNED. This application, which is presented in section 7.1, was also published in [75].

Regarding JET[4], it is the largest tokamak in operation nowadays and one of the most relevant experimental fusion facilities dedicated to testing technologies for ITER. Among the different projects carried out in this facility, UNED participates in the WPJET3 DT technological exploitation of DT operation project within the EUROfusion Consortium program[76]. Specifically, inside of the subproject "NEXP shutdown dose rate experiments".

The principal aim of NEXP project is to provide experimental data to validate the codes dedicated to the SDR estimation in ITER. Specifically, UNED participates in order to verify R2S-UNED and D1S-UNED codes, which are applied in ITER neutronic analyses.

The work performed in this thesis allows assessing the uncertainty in the R2S-UNED estimation due to the numerical calculation method. Consequently, it enables a better comparison of the calculation method R2S with the experimental data, and therefore, a better code validation.

¹ The principal difficulty in estimating the SDR stochastic uncertainty using R2S is to calculate the neutron flux stochastic uncertainty. See section 5.1. This section proposes different methodologies to overcome this issue.

Section 7.2 presents the uncertainty estimation of the air-kerma in the detector of the octant 2 at 6 hours of cooling time after the DD campaign of 2016¹.

Finally, the conclusions about the applicability of the tool are presented in section 7.3.

¹ This campaign aims to minimize the experimental and computational uncertainties in order to prepare the next DT campaign.

7.1 ITER benchmark exercise

This section describes the R2S-UNED application to the ITER benchmark exercise. This exercise, described in section 7.1.1, is a widespread computational benchmarking where the developments of the codes used for the estimation of the SDR are usually tested. In addition, this exercise was chosen because there are few contributing regions¹ to the SDR. This fact allows calculating the stochastic SDR uncertainty of the neutron flux.

The goals of this section were the following:

- i. To present the guideline developed to estimate the actual SDR uncertainty of the R2S calculation. This guideline is described in section 7.1.2.
- ii. To show the analysis of the R2S relevant output, such as the estimation of the DGS contribution, the isotopic contribution, or the stochastic SDR uncertainty. These results are detailed in section 7.1.3
- iii. To analyze the possible use of the assumptions² of the neutron flux covariance to estimate the SDR uncertainty in realistic cases.
- iv. To analyze the effect of relevant variance reduction techniques, as the GVR, in the correlation of the neutron flux and in the SDR uncertainty.

Section 7.1.4 describes both analyses.

7.1.1 Computational assumptions

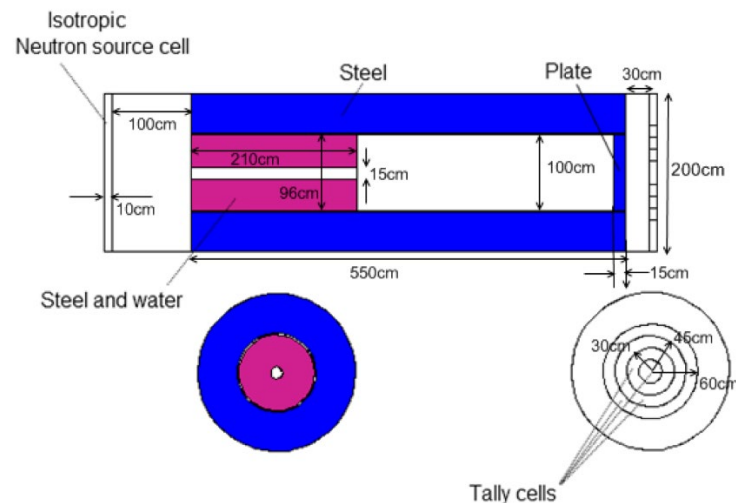


Figure 7.1 ITER benchmark scheme

¹ The regions are defined as the mesh element of the superimposed mesh

² R2S-UNED allows assuming that the neutron flux covariance matrix is completely correlated, uncorrelated or decorrelated, in order to provide an approximate estimation when this matrix cannot be calculated.

Figure 7.1 shows the geometry of the ITER benchmark exercise. This exercise represents, in a very schematic way, the typical characteristics (dimensions, materials, and shape) of an ITER equatorial port.

An external, 550 cm long, hollowed steel cylinder compounds the geometry of this exercise. The internal and external radii are 50 and 100 cm respectively. A steel disk occupies the last 15 cm of the inner of the cylinder. Between the two steel pieces, there is a 2 cm gap. Another 210 cm long cylinder of a water-steel mixture, with 7.5 and 48 cm internal and external radii, fills the inner front part of the cylinder respectively.

This geometry is irradiated by an isotopic 14 MeV neutron source, uniformly emitted from the front of the geometry. The material activation is calculated considering the SA-2 [70] irradiation scenario given in Table 7.1.

Table 7.1 SA-2 irradiation scenario

Source strength (n/s)	Duration	Repetitions
1.0714×10^{17}	2 years	1
8.25×10^{17}	10 years	1
0	0.667 years	1
1.6607×10^{18}	1.33 years	1
0	3920 seconds	17
2.0×10^{19}	400 seconds	
0	3920 seconds	4
2.8×10^{19}	400 seconds	

The SDR produced by the decay gammas is measured in a cylindrical slab of 15cm radius located at 30 cm from the rear face of the cylinder. The cooling time considered is 10^6 seconds after shutdown.

7.1.2 Guideline to estimate the SDR stochastic uncertainty of the R2S-UNED calculation

In general, the R2S simulations use meshes with a high number of mesh elements in order to achieve a fine spatial resolution. In fact, in the most challenging applications, several simulations are needed to calculate the DGS of the facility [77]. This problem is due to the RAM limitation of the current computers.

This fact is even more problematic to estimate the SDR uncertainty, because the covariance matrix of the neutron flux, associated with these meshes, cannot be calculated¹. However, in many practical applications, most of the activated regions² do not contribute to the specific SDR tallies. Thus, the spatial discretization can be reduced to a mesh covering only the regions contributing to the SDR tally. Therefore, we can obtain the neutron flux covariance if the number

¹ The size of the covariance matrix is prohibitive, as section 5.1 shows.

² Note that region is understood as mesh element

of DGS contributing regions is not excessively large. Hence, in these cases, we can calculate the stochastic uncertainty of the SDR in the R2S simulation.

This section proposes a guideline, presented in Figure 7.2, to estimate the SDR stochastic uncertainty in these cases. Its application requires two R2S simulations¹: The first simulation aims to define the so-called reduced mesh, which covers the most relevant regions to the SDR². This mesh is defined based on the DGS contribution obtained during this R2S simulation, which is performed with a so-called complete mesh covering the complete geometry.

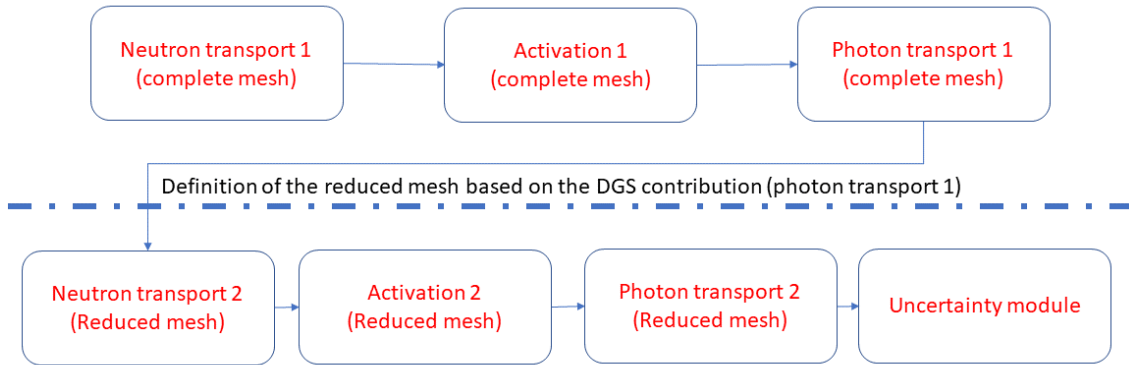


Figure 7.2 Computational scheme of the guideline applied in the ITER benchmark

The second R2S simulation is carried out using this reduced mesh. During the neutron transport of this simulation, the covariance matrix of the neutron flux is estimated. In addition, this R2S simulation includes the execution of the R2S-UNED uncertainty module, calculating the stochastic SDR uncertainty.

The application of this guideline is described in sections 7.1.2.1 (definition of the reduced mesh) and 7.1.2.2 (R2S simulation using the reduced mesh).

7.1.2.1 Estimation of the reduced mesh

This section presents the analysis performed to define the reduced mesh³. For that, we compute the DGS intensity contribution to the SDR tally (defined in section 5.3) in order to filter the most important regions contributing to the SDR.

In this R2S simulation, we consider the spatial and energy discretization defined in [24]. This complete mesh covers all the geometry. In addition, it guarantees an appropriate result because

¹ Neutron transport, activation, and photon transport

² Other alternatives, such as the adjoint neutron flux calculated by deterministic codes by MS-CADIS[30] or GT-CADIS[35] methodologies, can be used to estimate the reduced mesh. However, these S_N codes are not available in R2S-UNED, and they are less accurate than MC codes.

³ Mesh, which covers the contributing regions to the SDR, small enough to be able to compute the covariance matrix of the neutron flux.

it is in good agreement with the benchmark result. The definition of this complete mesh is described below and shown in Figure 7.3.

- The Z-axis was divided into 5 cm intervals from 0 to 545 cm, 2 cm intervals to 549 cm, and the last interval of 1 cm.
- The R-axis was divided into 2 intervals from 0 to 7.5cm, 8 intervals from 7.5 to 48 cm, 1 interval from 48 to 50 cm, and 10 intervals from 50 to 100 cm.
- Only one bin from 0 to 2π was considered for the θ angle.

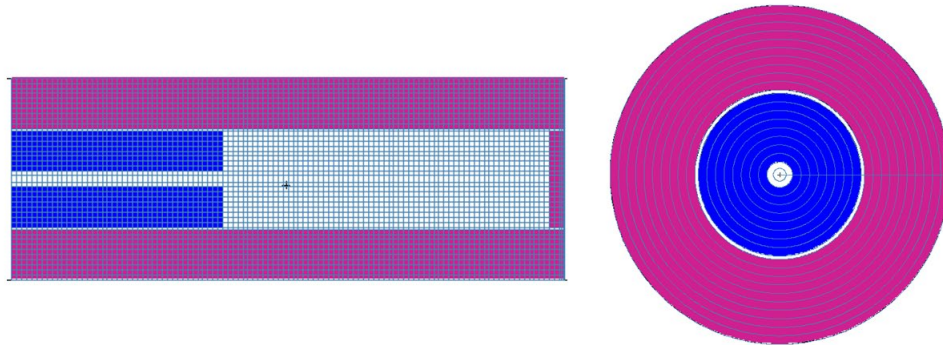


Figure 7.3 Complete mesh superimposed to the ITER benchmark geometry

The neutron flux was estimated simulating 10^{10} histories using the VitaminJ [66] energy group structure. The statistical uncertainty of most energy groups of all material regions was good (<10%). Only the stochastic uncertainty of the upper right region overcomes the 20%. The neutron flux and its uncertainty Figure 7.4.

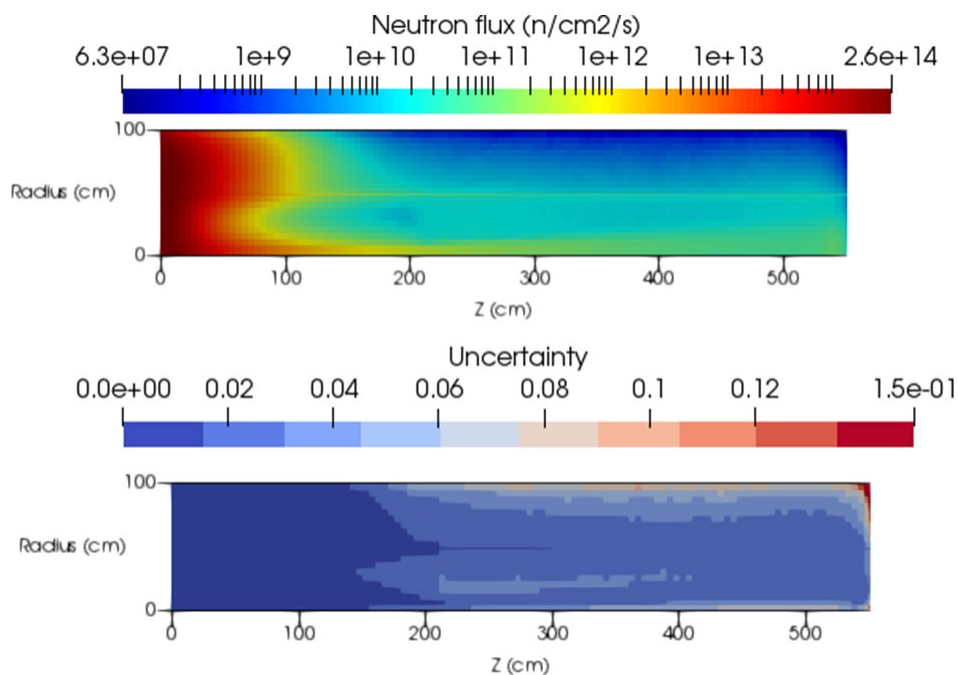


Figure 7.4 Neutron flux at power of $2 \cdot 10^{19} \text{ n} \cdot \text{s}^{-1}$ and its uncertainty (represented in 2D using axial symmetry around the Z-axis)

Chapter 7
Application of the uncertainty module of R2S-UNED

The DGS was built using the 24 energy groups recommended in FISPACT [22] and presented in ANNEX C. Afterwards, 10^8 photon histories were simulated using this DGS in order to estimate the DGS contribution.

Figure 7.5 presents the DGS contribution (the importance of each region) and its uncertainty. This figure shows that the last 15 cm of the activated cylinder is the most contributing region to the SDR. Consequently, the reduced mesh was defined, based on Figure 7.5, as follows:

- The Z-axis was divided into 2 cm intervals from 545 to 549 cm and a last interval of 1 cm.
- The R-axis was divided into 2 intervals from 0 to 7.5cm, 8 intervals from 7.5 to 48 cm, 1 interval from 48 to 50 cm, and 10 intervals from 50 to 100 cm.
- Only one bin from 0 to 2π for θ .

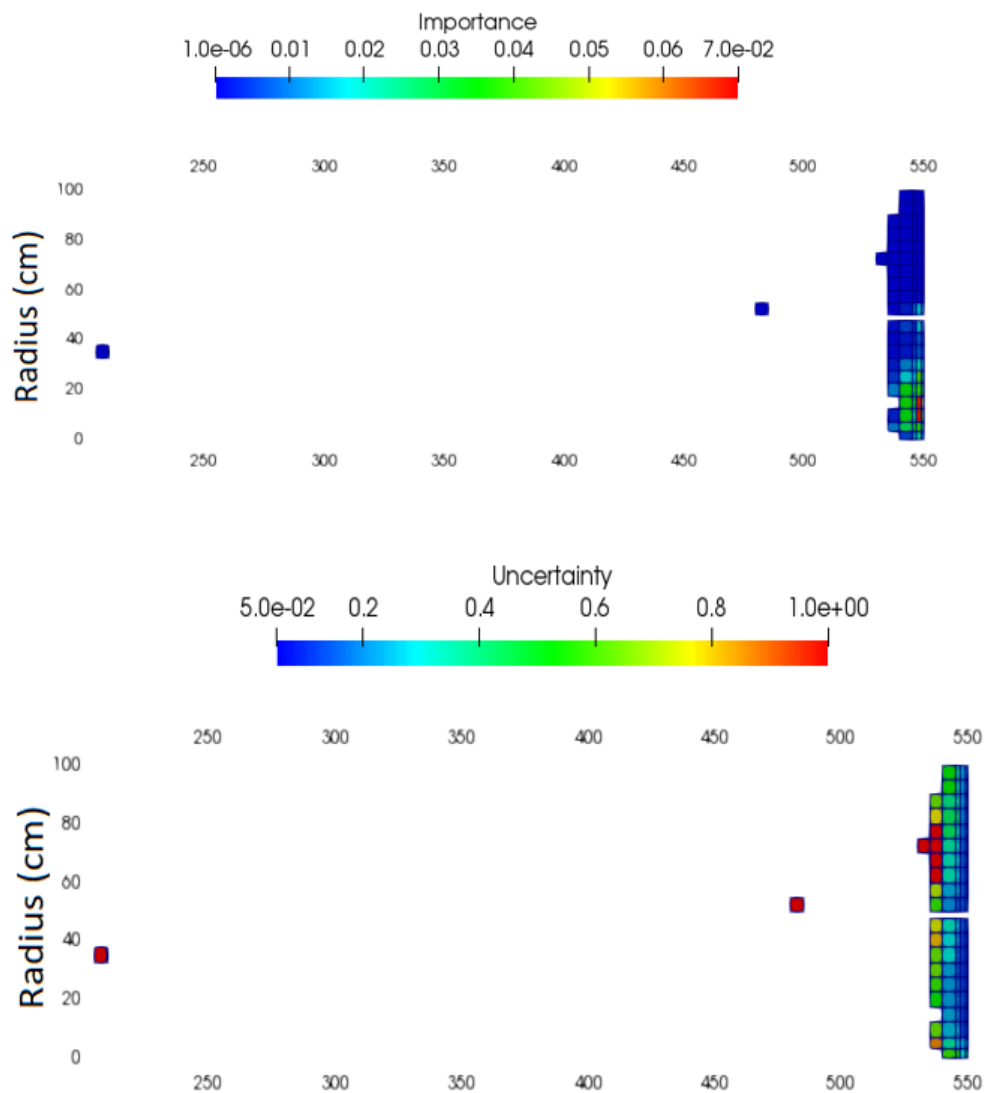


Figure 7.5 DGS contribution to the SDR (represented in 2D using cylindrical symmetry around the Z-axis)

The size of the neutron flux covariance matrix (Equation 7.1) for both (complete and reduced) meshes is compared in Table 7.2. The estimation of the reduced mesh requires 600 times less computational memory. It is worth noticing that the size of the neutron flux covariance matrix of the reduced mesh size can be handled by Marconi¹ supercomputer [33]. Therefore, we can estimate the uncertainty of the SDR using this mesh.

$$size = \left(\frac{\left(\frac{\#_{bins}^{energy} \cdot \#_{voxel}^{mesh}}{2} \right)^2}{2} + \frac{\#_{bins}^{energy} \cdot \#_{voxel}^{mesh}}{2} \right)$$

Equation 7.1

Table 7.2 Size of the defined meshes and the covariance matrix of the neutron flux

Mesh	Complete mesh	Reduced mesh
Energy resolution	175 bins	175 bins
Spatial resolution	2252 regions	105 regions
Size of the covariance matrix (number of elements)	$8.47 \cdot 10^{10}$	$1.69 \cdot 10^8$
Size of the covariance matrix (GB)	677.7	1.35

7.1.2.2 Application of the uncertainty module of R2S-UNED using a reduced mesh in the ITER benchmark

This section details the second R2S simulation of the guideline depicted in Figure 7.2, where the reduced mesh is used to estimate the SDR and its uncertainty.

The first stage of this R2S simulation is the neutron flux simulation. This simulation includes the estimation of the neutron flux covariance, using the reduced mesh. The rest of the parameters are the same as those applied in section 7.1.2.1.

The next steps are the activation and photon transport, which were also carried out just like in section 7.1.2.1.

The last step corresponds to the execution of the uncertainty module of R2S-UNED. The simulation took into account 99.5% of the relevant quantities (region, isotopes, and reaction rate filters described in Chapter 5). The output of the R2S-UNED uncertainty module will be presented in section 7.1.3.

7.1.3 Stochastic uncertainty estimated with R2S-UNED

This section presents the results² of the simulation described in section 7.1.2. They are divided in two groups:

¹ Marconi is one of the most relevant supercomputers in Europe for fusion applications. Their cores have 4.1 GB of RAM currently.

² Only the results related to the uncertainty of the different quantities due to the MC calculation method are presented in this section.

Chapter 7
Application of the uncertainty module of R2S-UNED

- i. The uncertainty of the activity, which is presented in section 7.1.3.1.
- ii. The uncertainty of the SDR, which is presented in section 7.1.3.2

7.1.3.1 *Uncertainty of the isotopic activity*

This section shows the uncertainty of the activity of the most contributing radioisotopes to the SDR in the ITER benchmark (presented in section 7.1.4.2). Table 7.3 presents these uncertainties calculated using the *SNILB* solver¹ or the *general* solver (see Chapter 5).

Table 7.3 Statistical uncertainty of the isotopic activity calculated with R2S-UNED

<i>Isotopes</i>	Activity (Bq)	Uncertainty (Bq) General Approach	Uncertainty (Bq) SNILB Approach
<i>⁵⁸Co</i>	$1.24 \cdot 10^{11}$	$1.07 \cdot 10^{10}$	$1.07 \cdot 10^{10}$
<i>⁵⁴Mn</i>	$7.62 \cdot 10^{10}$	$6.64 \cdot 10^9$	$6.64 \cdot 10^9$
<i>⁶⁰Co</i>	$8.65 \cdot 10^9$	$6.61 \cdot 10^8$	$6.63 \cdot 10^8$
<i>⁵⁷Co</i>	$2.93 \cdot 10^{10}$	$3.52 \cdot 10^9$	$3.52 \cdot 10^9$
<i>⁵¹Cr</i>	$4.61 \cdot 10^{10}$	$4.32 \cdot 10^9$	$4.32 \cdot 10^9$
<i>¹⁸²Ta</i>	$1.30 \cdot 10^9$	$9.68 \cdot 10^7$	$9.69 \cdot 10^7$
<i>⁵⁹Fe</i>	$6.58 \cdot 10^8$	$4.45 \cdot 10^6$	$4.45 \cdot 10^6$
<i>⁹⁵Nb</i>	$2.83 \cdot 10^7$	$3.81 \cdot 10^6$	$2.48 \cdot 10^6$

The results of Table 7.3 show an excellent agreement between both solvers². Only relevant differences are seen in the uncertainty of the ⁹⁵Nb activity.

Table 7.4 ⁹⁵Nb production pathways found in the relevant regions of the reduced mesh

<i>Number</i>	<i>Pathway</i>	<i>Contribution</i>
1	⁹⁵ Mo → ⁹⁵ Nb	61.87%
2	⁹⁸ Mo → ⁹⁵ Zr(β^-) → ⁹⁵ Nb	18.76%
3	⁹⁵ Mo → ^{95m} Nb(<i>IT</i>) → ⁹⁵ Nb	14.75%
4	⁹⁶ Mo → ⁹⁵ Nb	2.88%
5	⁹⁶ Mo → ^{95m} Nb(<i>IT</i>) → ⁹⁵ Nb	0.79%
6	⁹⁶ Mo → ⁹⁵ Zr(β^-) → ⁹⁵ Nb	0.51%

¹ The first step to use this solver is to guarantee that SNILB conditions are met. However, this has been proved previously in this [79] exercise and other similar ITER analyses.

² It was expected because both solvers were already verified in Chapter 6

Table 7.4 shows the relevant pathways that produce ^{95}Nb . SNILB solver cannot deal with all these pathways. Four of them¹ contain an intermediate decay nucleus that is $^{95\text{m}}\text{Nb}$ or ^{95}Zr . The contribution of these pathways explains the differences between both solvers.

It is worth underlining that the pathways, which contain $^{95\text{m}}\text{Nb}$, could be considered using the SNILB solver². Because the ratio between decay constants of $^{95\text{m}}\text{Nb}$ and ^{95}Nb is small (about ~ 0.1). However, the general solver must be used in order to consider the contribution to the SDR uncertainty to those pathways containing ^{95}Zr . Note that, in this case, the ratio of the decay constants of ^{95}Zr and ^{95}Nb elements is about 1.8.

7.1.3.2 *Uncertainty of the air-kerma*

The estimation of the SDR in the ITER benchmark with R2S-UNED is $16.3 \pm 0.16 \text{ mSv} \cdot \text{h}^{-1}$. The uncertainty module also shows the uncertainty due to each R2S MC transport simulation. In this R2S simulation, $0.12 \text{ mSv} \cdot \text{h}^{-1}$ is the statistical uncertainty due to the neutron transport and $0.10 \text{ mSv} \cdot \text{h}^{-1}$ is the stochastic uncertainty of the photon transport. Consequently, the distribution of the computational resources between both transport simulations is appropriate.

7.1.4 Comparison between D1S-UNED and R2S-UNED results of the ITER benchmark

This section presents a comparison of D1S-UNED and R2S-UNED results of the ITER benchmark exercise. It is worth underlining that both methodologies should estimate equivalent SDR results³. The results are presented in two sections:

The first one presents the comparison between the isotopic contributions to the SDR. This exercise allows validating the new R2S-UNED capability to estimate the isotopic contribution in a realistic application⁴. This comparison is presented in section 7.1.4.2.

The second one shows the importance of the SDR uncertainty estimations in the verification or validation exercise. As it was said, both methodologies are adequate for the estimation of the SDR in this exercise. Therefore, both estimations should be equivalents, although both methodologies have their own assumptions, which can introduce small differences between the results. Since we can estimate the difference due to the calculation method⁵, we can analyze the effect of the different assumptions or calculation methods in the results. This comparison is presented in section 7.1.4.3.

¹ Any of these two-step pathways were detected solving the ITER benchmark using D1S-UNED [79], because the Nb^{95} was considered negligible respect to the SDR tally.

² Sections 5.4.3.1 and 5.5.1 details the implementation and hypothesis of the SNILB solver. These assumptions are more than those imposed only by the SNILB conditions.

³ The R2S simulation was described in section 7.1.2, while the D1S simulation is described in 7.1.4.1.

⁴ It is worth noticing that D1S-UNED capabilities have been deeply tested[42].

⁵ Both D1S-UNED and R2S-UNED can estimate their stochastic uncertainty due to the calculation method

Chapter 7
Application of the uncertainty module of R2S-UNED

7.1.4.1 Computational assumptions of the D1S-UNED simulation of the ITER benchmark

D1S simulation used the same input as R2S neutron simulation but including the needed D1S parameters described in this section. In addition, this simulation also used a weight windows map, based on GVR [78], to speed up the calculation.

Table 7.5 D1S reaction data included in the simulation

Father isotope	Reaction	Daughter Isotope	Father isotope	Reaction	Daughter Isotope
^{59}Co	$(n,2n)+(n,2n)^*$	^{58}Co	^{58}Ni	(n,d)	^{57}Co
^{58}Ni	$(n,p)+(n,p)^*$	^{58}Co	$^{50}\text{Cr50}$	(n,γ)	^{51}Cr
^{55}Mn	$(n,2n)$	^{54}Mn	^{52}Cr	$(n,2n)$	^{51}Cr
^{54}Fe	(n,p)	^{54}Mn	^{54}Fe	(n,α)	^{51}Cr
^{56}Fe	(n,t)	^{54}Mn	^{181}Ta	$(n,\gamma)+$ $(n,\gamma)^*+(n,\gamma)**$	^{182}Ta
^{58}Ni	$(n,p\alpha)$	^{54}Mn	^{182}W	$(n,p)+$ $(n,p)^*+(n,p)**$	^{182}Ta
^{59}Co	$(n,\gamma)+ (n,\gamma)^*$	^{60}Co	^{183}W	$(n,np)+$ $(n,np)^*+(n,np)**$	^{182}Ta
^{60}Ni	$(n,p)+(n,p)^*$	^{60}Co	^{184}W	(n,α)	^{182}Ta
^{61}Ni	$(n,np)+(n,np)^*$	^{60}Co	^{58}Fe	(n,γ)	^{59}Fe
^{61}Ni	$(n,d)+(n,d)^*$	^{60}Co	^{59}Co	(n,p)	^{59}Fe
^{63}Cu	$(n,\alpha)+ (n,\alpha)^*$	^{60}Co	^{62}Ni	(n,α)	^{59}Fe
^{58}Ni	(n,np)	^{57}Co			

The reactions considered in the D1S simulation are listed in Table 7.5. This list was obtained adding to those reactions used in the D1S verification exercise [79], all available reactions[56] that produce the relevant isotopes detected in R2S-UNED simulation¹.

Table 7.6 presents the D1S time factors of the SA-2 [70] irradiation scenario (Table 7.1), normalized to $1.0714 \cdot 10^{17} \text{ n}\cdot\text{s}^{-1}$. The SDR was calculated at 10^6 seconds of cooling time, running the D1S simulation until $2 \cdot 10^9$ neutron histories were done.

¹ The contribution of these reactions can be considered negligible with respect to the SDR, but it could be useful to compare the isotopic contribution between D1S and R2S simulations.

Table 7.6 D1S time factor normalized to $1.0714 \cdot 10^{17}$ n/s

<i>Isotope</i>	Decay constant (s⁻¹)	D1S Time factor
⁵⁸ Co	$1.132 \cdot 10^{-7}$	13.76
⁵⁴ Mn	$2.570 \cdot 10^{-8}$	11.47
⁶⁰ Co	$4.167 \cdot 10^{-9}$	6.843
⁵⁷ Co	$2.952 \cdot 10^{-8}$	11.87
⁵¹ Cr	$2.896 \cdot 10^{-7}$	11.66
¹⁸² Ta	$6.994 \cdot 10^{-8}$	13.80
⁵⁹ Fe	$1.803 \cdot 10^{-7}$	12.98

7.1.4.2 Comparison of the isotopic contribution calculated with D1S-UNED and R2S-UNED

This section presents the isotopic contribution to the SDR in the ITER benchmark calculated with R2S-UNED and D1S-UNED. The results of both simulations, previously described, are presented in Table 7.7. This table shows that, in general, there is a good agreement between both methodologies.

Table 7.7 Radioisotope contributions to the SDR calculated by R2S and D1S methodologies

<i>Isotopes</i>	SDR R2S $\left(\frac{mSv}{h}\right)$	R2S contribution	SDR D1S $\left(\frac{mSv}{h}\right)$	D1S contribution	Relative uncertainty¹
⁵⁸ Co	9.15	56.25%	8.59	56.34%	0.018
⁵⁴ Mn	4.77	29.34%	4.67	30.66%	0.03
⁶⁰ Co	1.72	10.56%	1.57	10.34%	0.04
⁵⁷ Co	0.240	1.48%	0.154	1.01%	0.04
⁵¹ Cr	0.140	0.86%	0.117	0.77%	0.06
¹⁸² Ta	0.098	0.60%	0.093	0.61%	0.014
⁵⁹ Fe	0.061	0.37%	0.042	0.27%	0.07
⁹⁵ Nb	0.007	0.04%	0.0	0.0%	0.0
<i>Total</i>	16.3	100%	15.3	100%	0.016

Despite the good agreement, D1S-UNED results are systematically smaller than R2S ones. In this simulation, we cannot discern if the discrepancy can be due to the calculation method, or due to the assumptions of the methodology because, for that, we must take into account the R2S

¹ Actually, this is the uncertainty of the SDR produced by each isotope provided by D1S-UNED, not the relative contribution.

stochastic uncertainty in the isotopic contribution calculated by R2S. Despite this uncertainty can be estimated by combining appropriately the uncertainties of the isotopic activities and the DGS contributions, this capability is not currently available in R2S-UNED.

Otherwise, anticipating the conclusions of section 7.1.4.3, where the SDR results of D1S and R2S are compared¹, the MC uncertainty is enough to consider different the D1S and R2S results. This means that there are appreciable differences due to the different assumptions of both methodologies².

7.1.4.3 Uncertainty of the SDR response: Comparison of equivalent results of D1S and R2S

This section presents the statistical uncertainty of the SDR in both, D1S and R2S simulations of the ITER benchmark described in section 7.1. The results of both simulations and the difference of them are presented in Table 7.8. This result takes into account the independence between the R2S and D1S simulations³.

Table 7.8 SDR and its statistical uncertainty (one standard deviation) of R2S and D1S simulations of ITER benchmark exercise

	D1S(mSv · h⁻¹)	R2S(mSv · h⁻¹)	Ratio R2S/D1S
<i>SDR and uncertainty</i>	15.3 ± 0.24	16.3 ± 0.16	1.06 ± 0.02

The ratio is different from one by three standards deviations. Consequently, the D1S-UNED result is different from the R2S-UNED result⁴. Since both simulations consider the same data libraries, the reason for the difference must be the different assumptions of the methodologies such as the energy discretization during the estimation of the reaction rates or the homogeneous emission inside of the voxel in R2S. Nevertheless, the difference is small, and both methodologies are appropriate to assess the SDR in this exercise.

7.1.5 Effect of the GVR on the correlation of the neutron flux in the ITER benchmark

This section aims to study the impact of the correlation of the neutron flux on the SDR uncertainty. It is worth underlining again that the estimation of this quantity is currently the most limiting issue for the estimation of the stochastic uncertainty of the R2S calculations.

¹ Note that those comparison takes into account the MC uncertainty of each simulation

² Examples of these assumptions would be the spatial and energy discretization of R2S, or the SNILB assumption in the activation step of D1S

³ Note that the seed of the random number generator of MCNP was changed in D1S-UNED simulation

⁴ Or, at least, it is very probable that both results are different

For that, we estimated the actual statistical uncertainty calculated considering the evaluated correlations of the neutron flux¹. Then, this uncertainty is compared with those obtained assuming the neutron flux is fully correlated, or uncorrelated².

This study was carried out in two different R2S simulations solving the ITER benchmark: The first simulation does not use a GVR for the neutron transport simulation (case described in section 7.1.2). The second one is the same simulation but using GVR³ during the neutron transport⁴. The SDR and its uncertainty of all these cases are shown in Table 7.9.

Table 7.9 Uncertainty of the ITER benchmark exercise calculated in different R2S-UNED simulations

	Case	SDR $\left(\frac{mSv}{h}\right)$	Uncertainty $\left(\frac{mSv}{h}\right)$
<i>GVR</i>	Correlated assumption	16.6	4
	Calculated case		1.6
	Uncorrelated assumption		0.4
<i>No GVR</i>	Correlated assumption	16.32	1.6
	Calculated case		0.16
	Uncorrelated assumption		0.12

The uncertainties between the two cases, presented in Table 7.9, cannot be directly compared since the number of neutron histories are different for each simulation. However, we can result two results:

In the first place, we can see that the difference between the no correlated assumption and the calculated case is greater when the GVR is used. These differences are because the GVR induces a strong correlation in the neutron flux due to the splitting of the neutron particles. In order to understand this result, we must consider Equation 7.2, which describes the neutron flux correlation.

$$cov(\phi_i\phi_j) = \frac{\overline{\phi_{hi}\phi_{hj}} - \overline{\phi_{hi}} \cdot \overline{\phi_{hj}}}{NPS}$$

Equation 7.2

¹ Hereafter called calculated case when no hypothesis is assumed in the correlation matrix of the neutron flux

² These are two of the hypotheses that the uncertainty module of R2S-UNED can always consider

³ The GVR simulation is included to highlight the effect of the splitting techniques, which are commonly used in transport simulations to save computational time. Note that the effect of the GVR in the simulation depends on the method used to produce the weight windows map[103].

⁴ The number of neutron histories was reduced to 10⁸

In this equation, the mean values of the neutron flux $\overline{\phi_{h_i}}$ do not depend on the simulation parameters, but they depend on the physical problem simulated. On the contrary, $\overline{\phi_{h_i}\phi_{h_j}}$ depends on that the same neutron history can contribute to both regions. Consequently, splitting techniques such as GVR, increase the probability that the same neutron history contributes to two different regions in the simulation, increasing the correlation of the neutron flux².

The second result presented in Table 7.9 shows that the estimated uncertainty of the no GVR case is pretty like the uncertainty of the no correlated assumption. However, this does not mean that the no correlated assumption was a good estimation. Note that the estimated uncertainty contains two terms related to the MC neutron transport and the MC photon transport, respectively. The uncorrelated approach can be a sub-estimation of the real uncertainty. In addition, it can be also negligible compared with the MC photon transport. This motivates a deeper analysis of the uncertainty origin.

In order to perform this analysis, the different contributions of the uncertainty of Table 7.9 are detailed in Table 7.10.

Before presenting the analysis, it is worth remarking below three features, which were expected according to Chapter 4.

- i. TT term does not depend on the correlation of the neutron flux, because this term is only related to the gamma transport. In fact, this term is the uncertainty provided by the photon transport simulation, as expected.
- ii. ST term is negligible, as expected. Note that this term is directly ignored if the uncertainty propagation law is taken into account³ [29].
- iii. SS term contains the SDR uncertainty due to the neutron uncertainty. If the neutron flux is correlated, the SS is the most contributing term. In fact, it is the no diagonal SS term because there are more elements⁴ than the diagonal one. On the contrary, when the neutron flux is not correlated, the importance of this term is like the diagonal term, but not zero⁵.

Analyzing the uncertainty from the neutron flux more in detail (SS term), we can see that both approaches miscalculate the uncertainty⁶ in the SDR. Note that the SS term of the

¹ Where the index h indicates the neutron flux of an individual history

² [28] describes the relation between the neutron flux correlation and the distance. [31] proves this description.

³ Note that the estimation of the SDR uncertainty does not require extremely high precision. It is enough to know the first significant figure

⁴ We refer to the number of elements in the sum of the Equation 5.19 and Equation 5.20. Note that diagonal TT sum only the terms which contains the diagonal values of the covariance matrix of the DGS intensity. While the no diagonal TT sums the rest of them.

⁵ It is highlight that, despite of the neutron flux is not correlated, the DGS can be significantly correlated as equations of Chapter 4 predict

⁶ It was expected that the neutron flux was not completely correlated or uncorrelated

calculated¹ case is: $1.5 mSv \cdot h^{-1}$ in the GVR case, and $0.12 mSv \cdot h^{-1}$ in the no GVR case. While, the correlated case, which is the conservative hypothesis², are $4 mSv \cdot h^{-1}$ and $1.6 mSv \cdot h^{-1}$ respectively. This means that the neutron simulation must be run until the NPS was 10 times higher in the GVR case, and more than 100 times in the no GVR to guarantee the same uncertainty in these example cases³.

Otherwise, the SS term of the uncorrelated case is: $0.4 mSv \cdot h^{-1}$ in the GVR case, while the uncertainty in the no GVR case⁴ is $0.06 mSv \cdot h^{-1}$. This means that there is a factor 4 and 2 respectively. Despite this could be a better estimation, it is worth noticing that this option underestimates the uncertainty in both cases. From the point of view of the fusion facility analyses, the underestimation of the uncertainty is a risk. Consequently, this option must be considered only when we can assure that the neutron flux is not correlated.

As a summary of this section, the results of the analysis of the ITER benchmark show that⁵:

- i. The assumption considered in the correlation matrix of the neutron flux can lead to important misestimation of the SDR uncertainty.
- ii. Variance reduction techniques, such as the GVR, have a high influence on the correlation matrix of the neutron flux, and therefore in the final uncertainty. It is worth highlighting that the influence of the GVR comes from particle splitting. The splitting ratio due to the GVR depends on the way the GVR is carried out; that is, it depends on the weight windows map.

¹ Best estimation of the actual uncertainty

² Note that the completely correlated case was the superior boundary of the SDR stochastic uncertainty due to the neutron flux uncertainty

³ The difference between the ratio of the correlated and realistic estimation of the SDR uncertainty between the GVR or no GVR supports again the effect of the GVR technique in the neutron flux covariance

⁴ It is worth to highlight again that the difference is greater than Table 7.9 shows due to the photon transport uncertainty of the no GVR simulation is notable.

⁵ Note that this is a particular case, and the conclusion may be not general

Chapter 7
Application of the uncertainty module of R2S-UNED

Table 7.10 SDR and its uncertainty calculated with different correlation matrixes of the neutron flux, divided in different contributions

<i>Term</i>	No correlated assumption $\left(\frac{mSv}{h}\right)^2$	Completely Correlated assumption $\left(\frac{mSv}{h}\right)^2$	Calculated case $\left(\frac{mSv}{h}\right)^2$
<i>GVR CASE</i>			
<i>SDR covariance</i>	$1.9 \cdot 10^{-1}$	17	2.4
<i>TT Diag.</i>	$1.2 \cdot 10^{-2}$	$1.2 \cdot 10^{-2}$	$1.2 \cdot 10^{-2}$
<i>TT No Diag.</i>	$-2.7 \cdot 10^{-6}$	$-2.7 \cdot 10^{-6}$	$-2.7 \cdot 10^{-6}$
<i>SS Diag.</i>	$1.1 \cdot 10^{-1}$	$3.4 \cdot 10^{-1}$	$2.0 \cdot 10^{-1}$
<i>SS No Diag.</i>	$6.5 \cdot 10^{-2}$	17	2.2
<i>ST Diag.</i>	$3.9 \cdot 10^{-4}$	$1.0 \cdot 10^{-3}$	$6.3 \cdot 10^{-4}$
<i>ST No Diag.</i>	$-6.5 \cdot 10^{-10}$	$-1.7 \cdot 10^{-7}$	$-2.2 \cdot 10^{-8}$
<i>NO GVR CASE</i>			
<i>SDR covariance</i>	$1.4 \cdot 10^{-2}$	2.4	$2.4 \cdot 10^{-2}$
<i>TT Diag.</i>	$1.0 \cdot 10^{-2}$	$1.0 \cdot 10^{-2}$	$1.0 \cdot 10^{-2}$
<i>TT No Diag.</i>	$-2.6 \cdot 10^{-6}$	$-2.6 \cdot 10^{-6}$	$-2.6 \cdot 10^{-6}$
<i>SS Diag.</i>	$2.5 \cdot 10^{-3}$	$5.1 \cdot 10^{-2}$	$2.8 \cdot 10^{-3}$
<i>SS No Diag.</i>	$1.4 \cdot 10^{-3}$	2.4	$1.1 \cdot 10^{-2}$
<i>ST Diag.</i>	$4.8 \cdot 10^{-6}$	$8.0 \cdot 10^{-5}$	$5.6 \cdot 10^{-6}$
<i>ST No Diag.</i>	$-1.4 \cdot 10^{-11}$	$-2.4 \cdot 10^{-8}$	$1.2 \cdot 10^{-10}$

7.2 Application of the R2S-UNED uncertainty module in 2016 DD campaign of JET

This section presents the application of R2S-UNED to estimate the SDR uncertainty in JET reactor within the project "WP3JET: NEXP shutdown dose rate experiments"[76] under the EUROfusion program. This project is dedicated to exploit the JET results to validate the codes used to estimate the SDR and applied in ITER[80] [81]. Specifically, UNED activities are focused on R2S-UNED and D1S-UNED codes validation for the SDR estimation in fusion reactors environments.

Inside of NEXP project, R2S-UNED was applied to estimate the air-kerma (SDR) in a detector located in the octant 2 of JET at 6 hours after of 2016DD campaign¹ shutdown. There are two main reasons to apply the tool in this context.

The first one is to evaluate the applicability of the tool in a real scenario. Note that, nowadays, the campaign of JET is the most representative case of fusion environments.

The second one is to use the new capabilities implemented in R2S-UNED to improve the quality of the R2S-UNED code validation².

With respect to the capability to estimate the MC uncertainty of the R2S simulation, the estimation of the air-kerma uncertainty in this framework allows a better comparison with the JET results. In addition, it also improves the comparison with other D1S and R2S tools³ validated in the same framework.

Furthermore, the new capabilities implemented in R2S-UNED such as the estimation of contributing regions, isotopes, and reactions enable a better compression of JET campaign results as well as the R2S method. It is worth highlighting that these capabilities have helped in the detection of R2S miscalculations in the air-kerma in JET [82].

Concerning the R2S-UNED application in JET to estimate the air-kerma uncertainty, the initial approach consisted in the application of the previous guideline, which was presented in section 7.1.2. However, the number of contributing regions to the air-kerma is too high; therefore, this guideline cannot be applied⁴.

In this situation, a new computational scheme was developed to overcome this difficulty. This scheme is based on dividing the R2S simulation into a set of R2S simulations. Each one of them calculates the contribution of a specific region to the SDR. This division enables the SDR contributions and their stochastic uncertainties were calculated with the developed tool. Afterwards, the contributions are summed to estimate the SDR and the associated uncertainty.

The raw application of this strategy could increase the computational time to estimate the uncertainty if there are too many contributing regions, making the simulation unviable. For that reason, the division process of the R2S simulation was automatized and optimized to define the

¹ This campaign aimed to reduce experimental and computational uncertainties as preparation for the DTE2 campaign. This includes reducing the calculation uncertainty of the computational tools.

² This point is out of the scope of the thesis. Therefore, this thesis does not provide the details of this topic

³ The utility of this information was also shown in section 7.1.2

⁴ The raw application of the developed tool to estimate the air-kerma uncertainty still allows calculating the air kerma uncertainty considering the completely correlated or the uncorrelated approaches. See section 7.1.5

smallest number of regions. Despite the optimization scheme, there are still cases where the number of contributing regions can be prohibitive.

The presentation of the estimation of the air-kerma uncertainty in the JET detector of the octant 2 is presented in the next section as follows:

Section 7.2.1 presents the general computational assumptions, such as the model or the irradiation scenario.

Section 7.2.2 describes the estimation of the range of the air-kerma uncertainty calculated with R2S-UNED. That is, the estimation considering the complete correlated or uncorrelated approaches. In addition, this section also details the analysis of the DGS contribution to the air-kerma tally, because it is part of the application scheme.

Section 7.2.3 depicts this new computational scheme as well as its application to estimate the air-kerma and its MC uncertainty.

7.2.1 General computational assumptions of R2S air kerma estimation in octant 2 of JET

The experimental assembly and measurements analyses performed in the last 2016 DD benchmark are described in [83]. The MCNP model¹ of the octant 2 of this experiment was provided by EUROfusion [84]. The model, plotted in Figure 7.6, represents 45° of the tokamak. Reflective boundary condition on the lateral sides is applied to simulate a 360° reactor. Regarding the material described in the MCNP model, it includes impurities based on available chemical certificates.

Concerning the neutron irradiation scenario, the whole JET irradiation scenario (from 1983) was considered to activate the JET materials. A description of the DD and DT irradiation scenario² can be found in [85].

¹ The detail level of the MCNP model is high enough to obtain good agreement between experimental and simulated results.

² The TT neutron budget is negligible and therefore, it is not considered to the JET analysis thus far.

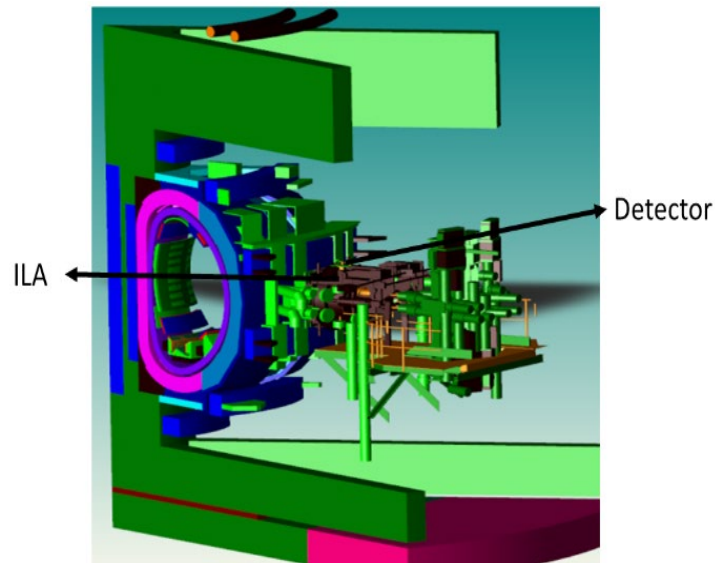


Figure 7.6 CAD model of principal regions of the octant 2 of JET

Because of the huge number of pulses, the irradiation history of JET is conveniently divided into some equivalent irradiation periods with a constant neutron emission rate averaged over their time duration. The early JET campaigns up to 2010 are represented as multiannual irradiation periods, while 2011–2016 JET campaigns are extracted from a detailed daily database. The neutron budget of these last years is presented in Table 7.11.

Table 7.11 2011-2016 yearly DD and DT neutron budget[85]

Year	DD	DT
2011	$2.05 \cdot 10^{17}$	$2.13 \cdot 10^{15}$
2012	$7.47 \cdot 10^{18}$	$3.21 \cdot 10^{16}$
2013	$7.67 \cdot 10^{18}$	$3.68 \cdot 10^{16}$
2014	$1.07 \cdot 10^{19}$	$8.49 \cdot 10^{16}$
2015	$4.07 \cdot 10^{18}$	$1.66 \cdot 10^{16}$
2016	$1.72 \cdot 10^{19}$	$2.27 \cdot 10^{17}$

It is worth underlining that the DD and DT neutron activation are considered individually in the R2S simulations. The fact to be able to consider this approach¹ implies that the activation is linear to the neutron flux. This means that SNILB conditions are assumed during JET analyses.

Regarding the nuclear data, R2S-UNED[24] simulations carried out in section 7.2 considered Fendl2.1 and 3.1 [86] library data to the neutron transport and MCPlib84 [73] to the photon transport. The activation was performed using EAF2007 [74] activation cross-section library.

¹ This hypothesis has also been verified.

With respect to the energy discretization, the neutron flux estimation is performed with CuV¹ capability and VitaminJ energy group structure [66]. While the decay gamma energy resolution was the usual recommended by FISPACT [22], which is described in annex A.

Concerning the spatial discretization, this will be described to each specific simulation in the following sections. In addition, it is also worth mentioning that GVR was used during the neutron transport (see section 7.1.5).

7.2.2 Estimation of the air-kerma and the bounding limits of its uncertainty using R2S-UNED

This section describes the application of the guideline presented in section 7.1.2 in order to estimate the MC air kerma uncertainty of the R2S simulation presented in NEXP project [55] [82]. As was commented, the number of contributing regions (which is calculated as part of the guideline application) is extremely high. Consequently, only the estimation of the uncertainty considering the neutron completely correlated or uncorrelated was performed.

Initially, we try to apply the guideline presented in section 7.1.2 in order to estimate the MC air kerma uncertainty of the R2S simulation presented in NEXP project [55] [82]. For that, the DGS contribution of the complete mesh must be analyzed to define an adequate reduced mesh, where the covariance matrix of the neutron flux can be estimated.

Regarding the organization of this section, section 7.2.2.1 presents the computation and analysis of the DGS contribution to the air kerma. Noting that the general mesh of this simulation consists in 8 meshes covering the whole MCNP model. The size of each mesh element is 10cm × 10cm × 10cm. Otherwise, section 7.2.2.2 presents the estimation of the uncertainty range of the air-kerma.

7.2.2.1 Air kerma estimation and DGS contribution

The R2S simulation was carried out according to the previous description. The neutron transport was run up to $4 \cdot 10^8$ histories. Figure 7.7 shows the neutron flux and its uncertainty in the DD simulation².

¹ It is worth noting that the estimation of the uncertainty does not consider the CuV. Nevertheless, this has no practical influence on the MC uncertainty estimation of the SDR as ANNEX D shows.

² DT neutrons are not presented because they are not relevant to the estimation of the air-kerma, as will be presented in this section

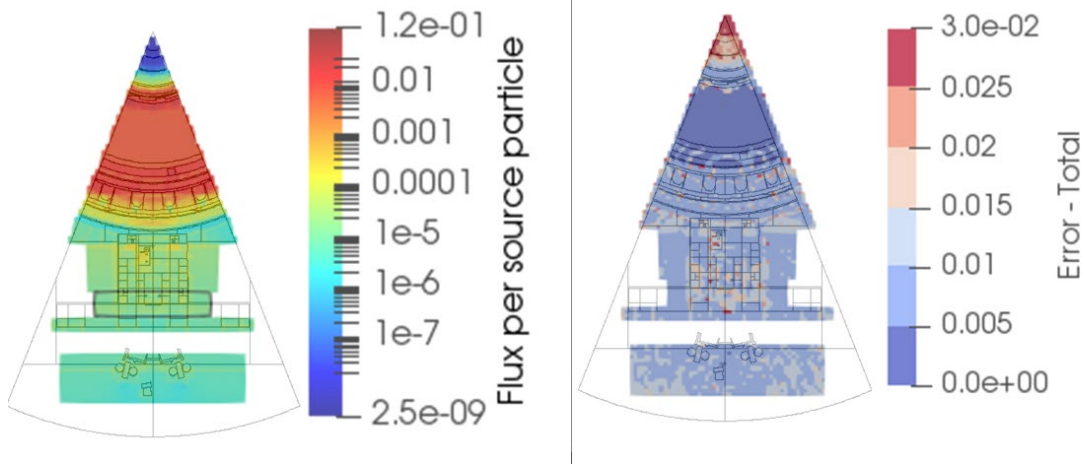


Figure 7.7 PZ=100 of the neutron flux uncertainty over the whole JET geometry

Decay gamma transport calculations were run up to 10^{10} photon source histories were tracked for the DGS produced by the DD neutrons, while $4 \cdot 10^9$ photon source histories were simulated for the DGS produced by the DT activation. The air kerma and the DGS contribution of each mesh (ANNEX B) are presented in Table 7.12.

The results presented in Table 7.12 shows that 96.73% of the response is due to the DD neutrons. Therefore, we can focus only in this neutron simulation to estimate the uncertainty of the case¹.

Table 7.12 Contribution to the air kerma tally

Mesh	DD ($\mu\text{Sv/h}$)	Contribution (%)	DT ($\mu\text{Sv/h}$)	Contribution (%)
1	$2.35 \cdot 10^{-4}$	0.01	$1.00 \cdot 10^{-4}$	0.004
2	$8.30 \cdot 10^{-3}$	0.39	$2.15 \cdot 10^{-4}$	0.01
3	1.22	57.54	$2.25 \cdot 10^{-2}$	1.06
4	0.78	37.00	$4.44 \cdot 10^{-2}$	2.10
5	$1.52 \cdot 10^{-2}$	0.72	$9.37 \cdot 10^{-4}$	0.04
6	$2.12 \cdot 10^{-3}$	0.10	$2.25 \cdot 10^{-4}$	0.01
7	0.0	0.00	$9.06 \cdot 10^{-5}$	0.004
8	$2.02 \cdot 10^{-2}$	0.96	$7.24 \cdot 10^{-4}$	0.03
Total	2.05	96.73	$6.92 \cdot 10^{-2}$	3.27
DD+DT	2.12 $\mu\text{Sv/h}$			

¹ Note that the estimation of the uncertainty does not require an extremely high accuracy

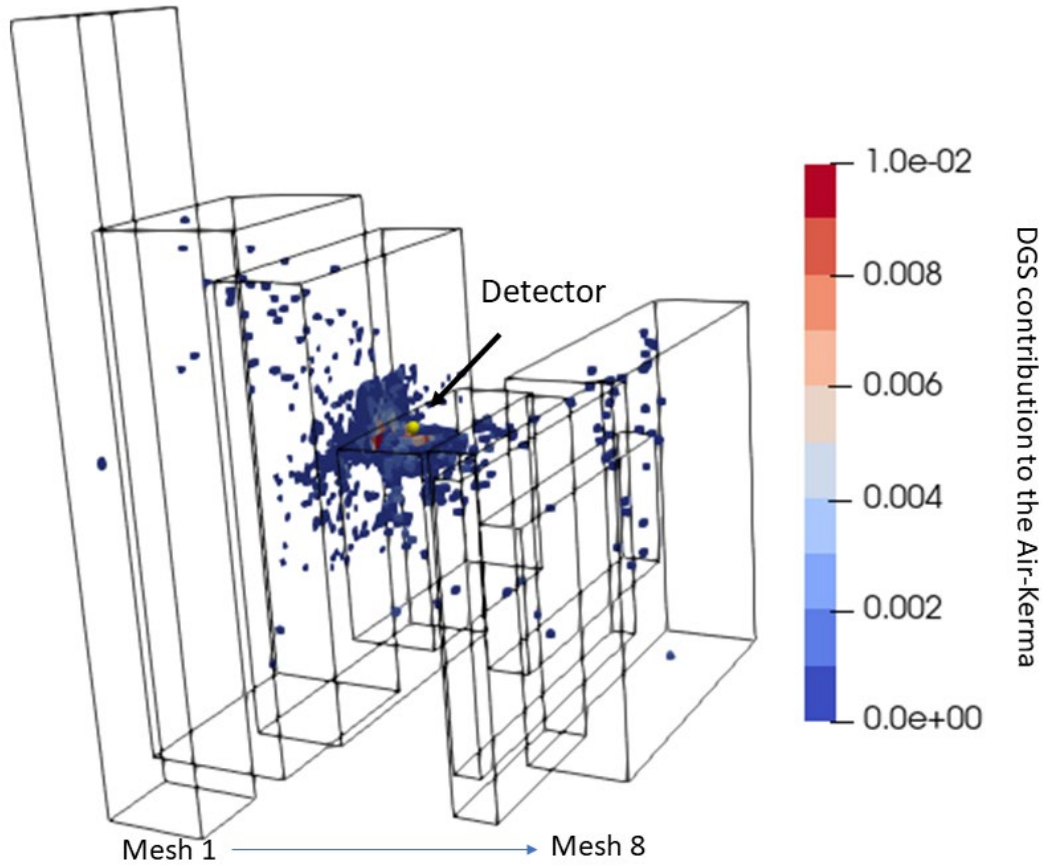


Figure 7.8 DGS contribution to the air-kerma in the detector (yellow sphere) due to the DD neutron activation

The DGS contribution due to the activation of the DD neutrons is detailed in Figure 7.8. This figure, and the results of Table 7.12, show that the contribution to the air kerma comes principally from meshes 3 and 4. However, the number of elements, which contribute to the air-kerma, are excessively high. Therefore, the guideline proposed to estimate the uncertainty in section 7.1 cannot be applied.

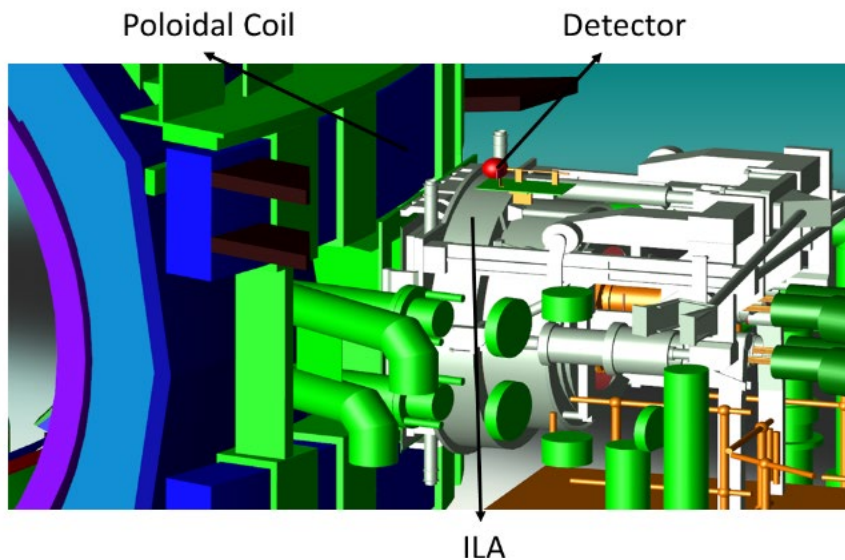


Figure 7.9 Contributing regions to the Air-Kerma [87].

The contributing regions, in the MCNP model, correspond to the poloidal coil (mesh 3) and the ILA (mesh 4). These regions are shown in Figure 7.9.

7.2.2.2 Estimation of the correlated or uncorrelated assumption bounding of the air kerma uncertainty

This section presents the estimation of the SDR uncertainty of the R2S simulation shown in section 7.2.2.1; that is, the R2S simulation considering the DD neutron activation from meshes 3 and 4. In addition, due to the high number of contributing elements, the uncertainty is estimated assuming correlated and uncorrelated approaches¹.

Neutron transport and activation step of the R2S simulation performed in 7.2.2.1 were reused to estimate the air-kerma uncertainty. However, the photon simulations of meshes 3 and 4 were run up to 10^{10} photons in order to reduce the stochastic uncertainty in this step. These new calculated DGS contributions were considered to perform the uncertainty calculation with the uncertainty module of R2S-UNED. Table 7.13 shows the superior boundary of the air kerma uncertainty due to meshes 3 and 4. These results show that the uncertainty of the air-kerma of this R2S-UNED simulation is smaller than 5%².

Table 7.13 Uncertainty estimation of the air-kerma contribution of mesh 3 and 4. Correlated neutron flux approach.

	<i>Mesh 3</i>	<i>Mesh 4</i>
<i>Air-kerma</i> ($\mu\text{Sv/h}$)	1.29	0.771
$\sigma_{\text{Air-kerma}}$ ($\mu\text{Sv/h}$)	0.05	0.011
$SS^{1/2}$ ($\mu\text{Sv/h}$)	0.048	0.011
$TT^{1/2}$ ($\mu\text{Sv/h}$)	0.017	0.0019

Regarding the uncorrelated case, the values of the uncertainty are presented in Table 7.14. In this case, the uncertainty is close to 1%.

Table 7.14 Uncertainty estimation of the air-kerma contribution of mesh 3 and 4. Uncorrelated neutron flux approach.

	<i>Mesh 3</i>	<i>Mesh 4</i>
K_a ($\mu\text{Sv/h}$)	1.286	0.771
σ_{K_a} ($\mu\text{Sv/h}$)	0.017	0.002
$SS^{1/2}$ ($\mu\text{Sv/h}$)	0.0017	0.0003
$TT^{1/2}$ ($\mu\text{Sv/h}$)	0.017	0.0019

¹ The correlated approach is a superior boundary, while the uncorrelated approach may be a more realistic inferior boundary. See 7.1.5.

² The neutron flux of both meshes was calculated at the same time. Therefore, the uncertainties of both simulations were combined also assuming that they are also correlated

Therefore, the results of this section show that the air-kerma was calculated with a good stochastic uncertainty (between 5% and 1%). In the worst case, the uncertainty is principally due to the neutron transport simulation, while in the uncorrelated case, the uncertainty from the photon transport is worse than the neutron transport uncertainty¹.

7.2.3 Estimation of the air-kerma and its actual stochastic uncertainty using R2S-UNED

This section calculates the uncertainty of the air-kerma in the octant 2 of JET. In this assessment, the air kerma is defined as the sum of a set of contributions. For that, the simulation is divided into a set of R2S cases. Each one of them allows calculating the correlation matrix of the neutron flux. It is worth highlighting that each R2S case calculates the contribution of a specific region to the air-kerma.

According to the results of section 7.2.2.1, the air kerma in the detector is practically those due to the activation of meshes 3 and 4 (hereafter called general meshes) in the DD neutron source calculation.

Considering this result, the estimation of the air-kerma uncertainty is reduced to estimate the uncertainty from the DD neutron contribution of each one of these meshes (97% of the air-kerma response).

The computational scheme followed to estimate the uncertainty in each general mesh is divided into 3 steps presented below:

I. Optimization of the definition of the set of R2S cases:

This step consists in defining a set of meshes (hereinafter called relevant meshes), which cover all contributing regions (considering the previous region filter). Each relevant mesh must be small enough to estimate the correlation matrix of the neutron flux.

II. Estimation of the air-kerma and its uncertainty of each R2S case:

This step consists in the estimation of the air-kerma contribution of each relevant mesh, as well as assessing its uncertainty using R2S-UNED. It is worth remarking that this step requires independent R2S simulations, which are achieved using different random seeds in each R2S simulation.

III. Combination of the uncertainties of the different R2S simulations:

Finally, the air kerma contributions and their associated uncertainties are combined. The result is the total SDR and the associated stochastic uncertainty of the complete calculation.

Concerning the application of these steps in the simulation of the air-kerma in JET: The definition of the relevant meshes is presented in section 7.2.3.1. The estimation of the stochastic

¹ This suggests a good distribution of the computational time spent in the neutron and photon transport

uncertainty of each air-kerma contribution is detailed in section 7.2.3.2. Finally, the combination of the results to estimate the total air kerma and its uncertainty is described in 7.2.3.3.

7.2.3.1 Optimization of the mesh definition to calculate the Air-kerma uncertainty

Figure 7.10 shows the element of the general meshes that contributes to the air kerma¹. The picture shows that the number of elements is extremely high to define the relevant meshes manually in any of the general meshes. Consequently, an algorithm to define the meshes was developed.

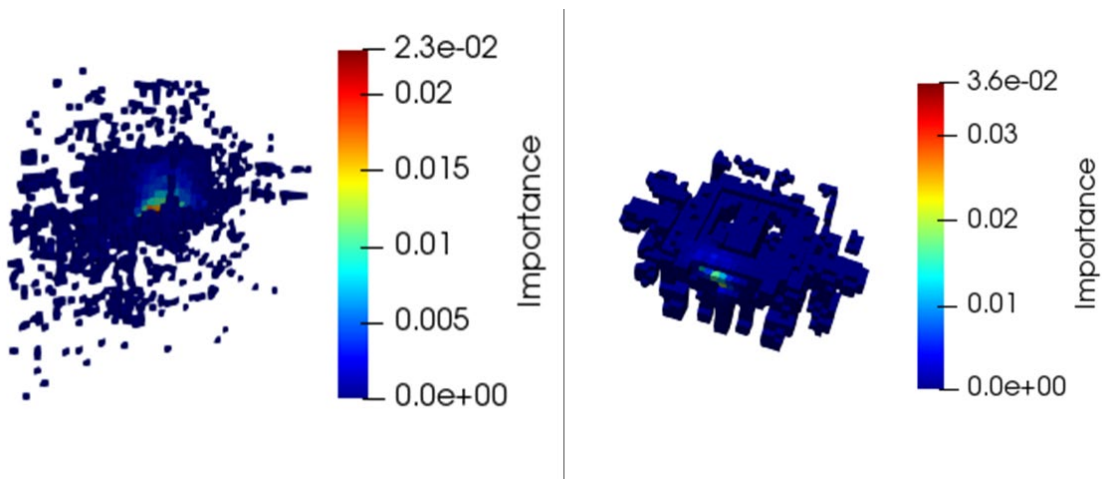


Figure 7.10 Contribution element of the mesh 3 (left) and 4 (right)

This algorithm, described in subsection I, defines the relevant meshes according to the order of the index of the contributing region in the input file. Therefore, the number of defined meshes depends on the algorithm input data (order of the array containing the relevant positions).

The raw application of this algorithm defines a huge number of relevant meshes, increasing the computational time because each mesh corresponds to one R2S simulation². For this reason, the algorithm was integrated inside another code that optimize the number of relevant meshes defined. Section II describes two options, which optimize the number of meshes.

Finally, section III presents the results of both options and the best definition of the relevant mesh.

I. Algorithm to define the relevant mesh

The algorithm, described in Figure 7.11 depicts the algorithm implemented to define the relevant meshes. The algorithm starts reading all relevant indexes³ and stores them in the

¹ This figure is obtained from Figure 7.8

² The R2S simulation includes the estimation of the MC uncertainty of the air-kerma contribution.

³ They are the DGS contribution elements. Note that, the practical implementation of the algorithm includes a filter, which discards those elements that almost do not contribute.

“relevant index vector”. Afterwards, it defines the possible relevant mesh, if the mesh is not small enough¹ the algorithm discards the last index of this array, and the mesh is built again. When the mesh is small enough, it is stored, and the algorithm starts again using all discarded elements as the new “relevant index vector”.

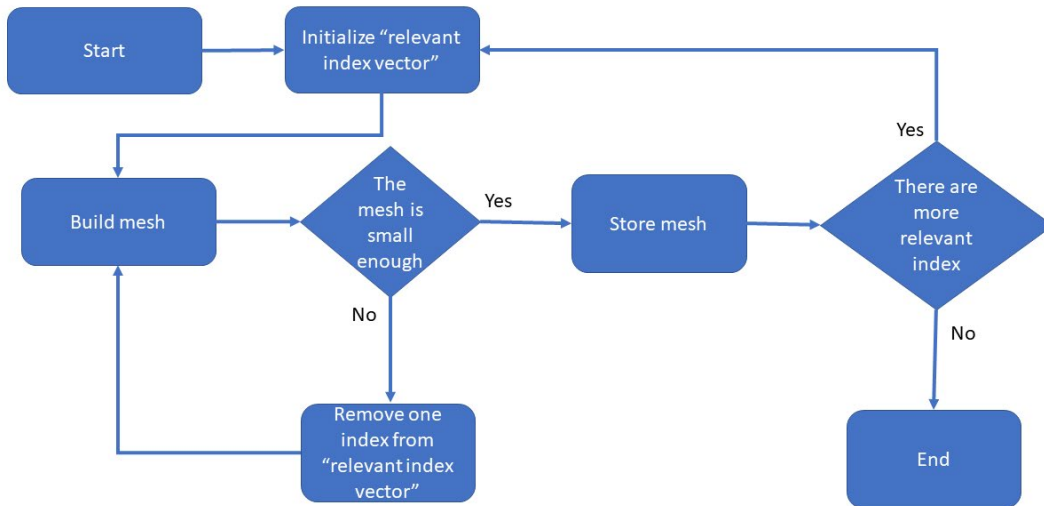


Figure 7.11 Algorithm implemented to define the meshes that contain the relevant regions

As it can be deduced from this description, the number of relevant meshes defined at the end of the algorithm depends on the input data. This means that it depends on the order in which the contributing elements are sorted in the “relevant index” array.

II. Algorithm to optimize the number of relevant mesh defined

As was previously said, the number of meshes defined by the algorithm described in subsection I depends on the order of the input data. Therefore, we can reduce the computational time to estimate the air-kerma and its uncertainty² by optimizing the number of defined meshes. However, the direct option to choose the optimal one (i.e. the evaluation of all possibilities input configuration) is not suitable. Because there are factorial of N possible input data, where N is the number of relevant elements. For that, below, we propose two different approaches which try to find an optimal solution:

- i. Sort the relevant elements according to the distance

The idea of this algorithm is to try to put together the closer elements. This way all these elements can be included in the same mesh, reducing the total number of meshes defined.

¹ Note that the small enough is defined according to the available computational resources

² Note that each mesh requires a complete R2S simulation (neutron transport, activation, photon transport, and uncertainty transport).

ii. *Simulated annealing* algorithm

Simulated annealing is a useful methodology, based on MC Markov chains. In this scope, we use the algorithm to minimize a function (commonly called "Energy" function). A very brief description of the algorithm is done below. More details about the methodology, including the scheme, can be found in [88].

The algorithm is an extension of the Metropolis algorithm[89] that appropriately samples the phase space¹ of the function, according to the probability of each system configuration. In the algorithm, the probability of a system² is assigned according to the number of meshes defined. Consequently, it leads to sample more systems whose energy is small. Hence, the algorithm ends by finding the system whose energy is minimum, ideally³.

III. Definition of the relevant meshes

The relevant meshes were defined from the contributing elements to the air kerma of meshes 3 and 4 using the three methodologies: Default definition, sorting by distance or using the *simulated annealing* algorithm.

The methods previously described were applied to define the relevant meshes considering:

- i. The maximum number of mesh elements is 120 (the available extra RAM in our cluster⁴ is around 1.8GB).
- ii. The mesh elements were filtered (97% of the contribution to the SDR) in order to delete isolated elements whose contribution is negligible.

Table 7.15 Number of meshes defined

	<i>Mesh 3</i>	<i>Mesh 4</i>
<i>Number of relevant elements</i>	738	742
<i>Number of raw meshes</i>	276	125
<i>Number of meshes according to the distance</i>	181	96
<i>Number of meshes using simulated annealing</i>	50	20

¹ In this scope, the phase space is the space of all possible "relevant index" arrays; That is, the space where are defined the possible inputs to build the relevant meshes

² One possible configuration of the input array (containing the relevant regions)

³ It is important to notice that the method tries only a few elements of the phase space. Consequently, the method only guarantees a good solution, not the best one. The quality of the solution is strongly related to the implementation of the method. For the aim of this application, the implementation performed in this thesis is considered good enough.

⁴ Our cluster, where the cases were run, is currently composed by 1000 processor Intel(R) Xeon(R) Silver 4210 CPU @ 2.20GHz

Table 7.15 summarizes the results achieved by default, sorting by distance, or using the *Simulated annealing* algorithm.

Clearly, *simulating annealing* algorithm produce the best option. The definition of these meshes is printed in Figure 7.12.

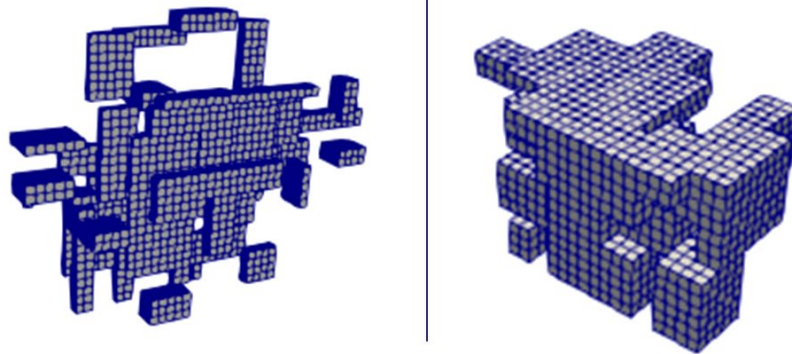


Figure 7.12 Distribution of the meshes to consider 95% of the contributing regions

7.2.3.2 Estimation of the air-kerma uncertainty of each defined R2S simulation

This section describes the R2S simulations performed to calculate the air kerma and its uncertainty in each relevant mesh plotted in Figure 7.12. Due to the high number of meshes, the NPS of each neutron and photon simulation was reduced. The different steps of each R2S simulation carried out are described below. It is important to remark again that the random seed of each transport simulation is different and, therefore, the results of each simulation were uncorrelated with each other.

In the case of the neutron transport, $2 \cdot 10^7$ histories were simulated. Figure 7.13 shows the uncertainty of the neutron flux of each mesh. The increase of the uncertainty is approximately $20^{1/2}$ the uncertainty presented in Figure 7.7, as was expected¹.

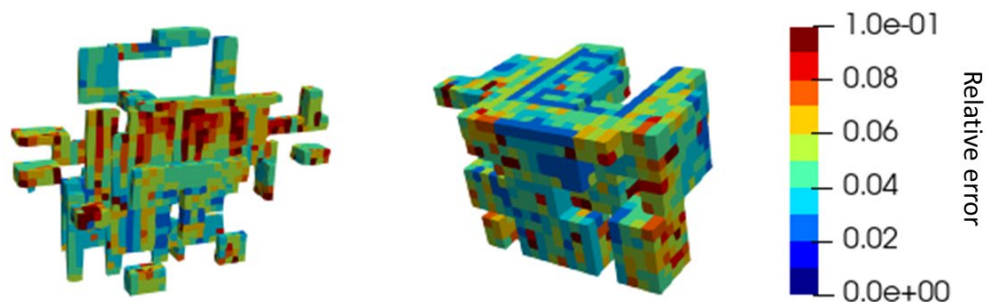


Figure 7.13 Neutron flux uncertainty in each mesh

¹ This is a required condition of the simulation convergence, although it does not guarantee the convergence by its-self

Afterwards, the activation step is performed in each mesh in order to obtain the DGS. The DGSs are post-processed to delete all crushes with other meshes. Each DGS is transported simulating 10^8 histories to calculate the contribution of each region (relevant mesh) to the air kerma.

The last step consists in calculating the uncertainty of the air kerma due to each mesh. The uncertainty of each mesh was calculated considering the three options for the neutron flux covariance: calculated (best estimation), completely correlated, and uncorrelated.

The results of the contribution of each mesh and its associated uncertainties are presented in Figure 7.14 and Figure 7.15¹. These results show that the correlated assumption widely overestimates the stochastic uncertainty due to the neutron flux in the air kerma.

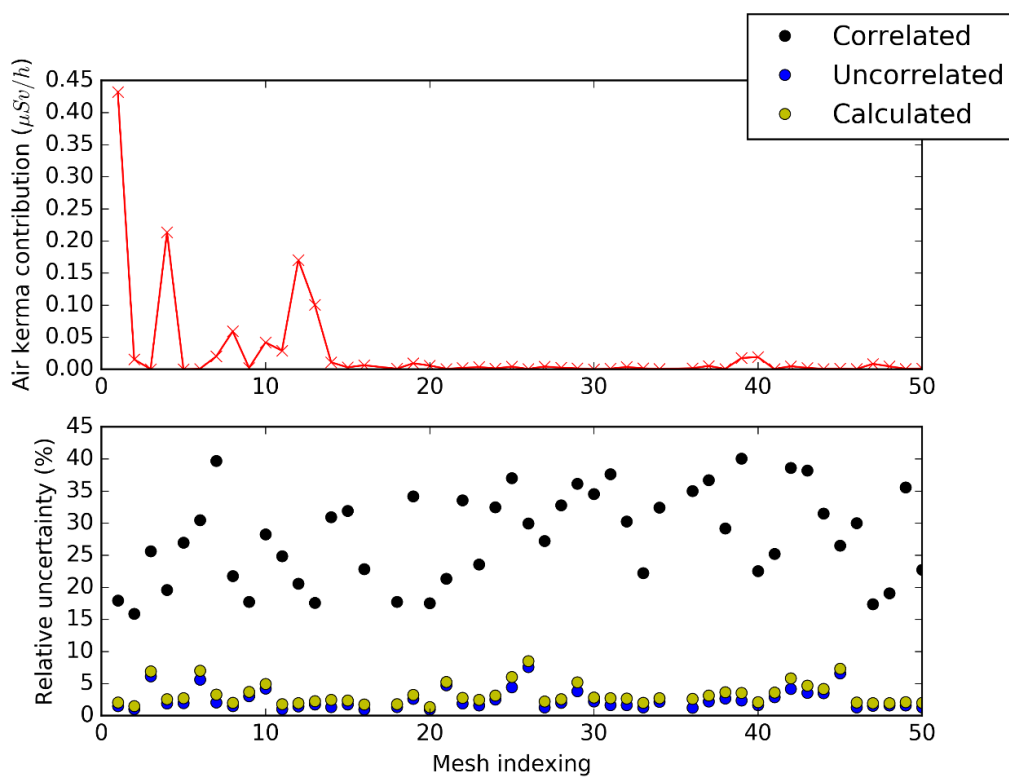


Figure 7.14 Contribution of each small mesh inside of mesh 3 to the air kerma and its uncertainty due to the neutron flux

¹ The most contributing case was also compared with the brute force method. This comparison is in agreement (but does not prove) the simulation convergence. In addition, it is another verification of the tool. The comparison is presented in ANNEX D

Chapter 7
Application of the uncertainty module of R2S-UNED

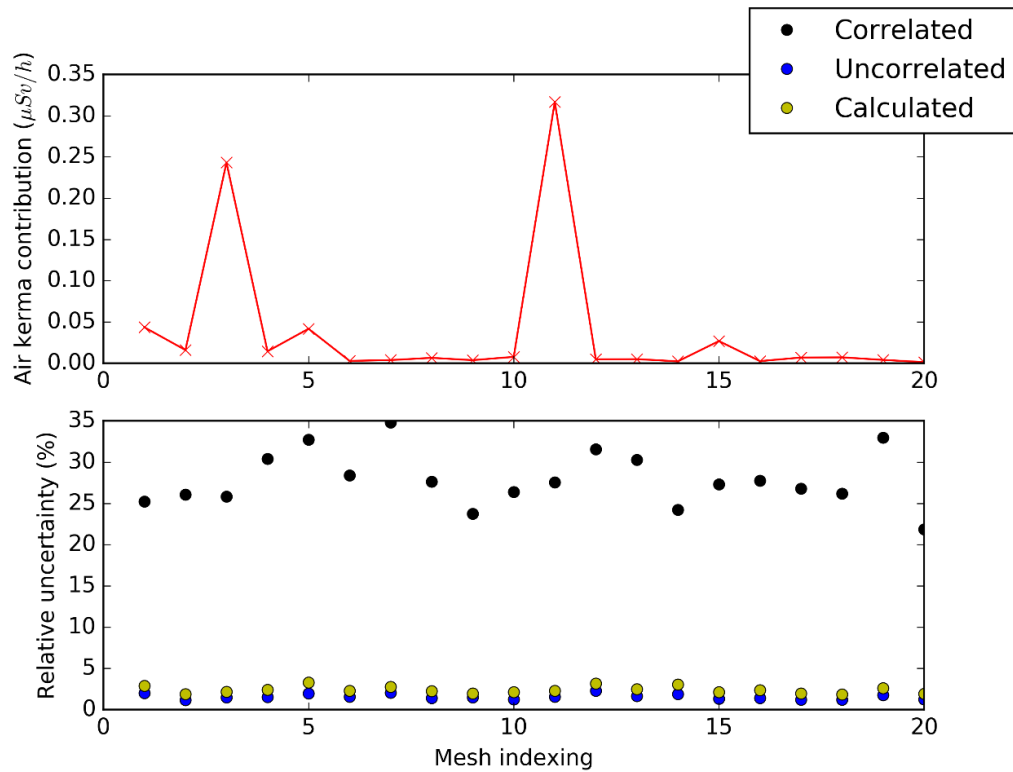


Figure 7.15 Contribution of each small mesh inside of mesh 4 to the air kerma and its uncertainty due to the neutron flux

Regarding the uncorrelated estimation of the air-kerma uncertainty, we can see that this assumption underestimates the calculated uncertainty of the case. Both quantities are compared in Figure 7.16 to clarify the scale of the previous plot. Notice that the plots show up to a factor of 0.5, which could be unacceptable.

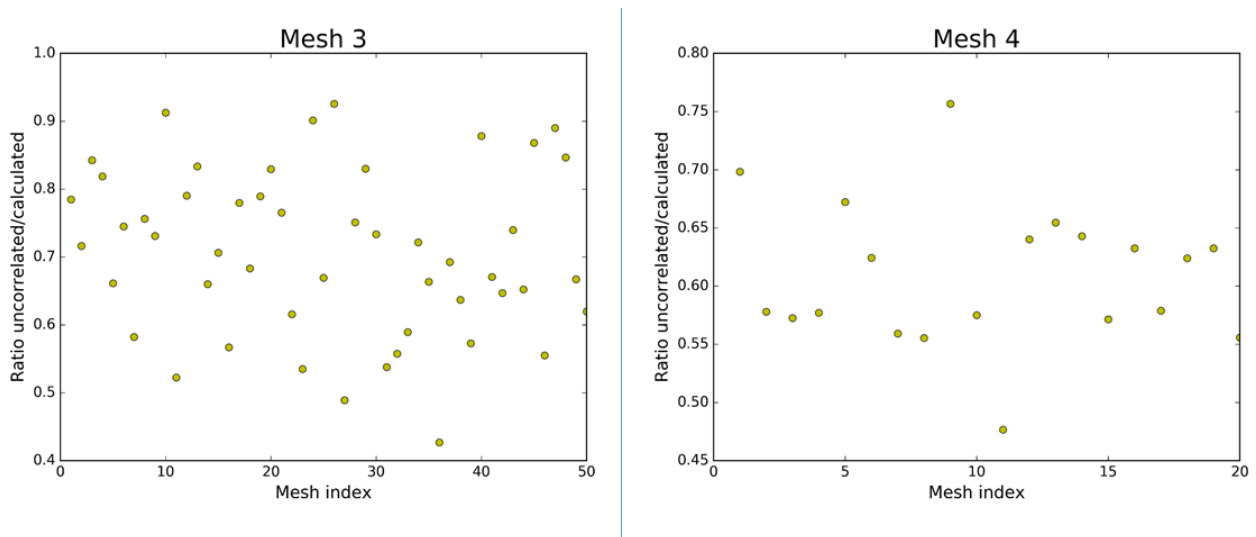


Figure 7.16 Uncertainty underestimation of the uncorrelated assumption of the correlation matrix of the neutron flux in JET

7.2.3.3 *Merging the uncertainty of the different regions.*

Since the different R2S estimations were performed using a different random seed, the results are uncorrelated. This means that, according to the law of uncertainty propagation, the uncertainty of the sum of them can be estimated as shown in Equation 7.3.

$$K_a = \sum_m K_{a_m} \rightarrow \sigma_{K_a} = \sqrt{\sum_m \sigma_{K_{a_m}}^2}$$

Equation 7.3

Table 7.16 R2S estimation of the Air Kerma and its stochastic uncertainty in the Octant 2 of JET

	<i>Correlated</i>	<i>Uncorrelated</i>	<i>Calculated</i>
K_a ($\mu\text{Sv/h}$)	1.97	1.967	1.967
σ_{K_a} ($\mu\text{Sv/h}$)	0.11	0.006	0.009
$SS^{1/2}$ ($\mu\text{Sv/h}$)	0.11	0.006	0.009
$TT^{1/2}$ ($\mu\text{Sv/h}$)	0.0011	0.0011	0.0011

The estimated air-kerma uncertainty, calculated using different assumptions of the correlation matrix of the neutron flux, is presented in Table 7.16.

Concerning the comparison between this simulation and the R2S simulation of section 7.2.2, we can see that they are in good agreement¹, as was expected. However, contrary to the R2S simulation presented in 7.2.2, the uncertainty due to the photon transport in this simulation is negligible². This is due to each simulation samples a small region. Therefore, the contributing region of the DGS is sampled better in this simulation than in those described in 7.2.2.

Regarding Table 7.16 results its-self, they also support the conclusion of section 7.2.3.2. The correlated case strongly overestimates the air-kerma (around a factor 7). While the uncorrelated case underestimates slightly the uncertainty. It is worth noting that, the uncorrelated case can be considered a good approach in this simulation³.

It is worth highlighting that, despite the uncertainty of the neutron flux was in general superior to 3% (Figure 7.13), the uncertainty of the SDR is around 0.5%. This is due to, in this case, the correlation between the different elements is low.

¹ Note that the simulation was filtered up to 97% of the contribution of the Air-Kerma. The actual estimation of the Air Kerma is 2.03

² This means that, if the simulation has converged, we should dedicate less computational time to the photon transport.

³ As commented previously, it is not a general conclusion, because different simulation parameters can modify the correlation of the neutron flux.

7.3 Summary and Conclusions

This chapter shows the applicability of the implemented uncertainty module of R2S-UNED in two different exercises: The computational SDR ITER benchmark and the estimation of the air-kerma in the detector of the octant 2 of JET at 6 hours after 2016 DD campaign shutdown.

Both exercises contribute to get the next conclusions:

I. Application range of the uncertainty module of R2S-UNED

One of the aims of the thesis was that the implemented tool could be applied in any case where R2S-UNED could be required. In this sense, the uncertainty module of R2S-UNED was successfully applied in both cases. However, it is worth highlighting that:

- a. Other types of analysis could require different outputs such as mesh tallies, where the proposed scheme to estimate the SDR uncertainty cannot be applied.
- b. The estimation of the real uncertainty of the case requires the calculation of the neutron flux correlation matrix. Usually, this assessment is prohibitive in most practical cases, as the cases of the ITER benchmark or the JET application¹.

In order to increase the applicability of the R2S-UNED uncertainty module, we propose different calculation guidelines, depending on the difficulties of the simulation:

- a. The simplest kind of calculations is those where the correlation matrix of the neutron flux can be directly estimated. An example of this is the thin slabs presented in Chapter 6
- b. A more complex kind of simulation requires redefining the simulation covering the relevant region by a single mesh. In these cases, we propose a guideline that uses the DGS contribution as a user guide to defining a reduced mesh. This simulation was the case of the ITER benchmark.
- c. Realistic simulations usually have a high number of contributing regions, which does not allow using the previous guideline. For this kind of situation, we develop an automatized process to define an optimal set of R2S simulations, where each simulation is small enough to estimate the uncertainty. This was the case for the JET application. It is worth highlighting that this case requires more computational time than the simple SDR estimation.

Despite these guidelines, there are cases where the computational requirement of the R2S simulation can be prohibitive to the estimation of the stochastic uncertainty. Therefore, this aim related to the applicability of the tool was only partially achieved.

¹ Note that the JET simulation, where the actual SDR uncertainty was estimated, only calculates around 95% of the SDR in the tally. It was due to the different applied filters.

II. Effects of the variance reduction in the correlation matrix

The variance reduction techniques are commonly used in R2S simulations to optimize the calculations. These techniques can considerably affect the correlation degree of the neutron flux because they lead to correlate the neutron flux. Despite seeing this relation, we cannot predict the degree of correlation due to these techniques.

III. Importance of the realistic estimation of the correlation matrix

When the guidelines commented on the point I cannot be applied, the uncertainty module can still provide useful information. We can assume that the correlation matrix of the neutron flux is completely correlated (superior bound of the uncertainty) or uncorrelated. However, important differences were found between these approaches and the real uncertainty. This means that an appreciable extra computational time must be spent in the neutron simulation to guarantee the uncertainty limit of the simulation.

IV. Relevance of the SDR uncertainty in the analysis

The estimation of the stochastic uncertainty of the calculation method of the R2S-UNED and D1S-UNED enables us to distinguish the differences between both results due to the calculation assumptions of each method.

In addition, the estimation of the uncertainty of the JET calculation enables estimating the numerical quality of the simulation. The uncertainty of the air-kerma calculated is close to 1%, which is considered a low uncertainty (due only to the calculation method).

V. Convergence

The simulation convergence is required for the results provided by R2S-UNED (both, SDR and its associated stochastic uncertainty) was meaningful. MCNP performs useful tests to evaluate the convergence of the different tallies. However, most of these tests are not suitable for mesh-tally simulation due to the enormous amount of data to be managed. Consequently, we do not know if we can take action based on the uncertainty calculated by the R2S-UNED uncertainty module. During this chapter, we deal with this topic performing some tests¹ (when it was possible)

¹ They are the total uncertainty, the behaviour of the uncertainty with the NPS and the visual inspection of its probability distribution

Chapter 7
Application of the uncertainty module of R2S-UNED

but it does not guarantee completely the convergence of the simulation. This is still an open issue in the mesh-tally calculation.

Chapter 8.

Summary and Conclusions

This thesis is focused on the uncertainty propagation in R2S method. In this framework, this work describes a methodology to perform the estimation of the stochastic uncertainty in R2S, as well as its implementation in R2S-UNED.

The milestones related to the theory and implementation of this methodology are described in section 8.1. However, it is worth mentioning those achievements directly related to the purpose of the thesis:

The first objective was that the methodology must be suitable to advanced MC R2S. This goal was successfully accomplished, as proven by the fact that the methodology was implemented in R2S-UNED.

The second one consisted in estimating the SDR stochastic uncertainty when SNILB¹ conditions are not met. In this case, dedicated validation exercises were successfully carried out in order to demonstrate that this aim was achieved.

Regarding the applicability of this method², important and expected issues were found. During this thesis, we propose different guidelines or methodologies to overcome them with different degrees of success. These propositions enabled the methodology to be used in two computational applications with different sophistication degrees: The ITER computational SDR benchmark and the estimation of the air-kerma in JET. However, they do not represent the whole typical analysis performed with R2S-UNED. This topic is deeper commented in section 8.2.

Finally, section 8.3 shows the visibility of the work performed during the thesis describing the transfer outcomes in conferences, articles, and so on.

¹ Single Neutron Interaction and Low Burn-up (considered during the activation step).

² The tool must be applied in any case where R2S-UNED was relevant.

8.1 Implementation and validation of the methodology

Common R2S implementations do not estimate the stochastic uncertainty of the estimated SDR. For that reason, during the last years, several methodologies have been implemented to mitigate this issue. However, all of them present the same relevant weakness. They cannot estimate the SDR stochastic uncertainty when SNILB conditions are not met. That is, in the cases where the R2S methodology is more relevant. As a consequence, the utility of these methodologies is limited.

In order to overcome this limitation, we have developed a new methodology that is described in depth in Chapter 4.

Concerning the milestones related to the implementation of the tool in R2S-UNED; we classified them into two types¹: The first ones are related to the correct transportation of the neutron flux uncertainty up to the SDR; while the second ones deal with the implementation of additional capabilities in R2S-UNED required to the correct transportation of the uncertainty. It is worth underlining that the achievement of each objective was adequately verified as shown in Chapter 6.

Regarding the first type, the milestones consisted in the correct estimation of the uncertainty of each relevant quantity in R2S. That is, the uncertainty of all relevant reaction rates, isotopic concentration or DGS intensity (in any contributing region) involved in the R2S simulation, and finally, the SDR uncertainty (in a specific location²), which was the principal goal of the thesis.

Among all the verification exercises related to these milestones, it is worth remarking the comparison of the SDR uncertainty, calculated with the developed tool and with the brute force method, when the SNILB conditions are not met. These exercises [63] [75], presented in Chapter 6, confirm that the proposed methodology overcomes the limitation previously commented, achieving one of the goals of the thesis.

With respect to the second type, the milestones are related to the adequate implementation of three new capabilities, which were included to complete the scheme of uncertainty propagation. Those are: the estimation of the isotopic contribution to the tally, the calculation of the pathway contribution to the production of an isotope, and the assessment of the derivatives of the concentration to the reaction rates (sensitivity coefficients). Below, we comment on the most relevant highlights and issues related to these new capabilities.

¹ Additional transversal milestones related to improvements of R2S-UNED performance were achieved [93]. However, they are not commented because they are transversal to the topic of the thesis.

² The methodology is adequate only to estimate the uncertainty of individual SDR tallies.

I. Isotopic contribution to the tally:

The purpose of this capability was to filter the isotopes that contribute to the SDR tally in order to speed up the estimation of the uncertainty. In addition, the information provided by this method is valuable to different nuclear analyses in fusion facilities, as for example, to find the reason for the differences between D1S and R2S estimation in the air-kerma in JET¹ [90].

II. Pathway contribution to the production of an isotope:

This capability aimed to filter the most relevant reactions to the SDR response. But, in addition, this provides relevant information to most of the nuclear analysis that includes the activation step. For that reason, it was extracted from R2S-UNED in an individual module (called Achains) coupled with ACAB. As an example of the applicability, the developed tool was the detection of all relevant pathways to the analysis of the SDR in ITER [56].

Regarding the implementation, we took into account that, in fusion environments, the most relevant pathways in SDR analysis do not contain loops². However, the methodology can still be improved to deal with more general problems. This will be mentioned as future work in section 9.1.1.

III. Estimation of the derivatives of the isotopic contribution with respect to the reaction rates:

The strategy followed in the thesis to estimate the sensitivity coefficients was to solve the ODEs system that describes their temporal evolution. For this task, we use ACAB since it has been extremely verified and validated in fusion environments [46].

The methodology works well in most of the cases; however, small miscalculations were found in no realistic cases when the burn-up was extremely high. The study of a more appropriate solver is proposed as future work in section 9.1.1. Nevertheless, the accuracy of the solver looks good enough to justify its application in realistic fusion facilities.

8.2 Applicability of R2S-UNED to estimate the SDR stochastic uncertainty

Chapter 7 demonstrates the applicability of the implemented uncertainty module of R2S-UNED in two different exercises: The computational SDR benchmark of ITER and the air-kerma estimation in JET. The first one is a headstone to verify the advances in SDR computational methodologies. In addition, its simple geometry makes it easy to define a proper mesh for the spatial distribution of the neutron flux and to identify the contributing regions doing the exercise

¹ This work will be sent to its publication in Nuclear Fusion

² The methodology can consider loops, but it does not estimate the importance of the loop. Consequently, it is not optimized to filter the most relevant reactions.

highly traceable. The second application of the uncertainty module was the estimation of the air-kerma in the octant 2 of JET. This application provides a realistic model (regarding dimensions and complexity) of a tokamak fusion facility.

These applications highlight one of the most important weaknesses of the methodology: The difficulty to calculate the neutron flux covariance matrix¹. For this reason, this thesis presents a guideline and a methodology to improve the uncertainty module applicability. Both are focused on simulating only the most relevant regions in the smallest number of individual R2S cases². Therefore, we must analyze in detail the simulation case in order to apply these strategies. Consequently, the computational resources required to calculate the stochastic uncertainty of R2S UNED are increased, and could even be prohibitive in some practical applications.

Despite such disadvantages of these strategies, their development has noticeably increased the applicability of the method. Therefore, it also increases the applicability of the R2S-UNED uncertainty module. It was proven by the application of R2S-UNED in the JET and the ITER benchmark.

These applications also allowed analyzing the importance of estimating the neutron covariance matrix in the calculation of the SDR uncertainty. For that reason, the uncertainty estimated using the calculated covariance matrix of the neutron flux was compared with the uncertainty calculated assuming the neutron flux was completely correlated or uncorrelated³. The comparison shows that it is important to calculate the correlation matrix of the neutron flux in order to perform an accurate estimation of the SDR uncertainty in R2S calculations. Consequently, the current methodology must be improved to completely consider the correlation of the neutron flux in general cases. Especially when VR techniques are applied because they could significantly increase the correlation of the neutron flux as it was shown in the ITER benchmark.

In addition, the applications of the uncertainty module of R2S also evidenced that D1S and R2S methodologies estimate different results because each one considers different physical assumptions. Nevertheless, the differences found in the thesis are irrelevant, as was expected, because they are smaller than other uncertainty sources, such as the geometry model. That is, both methodologies are adequate for the shutdown analysis of the current fusion facilities.

¹ In practical cases, the size of this matrix is usually too high to estimate it using MC transport codes. This weakness was expected because it is common in other methodologies that estimate the MC uncertainty in R2S.

² The guideline helps the user to define a small mesh covering the relevant regions, while the methodology automatizes the definition of several meshes optimally.

³ These approaches were implemented for those cases where the actual SDR uncertainty cannot be estimated because the computational resources required to do it are prohibitive.

8.3 Transfer Outcome

This section presents the transfer of the work performed during the thesis, as the developed code and methodologies.

In the first place, this thesis was performed in the frame of the national plan "Development of computational methods and tools to the calculation of residual dose in relevant fusion facilities to the nuclear fusion technology" (ENE2015-70733-R). In particular, it corresponds to the development of aim 4 "Development of a computational methodology suitable to the estimation of uncertainty in the prediction of residual dose". The work performed in this thesis successfully achieves this objective of the national plan. In addition, the transversal work of the thesis also contributed to achieving milestones of other points of the national plan such as aim 1 related to the new capabilities of R2S-UNED and its validation.

Regarding the publications, the work of this thesis was published in nine JCR articles; and it is expected to publish another two during the next year. Two of the published articles [63] [75], as well as the two unpublished ones, are directly related to the thesis. In addition, the transversal improvement¹ of the tools related to R2S-UNED was published in four of the articles [42] [91]–[93]. Finally, the newly developed capabilities enable the development of the last three articles [56] [94] [95]. The achievements or evolution of these works were presented also in ISFNT 2017, SOFT 2018, and 2020², as well as in international meetings such as ITER Neutronic Meeting and Annual General Monitor Meeting (AGMM) in the framework of JET³ during the years 2018, 2019, and 2020.

Finally, it is worth highlighting that the developed code⁴ could be sent to the NEA data bank[96] so that the neutronic community can access and use the tools.

¹ Improvements in the transport or activation codes, which are not directly related with the uncertainty estimation or transport in R2S. For example, the optimization of the memory management related to the geometry description in the transport codes based on MCNP.

² I only presented the work related to [63] [91] in SOFT 2018 and SOFT 2020.

³ I only presented the work in the AGMM. The results of the thesis, related with the application in JET, will be presented in the next event.

⁴ It includes the new module to transport the uncertainty in R2S as well as the update of the activation module of R2S-UNED.

Chapter 9.

Future Work

This chapter presents the perspective to continue the work of this thesis in different areas. The closest one to the work performed in this thesis is the application of the tool during the validation of R2S-UNED. The next milestone in this area is the blind SDR benchmark, which has been proposed inside of the EUROfusion PrIO¹ work package (in JET), to validate shutdown dose codes used in ITER.

The second one is the improvements of the methodology developed during this thesis and its implementation. This includes the development of new features, which the current methodology does not consider, as well as the improvement of the accuracy or speed of the tool. Section 9.1 presents this area.

The third area describes other possible applications of the developed tool², transporting other relevant uncertainties in R2S, or other computational methodologies. Section 9.2 briefly comments on this.

Finally, one last area comments other uncertainty sources in R2S related to the calculation methodology of R2S. These uncertainty sources still require the development of the methodology to quantify the uncertainty associated with the different approaches of R2S. The last area is briefly depicted in section 9.3.

It is worth noting that we are already working in some of the points of these areas as part of the EUROfusion project of NEXP shutdown dose rate experiments in JET.

¹ Preparation of ITER Operation. The proposal of the PrIO work package must still be approved based on the continuity of the JET operation.

² Remember that one of the capabilities of the tool is the transport of the uncertainty of the neutron flux until the SDR

9.1 Code and methodology improvements

9.1.1 Code improvements

As it was commented during the thesis, and in the conclusion in Chapter 8, some of the code features were developed or optimized considering the application of the tool by UNED. That is, taking into account the computational resources, as well as specific physical features of the fusion facilities where TEC3FIR uses R2S-UNED. Consequently, they can be modified or improved in order to increase the applicability of R2S-UNED. The most relevant ones are presented below.

I. ODE solver used to estimate the sensitivity coefficients¹

R2S-UNED calculates the sensitivity coefficients by solving the ODEs system that defines them. Specifically, we implemented a solver, based on ACAB solver², to perform this task because the ODEs system is very similar to the activation system which ACAB solves properly³ and because we can modify ACAB solver if needed.

In realistic cases, the solver works correctly, even when SNILB conditions are not met. However, minor miscalculations were found in the results provided by the solver when the burn-up is extremely elevated. Possibly, these discrepancies are due to the ACAB solver being modified to estimate negative results⁴. Nevertheless, these mistakes do not significantly affect the SDR uncertainty in the calculated cases because they are minor, even though they could be enough to reconsider the solver used in this application or to study the accuracy of ACAB calculating the sensitivity coefficients in fusion environments. It is worth highlighting that the analysis of the ODEs solver, such as ACAB, in the computational neutronic field is an important research line. Currently, this is one important research field studied in TEC3FIR.

II. Pathway estimation

We implemented an algorithm to detect and quantify the pathway contribution to the production of a determinate isotope. This algorithm aimed to filter the most relevant reactions to the SDR response. In SDR analysis of fusion facilities, the pathways usually do not include loops. However, in order to develop a more generic tool, the algorithm allows to the user including them in the pathway contribution, if needed. In any case, the algorithm does not quantify the relevance of the loops. That is, all the loops would be included, even if they are irrelevant.

¹ Derivatives of the isotopic concentration respect to the reaction rates

² It is worth highlighting that ACAB solver refers only to the three subroutines used in ACAB to solve the ODEs system, which were originally implemented in ORIGEN[48].

³ ACAB has been verified in depth in fusion environments. In addition, it has been considered reference codes in relevant fusion facilities such as ITER or IFMIF-EVEDA

⁴ Note that, as opposed to the isotopic concentration, the sensitivity coefficients can be negatives

On that account, the algorithm can be improved by quantifying the loop contribution in order to perform a better filter of reactions when the loops are actually relevant. In this regard, we consider two possible options: The first one consists in considering ODEs solver based on linearizing the pathways (as ALARA or ACTYS-go [39] [40]). The other possible option, which does not require changing the ODEs solver, is to delete the loop of the pathway in order to quantify its importance.

III. Code performance

The computational time required to apply the tool developed during the thesis was considered adequate. One of the reasons for the good performance was that the algorithm was parallelized using MPI, because we have access to huge clusters such as Marconi[33] or the cluster of TECF3IR group¹. However, if the code was run in personal computers, it would be worth improving the performance due to the computer time that is required. In section 5.7, we discussed how we can improve the code performance, at the expense of reducing the outputs that the tool could calculate. The implementation of these options could be considered in the future.

9.1.2 Methodology improvements

The methodology developed to estimate the MC uncertainty in R2S simulations has two principal drawbacks. The first one is related to the reliability of the result provided by the tool, and the second one, with the capability to apply it.

Regarding the reliability, R2S-UNED does not include tests about the convergence of the SDR tally. This means that, although we can calculate the uncertainty of the calculation, this value can be meaningless, because we cannot guarantee that the distribution of the simulation variables is a gaussian distribution. Therefore, its use could lead to incorrect conclusions. In order to improve this situation, statistical tests, similar to those implemented in MCNP tallies, may be implemented.

Regarding the applicability, as commented in section 8.2, the most relevant limitation to estimating the stochastic SDR uncertainty is the estimation of the neutron flux correlation matrix. Consequently, one potential research topic is to overcome this limitation. Three possible lines to be researched are:

- i. At this time, teams are studying the features of the covariance matrix [31]. These studios aim to develop a methodology to estimate the neutron correlation using the currently available computational resources.

¹ Our cluster is currently composed by 1000 processor Intel(R) Xeon(R) Silver 4210 CPU @ 2.20GHz

- ii. Optimizing the R2S simulation to allow the estimation of the SDR uncertainty with the currently available computational resources. This line was studied in this thesis, as commented in section 8.2. However, the developed methodologies can still be improved.
- iii. Introducing the estimation of the SDR uncertainty inside of the MC transport simulation. This simulation could require massive computational time.

9.2 Other applications of the developed methodology

The main feature of the developed tool is to transport the neutron flux uncertainty to the SDR. It can also be considered to transport other uncertainty in R2S-UNED, whether they are due to MC or not. One relevant example in R2S is the uncertainty due to the activation cross-section¹, which was commented in section 4.2. But also, uncertainties associated with the transport cross-section, material definition, etc. could be transported.

In addition, the method developed to estimate the SDR uncertainty can be applied to other methodologies currently used in neutronic analysis. For example, SRC-UNED produces an intermediate source² in a surface from the set of particles stored when they cross it. Consequently, the uncertainty propagation of this source to the tally can be carried out using the scheme proposed in this thesis.

9.3 Other uncertainty sources in R2S method

The stochastic uncertainty of the R2S simulation is neither the only uncertainty of the estimated SDR, nor the most important one in all circumstances. There are other types of systematic uncertainties related to different approaches considered in common implementations of the R2S method.

Two of them are the spatial and energy discretization considered during the coupling of the activation and the transport. Their importance was detected [90] in the project of NEXP shutdown dose rate experiments and we are currently working in a methodology to overcome them.

¹ It is worth underlining that the literature shows that this uncertainty is as relevant as the stochastic uncertainty of the neutron flux in fusion applications[57] [104] [105].

² This source is equivalent to the DGS in R2S methodology. In addition, the covariance matrix associated to this source can be directly estimated during its production.

ANNEX A.

Neutron uncertainty in JET

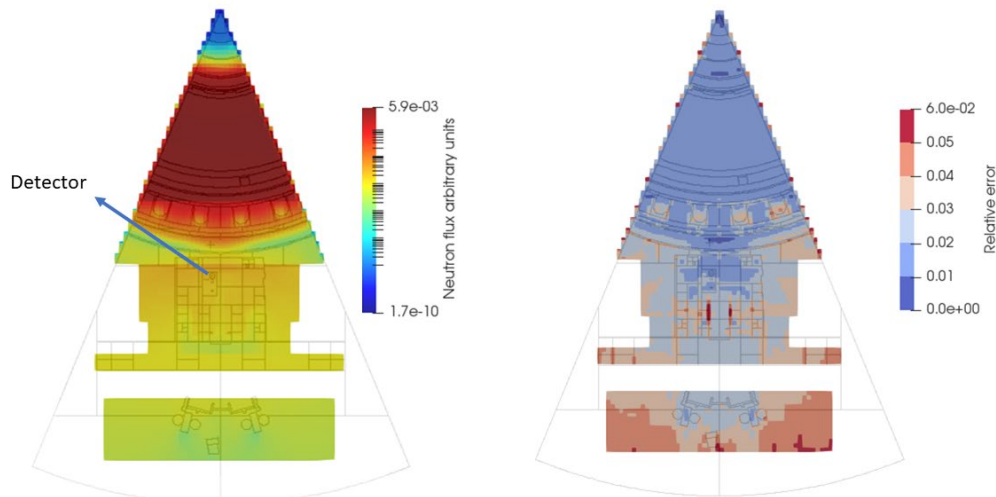


Fig 1 Neutron flux calculated with MC code based on MCNP5 [6] in PZ = 100cm of octant 2 JET model.

Fig 1 presents an example of the complexity of the neutron flux estimation in relevant fusion facilities. This figure shows the neutron flux calculated in Joint Europeans Torus (JET)¹. The calculation required four neutron transport simulations, where each one spent around 8150 hr·cpu in our cluster² in order to consider the activation of the complete facility with fine spatial resolution. It is worth highlighting that the total number of elements used to describe the spatial distribution of the neutron flux spectra, including the energy discretization is $5.7 \cdot 10^7$.

It is important to note that the uncertainty represented in Fig 1 is the uncertainty of the total flux in each region. The uncertainty of each energy element can be bigger than the uncertainty of the total flux in the region. In addition, it is remarkable that the neutron flux was calculated using Global Variance Reduction (GVR). As shown in Chapter 7 of this thesis, this VR method correlates the fluxes increasing the uncertainty with respect to the feeling that this figure transmits. Consequently, the uncertainty level expected from the neutron flux in the decay photon responses maybe around 5% near to detector region.

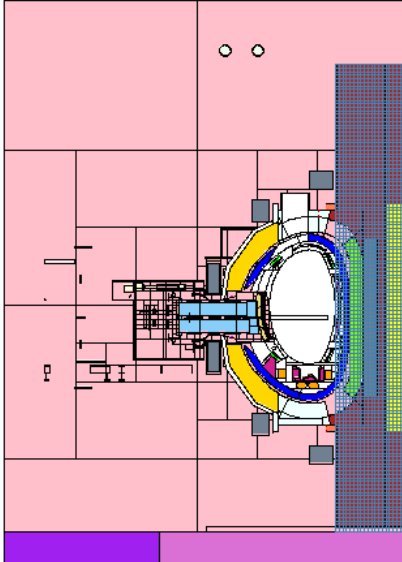
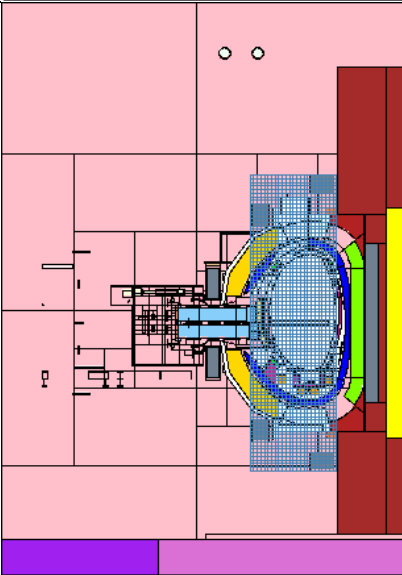
¹ This is the neutron transport of an R2S simulation to estimate the decay photon flux and SDR in a detector of the octant 2 of JET after the 2016 DD campaign [55].

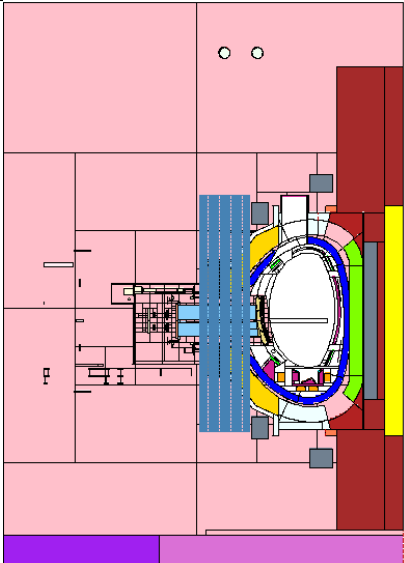
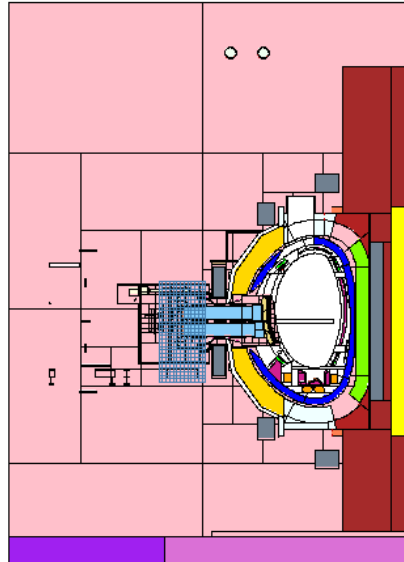
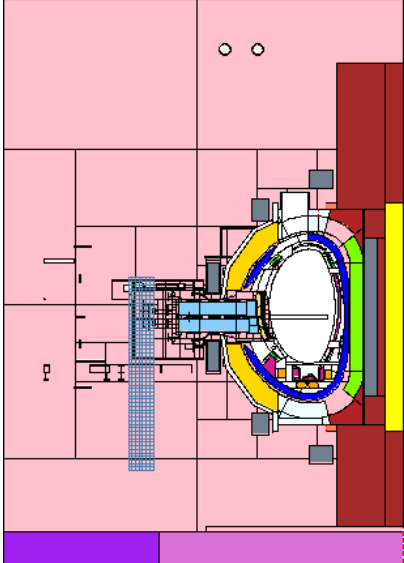
²Our cluster is currently composed by 1000 processor Intel(R) Xeon(R) Silver 4210 CPU @ 2.20GHz

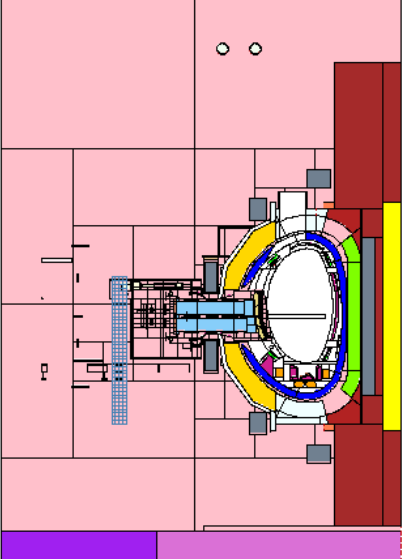
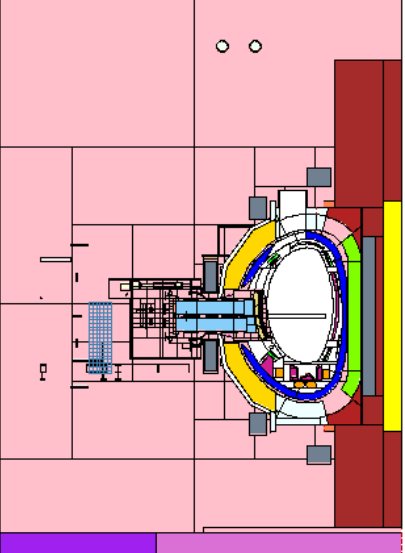
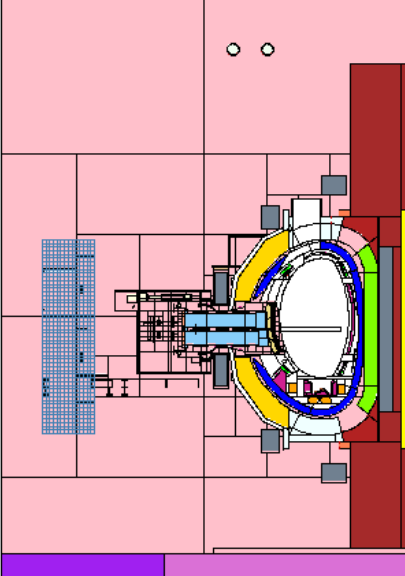
ANNEX B.

Meshes covering JET geometry

This annex presents the MCNP definition and a plot of each one of the eight general meshes used to activate the JET geometry in the R2S simulation.

Mesh	MCNP fmesh card	MCNP plotter
1	Fmesh914:n geom=rec origin= -80 -118 -600 Imesh= 80 iints=16 Jmesh= 2 jints=19 Kmesh= 710 kints=131	
2	Fmesh924:n geom=rec origin= -180 -428 -410 Imesh= 180 iints=36 Jmesh= -118 jints=24 Kmesh= 410 kints=82	

3	<p>Fmesh934:n geom=rec origin= -235 -568 -310 Imesh= 235 iints=47 Jmesh= -428 jints=44 Kmesh= 350 kints=66</p>	
4	<p>Fmesh944:n geom=rec origin= -180 -698 -170 Imesh= 180 iints=36 Jmesh= -568 jints=13 Kmesh= 110 kints=28</p>	
5	<p>Fmesh954:n geom=rec origin= -160 -768 -430 Imesh= 160 iints=32 Jmesh= -698 jints=7 Kmesh= 110 kints=54</p>	

6	<p>Fmesh964:n geom=rec origin= -280 -808 -300 Imesh= 280 iints=56 Jmesh= -768 jints=4 Kmesh= 110 kints=41</p>	
7	<p>Fmesh974:n geom=rec origin= -240 -868 -160 Imesh= 240 iints=56 Jmesh= -808 jints=6 Kmesh= 40 kints=20</p>	
8	<p>Fmesh984:n geom=rec origin= -260 -1008 -280 Imesh= 240 iints=52 Jmesh= -868 jints=14 Kmesh= 240 kints=52</p>	

ANNEX C.

Decay gamma groups recommended by FISPACT

This annex presents the photon energy structure, suggested by FISPACT[22], which is widely used during the thesis.

Table 1 Upper limits for the decay gamma energy bins in MeV.

2.00E+01	1.40E+01	1.20E+01	1.00E+01	8.00E+00	6.50E+00	5.00E+00	4.00E+00
3.00E+00	2.50E+00	2.00E+00	1.66E+00	1.44E+00	1.22E+00	1.00E+00	8.00E-01
6.00E-01	4.00E-01	3.00E-01	2.00E-01	1.00E-01	5.00E-02	2.00E-02	1.00E-02

ANNEX D.

Isotopic contribution to the Air-Kerma

This annex presents the raw results of the isotopic contribution to the air-kerma calculated with R2S-UEND in the octant 2 at 6 hours after of 2016 DD campaign shutdown. It is worth highlighting that these results correspond only to the contribution of the DD neutron activation of meshes 3 and 4.

Table 2 Isotopic contribution to the air-kerma in the octant 2 at 6 hours after of 2016 DD campaign shutdown calculated with R2S-UNED

Isotope	R2S contribution ($\gamma \cdot h^{-1}$)
Cu64	$6.66 \cdot 10^5$
Mn54	$2.44 \cdot 10^5$
Co60	$6.18 \cdot 10^4$
Co58	$9.15 \cdot 10^3$
Mo99+Tc99m	$1.01 \cdot 10^4$

ANNEX E.

Comparison of the brute force method and the implemented method in JET

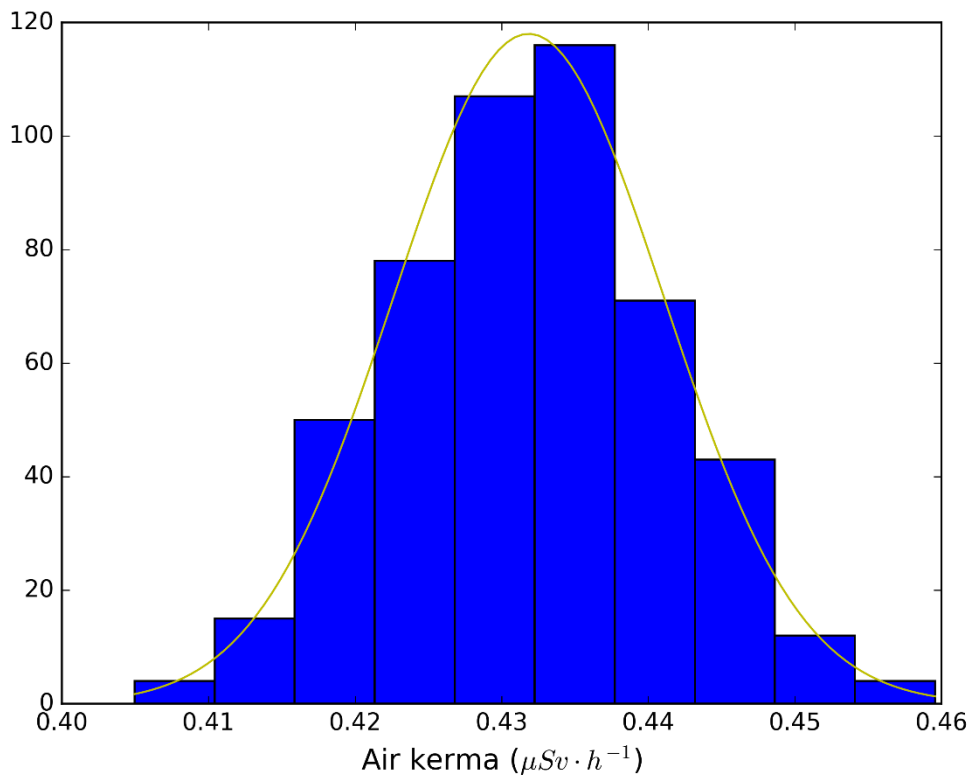


Fig 2 Histogram of the 500 R2S estimations of the air-kerma contribution of the studied case.

The most contributing mesh of the "relevant" ones in R2S simulation (case 1 of general mesh 3) was used to verify the correct estimation of the methodology in a realistic case. For that, the stochastic uncertainty calculated with R2S-UNED is compared with those calculated with the brute force method. The brute force method consisted in 500 R2S simulations of the air kerma contribution. The results of the brute force method are presented in the upper figure, while the estimation of the mean and standard deviation of both methods are presented below.

Table 3 Mean and standard deviation of the R2S simulation calculated by R2S-UNED or by the brute force method

	<i>Air kerma contribution (μSv · h⁻¹)</i>	<i>σ (μSv · h⁻¹)</i>
<i>R2S-UNED uncertainty</i>	$4.320 \cdot 10^{-1}$	$9.1 \cdot 10^{-3}$
<i>Brute force estimation</i>	$4.318 \cdot 10^{-1}$	$9.2 \cdot 10^{-3}$

References

- [1] L. El-Guebaly "History and evolution of fusion power plant studies: Past, Present and Future Prospects" *International Journal of Energy, Environment and Economics* vol. 18 pp. 115–167 2011.
- [2] R. Pampin *et al.* "Developments and needs in nuclear analysis of fusion technology" *Fusion Engineering and Design* vol. 88, no. 6–8 pp. 454–460 2013 doi: 10.1016/j.fusengdes.2013.03.049.
- [3] W. Biel *et al.* "Diagnostics for plasma control – From ITER to DEMO" *Fusion Engineering and Design* vol. 146, no. December 2018 pp. 465–472 2019 doi: 10.1016/j.fusengdes.2018.12.092.
- [4] "JET." <https://www.euro-fusion.org/devices/jet/> (accessed Oct. 18, 2020).
- [5] "ITER goals." <https://www.iter.org/sci/Goals> (accessed Oct. 16, 2020).
- [6] "DEMOstration power plant." <https://www.euro-fusion.org/programme/demo/> (accessed Jun. 14, 2021).
- [7] U. Fischer, D. Leichtle, A. Serikov, P. Pereslavytsev, and R. Villari "Review and validation of shutdown dose rate estimation techniques for application to ITER" *Fusion Science and Technology* vol. 64, no. 3 pp. 563–570 2013 doi: 10.13182/FST13-A19153.
- [8] U. Fischer *et al.* "Neutronic analyses and tools development efforts in the European DEMO programme" *Fusion Engineering and Design* vol. 89, no. 9–10 pp. 1880–1884 2014 doi: 10.1016/j.fusengdes.2014.02.013.
- [9] L. Lu, U. Fischer, and P. Pereslavytsev "Improved algorithms and advanced features of the CAD to MC conversion tool McCad" *Fusion Engineering and Design* vol. 89, no. 9–10 pp. 1885–1888 2014 doi: 10.1016/j.fusengdes.2014.05.015.
- [10] L. Hu *et al.* "SuperMC cloud for nuclear design and safety evaluation" *Annals of Nuclear Energy* vol. 134 pp. 424–431 2019 doi: 10.1016/j.anucene.2019.07.019.
- [11] P. P. H. Wilson, T. J. Tautges, J. A. Kraftcheck, B. M. Smith, and D. L. Henderson "Acceleration techniques for the direct use of CAD-based geometry in fusion neutronics analysis" *Fusion Engineering and Design* vol. 85, no. 10–12 pp. 1759–1765 2010 doi: 10.1016/j.fusengdes.2010.05.030.
- [12] P. P. H. Wilson *et al.* "State-of-the-art 3-D radiation transport methods for fusion energy systems" *Fusion Engineering and Design* vol. 83, no. 7–9 pp. 824–833 2008 doi:

10.1016/j.fusengdes.2008.05.038.

- [13] T. M. Evans, A. S. Stafford, R. N. Slaybaugh, and K. T. Clarno "Denovo: A new three-dimensional parallel discrete ordinates code in SCALE" *Nuclear Technology* vol. 171, no. 2 pp. 171–200 2010 doi: 10.13182/NT171-171.
- [14] B. L. Granovskii and S. M. Ermakov "The Monte Carlo method" *Journal of Soviet Mathematics* vol. 7, no. 2 pp. 161–192 1977 doi: 10.1007/BF01084250.
- [15] S. W. Mosher *et al.* *ADVANTG — An Automated Variance Reduction Parameter Generator November 2013*, no. November. 2013.
- [16] X.-5 M. C. Team *MCNP - A General Monte Carlo N-Particle Transport Code Version 5, User's Guide*. 2003.
- [17] P. K. Romano and B. Forget "The OpenMC Monte Carlo particle transport code" *Annals of Nuclear Energy* vol. 51 pp. 274–281 2013 doi: 10.1016/j.anucene.2012.06.040.
- [18] S. Agostinelli *et al.* "GEANT4 - A simulation toolkit" *Nuclear Instruments and Methods in Physics Research, Section A: Accelerators, Spectrometers, Detectors and Associated Equipment* vol. 506, no. 3 pp. 250–303 2003 doi: 10.1016/S0168-9002(03)01368-8.
- [19] D. Valenza, H. Iida, R. Plenteda, and R. T. Santoro "Proposal of shutdown dose estimation method by Monte Carlo code" *Fusion Engineering and Design* vol. 55, no. 4 pp. 411–418 2001 doi: 10.1016/S0920-3796(01)00188-0.
- [20] Y. Chen and U. Fischer "Rigorous MCNP based shutdown dose rate calculations: Computational scheme, verification calculations and application to ITER" *Fusion Engineering and Design* vol. 63–64 pp. 107–114 2002 doi: 10.1016/S0920-3796(02)00144-8.
- [21] G. Mariano, D. Flammini, N. Fonesu, F. Moro, and R. Villari "Progress in development of advanced D1S dynamic code for three-dimensional shutdown dose rate calculations" *Fusion Engineering and Design* vol. 157, no. September 2019 p. 111631 2020 doi: 10.1016/j.fusengdes.2020.111631.
- [22] R. A. Forrest *FISPACT-2007: User Manual*. UKAEA-FUS-534, 2007.
- [23] A. Davis and R. Pampin "Benchmarking the MCR2S system for high-resolution activation dose analysis in ITER" *Fusion Engineering and Design* vol. 85, no. 1 pp. 87–92 2010 doi: 10.1016/j.fusengdes.2009.07.002.
- [24] P. Sauvan, J. P. Catalán, F. Ogando, R. Juárez, and J. Sanz "Development of the R2SUNED Code System for Shutdown Dose Rate Calculations" *IEEE Transactions on Nuclear Science* vol. 63, no. 1 pp. 375–384 2016 doi: 10.1109/TNS.2015.2507138.

- [25] T. Eade, D. Stonell, and A. Turner "MCR2S unstructured mesh capabilities for use in shutdown dose rate analysis" *Fusion Engineering and Design* vol. 100 pp. 321–333 2015 doi: 10.1016/j.fusengdes.2015.06.189.
- [26] P. Kanth and P. V. Subhash "ACTYS-ASG, tool for coupling ACTYS-1-GO with ATTILA" *Fusion Engineering and Design* vol. 129, no. February pp. 196–201 2018 doi: 10.1016/j.fusengdes.2018.02.092.
- [27] M. Z.Youssef, R. Feder, K. Thompson, I. Davis, and G. Failla "Benchmarking the three-dimensional cad-based discrete ordinates code attila using integral dose-rate experiments and comparison to mcnp results" *Fusion Science and Technology* vol. 56, no. 2 pp. 718–725 2009 doi: 10.13182/fst09-a8993.
- [28] D. E. Peplow, A. M. Ibrahim, and R. E. Grove "Propagation of uncertainty from a source computed with Monte Carlo" *Transactions of the American Nuclear Society* vol. 108, no. 5 pp. 643–646 2013.
- [29] H. H. Ku "Notes on the use of propagation of error formulas" *Journal of Research of the National Bureau of Standards, Section C: Engineering and Instrumentation* vol. 70C, no. 4 p. 263 1966 doi: 10.6028/jres.070c.025.
- [30] A. M. Ibrahim, D. E. Peplow, R. E. Grove, J. L. Peterson, and S. R. Johnson "The multi-step cadis method for shutdown dose rate calculations and uncertainty propagation" *Nuclear Technology* vol. 192, no. 3 pp. 286–298 2015 doi: 10.13182/NT15-1.
- [31] M. S. Harb "Propagation of statistical uncertainty in mesh-based shutdown dose rate calculations," University of wisconsin-madison, 2019.
- [32] G. Y. Han, D. H. Kim, C. H. Shin, S. H. Kim, B. K. Seo, and G. M. Sun "On-the-fly Estimation Strategy for Uncertainty Propagation in Two-Step Monte Carlo Calculation for Residual Radiation Analysis" *Nuclear Engineering and Technology* vol. 48, no. 3 pp. 765–772 2016 doi: 10.1016/j.net.2016.01.009.
- [33] F. Iannone *et al.* "MARCONI-FUSION: The new high performance computing facility for European nuclear fusion modelling" *Fusion Engineering and Design* vol. 129, no. November 2017 pp. 354–358 2018 doi: 10.1016/j.fusengdes.2017.11.004.
- [34] S. C. Wilson, S. W. Mosher, K. E. Royston, C. R. Daily, and A. M. Ibrahim "Validation of the MS-CADIS Method for Full-Scale Shutdown Dose Rate Analysis" *Fusion Science and Technology* vol. 74, no. 4 pp. 288–302 2018 doi: 10.1080/15361055.2018.1483687.
- [35] E. D. Biondo and P. P. H. Wilson "Transmutation approximations for the application of hybrid Monte Carlo/deterministic neutron transport to shutdown dose rate analysis" *Nuclear Science and Engineering* vol. 187, no. 1 pp. 27–48 2017 doi:

10.1080/00295639.2016.1275848.

- [36] B. T. Rearden and M. A. Jessee *SCALE Code System*, no. 6.2.3. 2016.
- [37] A. Davis "Radiation shielding of fusion systems," Birmingham, 2010.
- [38] A. C. Hindmarsh *ODEPACK, A Systematized Collection of Ode Solvers*. Lawrence Livermore National Laboratory, 1982.
- [39] P. Kanth, S. C. Tadepalli, R. Srinivasan, and P. V. Subhash "ACTYS-1-GO: A faster and accurate algorithm for multipoint nuclear activation calculations" *Fusion Engineering and Design* vol. 122, no. May pp. 154–162 2017 doi: 10.1016/j.fusengdes.2017.08.022.
- [40] P. P. H. Wilson "ALARA: Analytic and Laplacian Adaptive," 1999.
- [41] J. Sanz, O. Cabellos, and N. Garcia-Herranz "ACAB Inventory code for nuclear applications: User's Manual V" 2008.
- [42] P. Sauvan *et al.* "D1SUNED system for the determination of decay photon related quantities" *Fusion Engineering and Design* vol. 151 2020 doi: 10.1016/j.fusengdes.2019.111399.
- [43] R. Villari *et al.* "Shutdown dose rate assessment with the Advanced D1S method: Development, applications and validation" *Fusion Engineering and Design* vol. 89, no. 9–10 pp. 2083–2087 2014 doi: 10.1016/j.fusengdes.2014.01.071.
- [44] F. Ogando, P. Sauvan, D. López, J. Sanz, B. Brañas, and F. Arranz "Activation analysis of the water cooling system of the LIPAc beam dump" *Fusion Engineering and Design* vol. 89, no. 9–10 pp. 2053–2056 2014 doi: 10.1016/j.fusengdes.2014.03.022.
- [45] R. Villari *et al.* "Shutdown dose rate benchmark experiment at JET to validate the three-dimensional Advanced-D1S method" *Fusion Engineering and Design* vol. 87, no. 7–8 pp. 1095–1100 2012 doi: 10.1016/j.fusengdes.2012.02.081.
- [46] E. T. Cheng, S. Beach, R. A. Forrest, and A. B. Pashchenko "Report on the second international activation calculation benchmark comparison study" *IAEA Nuclear data section* no. February 1994.
- [47] A. P. Belian, J. F. Latkowski, and E. C. Morse "Experimental studies of concrete activation at the National Ignition Facility using the Rotating Target Neutron Source" *Fusion Technology* vol. 34, no. 3 pt 2 pp. 1028–1032 1998 doi: 10.13182/fst98-a11963749.
- [48] A. G. Croff "ORIGEN2: A Versatile Computer Code for Calculating the Nuclide Compositions and Characteristics of Nuclear Materials" *Nuclear Technology* vol. 62, no. 3 pp. 335–352 1983 doi: 10.13182/nt83-1.

- [49] H. Bateman *Partial Differential Equations of Mathematical Physics*. 1932.
- [50] A. Saltelli, M. Ratto, S. Tarantola, and F. Campolongo "Sensitivity analysis for chemical models" *Chemical Reviews* vol. 105, no. 7 pp. 2811–2827 2005 doi: 10.1021/cr040659d.
- [51] S. C. Tadepalli and P. V. Subhash "Simplified recursive relations for the derivatives of Bateman linear chain solution and their application to sensitivity and multi-point analysis" *Annals of Nuclear Energy* vol. 121 pp. 479–486 2018 doi: 10.1016/j.anucene.2018.08.004.
- [52] D. G. Cacuci *Sensitivity and uncertainty analysis Volume I*. 2018.
- [53] R. P. Dickinson and R. J. Gelinias "Sensitivity Analysis of Ordinary Differential Direct Method" *Journal of computational physics* vol. 21 pp. 123–143 1976.
- [54] A. Bidaud *et al.* "Understanding Total Monte Carlo uncertainty propagation in burn-up calculations with Generalized Perturbation Theory." International Conference on Nuclear Data for Science and Technology (ND2016), Bruges, Belgium, 2016.
- [55] ENEA, CCFE, UNED, and KIT "WPJET3 D NEXP D20 Shutdown dose rate calculations with different numerical approaches for the DD shutdown." [Online]. Available: <https://idm.euro-fusion.org/?uid=2NFBMG>.
- [56] G. Pedroche, P. Sauvan, J. Alguacil, J. Sanz, and R. Ju "Nuclear data for D1SUNED for the study of ITER planned in-situ maintenance dose scenarios" *Fusion Engineering and Design* vol. 170 pp. 1–7 2021 doi: 10.1016/j.fusengdes.2021.112646.
- [57] J. W. Eastwood, J. G. Morgan, and J. C. Sublet "Inventory Uncertainty Quantification using TENDL Covariance Data in Fispact-II" *Nuclear Data Sheets* vol. 123 pp. 84–91 2015 doi: 10.1016/j.nds.2014.12.015.
- [58] G. Bailey, D. Foster, P. Kanth, and M. Gilbert *The FISPACT-II User Manual*, no. UKAEA. 2021.
- [59] M. Pusa "Rational approximations to the matrix exponential in burnup calculations" *Nuclear Science and Engineering* vol. 169, no. 2 pp. 155–167 2011 doi: 10.13182/NSE10-81.
- [60] J. C. Sublet, J. W. Eastwood, J. G. Morgan, M. R. Gilbert, M. Fleming, and W. Arter "FISPACT-II: An Advanced Simulation System for Activation, Transmutation and Material Modelling" *Nuclear Data Sheets* vol. 139 pp. 77–137 2017 doi: 10.1016/j.nds.2017.01.002.
- [61] A. Khursheed "Neutron-Induced Activation of Materials for the First Wall of Conceptual Fusion Reactors," London University, 1989.
- [62] A. J. Lopez-Revelles "Neutron analyses and design of components for ITER," Universidad Nacional de Educación a Distancia (UNED), 2018.

- [63] J. Alguacil, P. Sauvan, J. P. Catalan, and J. Sanz "Uncertainty propagation from neutron flux to decay gamma source in R2S methodology" *Fusion Engineering and Design* vol. 146 pp. 1100–1103 2019 doi: 10.1016/j.fusengdes.2019.02.016.
- [64] S. Van der Walt, S. C. Colbert, and G. Varoquaux "The NumPy Array: A Structure for Efficient Numerical Computation" *Computing in Science* vol. 13 pp. 22–30 2011 doi: 10.1109/MCSE.2011.37.
- [65] "Python: a Dynamic, Open Source Programming Language." <https://www.python.org/> (accessed Nov. 02, 2020).
- [66] "VitaminJ energy structure." http://serpent.vtt.fi/mediawiki/index.php/Pre-defined_energy_group_structures (accessed Oct. 22, 2020).
- [67] R. Garcia "Resolution of neutronic challenges for the development of ITER and DEMO-EU magnetic fusion reactors," Universidad Nacional de Educación a Distancia (UNED), 2017.
- [68] R. Garcia, M. Garcia, R. Pampin, and J. Sanz "Status of reliability in determining SDDR for manual maintenance activities in ITER: Quality assessment of relevant activation cross sections involved" *Fusion Engineering and Design* vol. 112 pp. 177–191 2016 doi: 10.1016/j.fusengdes.2016.08.016.
- [69] "D1-3 Activation study and D1SUNED v312 nuclear data set (ITER_D_WDQR2F)," 2018.
- [70] "Recommendation on Plasma scenarios (ITER_D_2V3V8Gv12)."
- [71] P. Virtanen *et al.* "SciPy 10: fundamental algorithms for scientific computing in Python" *Nature Methods* vol. 17, no. 3 pp. 261–272 2020 doi: 10.1038/s41592-019-0686-2.
- [72] C. Konno, S. Kwon, O. Masayuki, and S. Sato "FENDL-31b test(JAEA-Conf-2017-0001)," 2018.
- [73] M. C. White "Further Notes on MCPLIB03/04 and New MCPLIB63784 Compton Broadening Data For All Versions of MCNP5," 2012.
- [74] R. A. Forrest, J. Kopecky, and J. C. Sublet "The European Activation File EAF-2007 neutron induced cross section library," 2007.
- [75] J. Alguacil, P. Sauvan, J. P. Catalan, and J. Sanz "Development of a methodology to estimate the statistical SDR uncertainty with R2S-UNED" *Fusion Engineering and Design* 2021 doi: 10.1016/j.fusengdes.2021.112696.
- [76] P. Batistoni *et al.* "Technological exploitation of Deuterium–Tritium operations at JET in support of ITER design, operation and safety" *Fusion Engineering and Design* vol. 109–111, no. 2016 pp. 278–285 2016 doi: 10.1016/j.fusengdes.2016.03.012.

- [77] R. Juárez, R. Pampin, B. Levesy, F. Moro, A. Suarez, and J. Sanz "Shutdown dose rates at ITER equatorial ports considering radiation cross-talk from torus cryopump lower port" *Fusion Engineering and Design* vol. 100 pp. 501–506 2015 doi: 10.1016/j.fusengdes.2015.07.027.
- [78] A. J. Van Wijk, G. Van Den Eynde, and J. E. Hoogenboom "An easy to implement global variance reduction procedure for MCNP" *Annals of Nuclear Energy* vol. 38, no. 11 pp. 2496–2503 2011 doi: 10.1016/j.anucene.2011.07.037.
- [79] "D2-2 Computational Benchmark of D1SUNED v312 IDM_UID WEP47J," 2018.
- [80] L. Petrizzi, M. Angelone, P. Batistoni, U. Fischer, M. Loughlin, and R. Villari "Benchmarking of Monte Carlo based shutdown dose rate calculations applied in fusion technology: From the past experience a future proposal for JET 2005 operation" *Fusion Engineering and Design* vol. 81, no. 8-14 PART B pp. 1417–1423 2006 doi: 10.1016/j.fusengdes.2005.10.014.
- [81] R. Villari *et al.* "ITER oriented neutronics benchmark experiments on neutron streaming and shutdown dose rate at JET" *Fusion Engineering and Design* vol. 123 pp. 171–176 2017 doi: 10.1016/j.fusengdes.2017.03.037.
- [82] R. Villari *et al.* "D029– Analysis of the measurements of the DD shutdown Shutdown dose rate calculations with different numerical approaches for the DD shutdown."
- [83] R. Villari *et al.* "Shutdown dose rate neutronics experiment during high performances DD operations at JET" *Fusion Engineering and Design* vol. 136 pp. 1545–1549 Nov. 2018 doi: 10.1016/j.fusengdes.2018.05.053.
- [84] R. Villari, D. Flammini, and J. P. Catalan "D17 - Final Version of MCNP Input for Shutdown Dose Rate Experiment," 2015. [Online]. Available: <https://idm.euro-fusion.org/?uid=2MMSQ5%0A>.
- [85] N. Fonnesu, R. Villari, D. Flammini, P. Batistoni, U. Fischer, and P. Pereslavitsev "Shutdown dose rate studies for the DTE2 campaign at JET" *Fusion Engineering and Design* vol. 161, no. 2019 pp. 1–5 2020 doi: 10.1016/j.fusengdes.2020.112009.
- [86] "FENDL: Fusion Evaluated Nuclear Data Library." <https://www-nds.iaea.org/fendl/> (accessed Nov. 03, 2020).
- [87] R. Villari *et al.* "Experimental validation of shutdown dose rate computational tools at JET tokamak in DD operations," 2020.
- [88] D. R. Greening "Parallel simulated annealing techniques" *Physica D: Nonlinear Phenomena* vol. 42, no. 1–3 pp. 293–306 1990 doi: 10.1016/0167-2789(90)90084-3.

- [89] "Metropolis algorithm." https://es.wikipedia.org/wiki/Algoritmo_de_Metropolis-Hastings (accessed Apr. 26, 2021).
- [90] ENEA, CCFE, UNED, and KIT "Report D24 Shutdown dose rate calculation for DD: Analysis of discrepancies between codes."
- [91] J. Alguacil, J. P. Catalan, M. De Pietri, P. Sauvan, and J. Sanz "A method for assessing 3D decay heat and temperature considering accurate distributions of the decay gamma fields" *Fusion Engineering and Design* vol. 168 p. 112610 2021 doi: 10.1016/j.fusengdes.2021.112610.
- [92] M. De Pietri, J. Alguacil, A. Kolsek, G. Pedroche, N. Ghirelli, and E. Polunovskiy "Integral modelling of the ITER cooling water systems radiation source for applications outside of the Bio-shield" *Fusion Engineering and Design* vol. 171 p. 112575 2021 doi: 10.1016/j.fusengdes.2021.112575.
- [93] J. Alguacil, P. Sauvan, R. Juarez, and J. P. Catalan "Assessment and optimization of MCNP memory management for detailed geometry of nuclear fusion facilities" *Fusion Engineering and Design* 2018 doi: 10.1016/j.fusengdes.2018.02.048.
- [94] R. Juarez *et al.* "A full and heterogeneous model of the ITER tokamak for comprehensive nuclear analyses" *Nature Energy* vol. 6 2021 doi: 10.1038/s41560-020-00753-x.
- [95] R. Juárez *et al.* "Update in the nuclear responses of the European TBMs for ITER during operation and shutdown" *Fusion Engineering and Design* vol. 134 2018 doi: 10.1016/j.fusengdes.2018.06.022.
- [96] "NEA data bank." https://www.oecd-nea.org/jcms/pl_28124/about-the-data-bank (accessed Jul. 26, 2021).
- [97] L. L. Briggs, W. F. Miller, and E. E. Lewis "Ray-Effect Mitigation in Discrete Ordinate-Like Angular Finite Element Approximations in Neutron Transport" *Nuclear Science and Engineering* vol. 57, no. 3 pp. 205–217 1975 doi: 10.13182/NSE75-A26752.
- [98] A. Davis and A. Turner "Comparison of global variance reduction techniques for Monte Carlo radiation transport simulations of ITER" *Fusion Engineering and Design* vol. 86, no. 9–11 pp. 2698–2700 2011 doi: 10.1016/j.fusengdes.2011.01.059.
- [99] J. C. Wagner, D. E. Peplow, and S. W. Mosher "Fw-cadis method for global and regional variance reduction of monte carlo radiation transport calculations" *Nuclear Science and Engineering* vol. 176, no. 1 pp. 37–57 2014 doi: 10.13182/NSE12-33.
- [100] J. P. Catalán *Nuclear analysis in Magnetic Fusion reactors: Computational development and application in DEMO and ITER*, UNED. Madrid, 2015.

- [101] J. Sanz, R. Falquina, A. Rodriguez, O. Cabellos, S. Reyes, and J. F. Latkowski "Monte Carlo uncertainty analyses of pulsed activation in the national ignition facility gunite shielding" *Fusion Science and Technology* vol. 43, no. 3 pp. 473–477 2003 doi: 10.13182/FST03-A293.
- [102] O. W. Hermann and R. M. Westfall "Origen-S: Scale system module to calculate fuel depletion, actinide transmutation, fission product buildup and decay, and associated radiation source terms," 1998.
- [103] J. Zhao *et al.* "An automatic adaptive mesh generation method for weight window in Monte Carlo particle transport" *Annals of Nuclear Energy* vol. 91 pp. 105–110 2016 doi: 10.1016/j.anucene.2015.12.011.
- [104] O. Cabellos *et al.* "Sensitivity and uncertainty analysis to burnup estimates on ADS using the ACAB code," in *AIP Conference Proceedings*, 2005, vol. 769, pp. 1576–1579, doi: 10.1063/1.1945307.
- [105] O. Cabellos *et al.* "Propagation of nuclear data uncertainties in transmutation calculations using ACAB code" *Journal of the Korean Physical Society* vol. 59, no. 23 pp. 1268–1271 2011 doi: 10.3938/jkps.59.1268.